UC San Diego

UC San Diego Electronic Theses and Dissertations

Title

Adaptation to the aquatic environment: from penguin heart rates to cetacean brain morphology

Permalink

https://escholarship.org/uc/item/571885zg

Author

Wright, Alexandra

Publication Date

2016

Peer reviewed|Thesis/dissertation

eScholarship.org Powered by the California Digital Library
University of California

UNIVERSITY OF CALIFORNIA, SAN DIEGO

Adaptation to the aquatic environment: from penguin heart rates to cetacean brain morphology

A dissertation submitted in partial satisfaction of the requirements for the degree

Doctor of Philosophy

in

Marine Biology

by

Alexandra Katharine Wright

Committee in charge:

Paul Ponganis, Chair
Timothy Gentner
Gerald Kooyman
Jill Leutgeb
Miriam Scadeng
Rebecca Theilmann

2016

The Dissertation of Alexandra Katharine Wright is approved, and it is acceptable in quality and form for publication on microfilm and electronically:

_____

_____

_____

_____

_____

_____
Chair

University of California, San Diego

2016

DEDICATION

To Jason Garber, you believed in me and with your friendship, you made this possible.

To my puppy, Viva, for your unwavering love and bulldog spirit.

To my husband, Patrick, for your boundless love and support and for your encouragement and patience throughout this process. Without you, I could not have achieved this. With you, I know true love and joy.

TABLE OF CONTENTS

LIST OF ABBREVIATIONS

Aerobic dive limit	ADL
Anterior thalamic radiation	ATR
Arcuate fasciculus	ARC
Axial diffusivity	A_D
Brain mass	BM
Cerebrospinal fluid	CSF
Cingulum	CG
Corpus callosum mid-sagittal area	CCA
Corticocaudate tract	CCA
Diffusion tensor imaging	DTI
Electrocardiogram	ECG
Electroencephalogram	EEG
External capsule	EC
Forceps minor of the corpus callosum	CCFM
Fornix	FX
Fractional anisotropy	FA
Functional magnetic resonance imaging	fMRI
Gray matter	GM
Heart rate	f_H
Inferior colliculus	IC
Lateralization index	LI
Magnetic resonance imaging	MRI
Mean diffusivity	M_D
Radial diffusivity	R_D
Rapid eye movement	REM
Region(s) of interest	ROI
Superior colliculus	SC
Superior longitudinal fasciculus	SLF
Time depth recorder	TDR
Unihemispheric slow wave sleep	USWS
White matter	WM

LIST OF FIGURES

LIST OF TABLES

ACKNOWLEDGEMENTS

I would like to express my gratitude to my advisor Paul Ponganis for his guidance and support throughout this process. It has been a long and challenging journey that I doubt I could have completed if it were not for his mentorship, kindness, understanding, and patience. Thank you, Paul, for welcoming me into your lab and for helping to shape me into the scientist I am today.

I would also like to thank Miriam Scadeng and Rebecca Theilmann for their contributions to my intellectual, scientific, and professional development. Thank you for your mentorship, advice, and good humor. I am grateful to Sam Ridgway for his openness to collaboration, invaluable guidance, and constructive feedback and for allowing me to work with his fantastic cetacean brains. I am truly privileged to have had the opportunity to learn from and work with you, Sam. I would also like to thank Judy St. Leger for helping my dissertation to take on a new course by providing me with the opportunity to pursue my dual interests in marine biology and neuroscience with her generous provision of a killer whale brain.

Finally, I would like to thank my dissertation committee members Paul Ponganis, Miriam Scadeng, Rebecca Theilmann, Jerry Kooyman, Jill Leutgeb, and Tim Gentner for serving on my committee and for providing helpful insights and recommendations.

Chapter 1, in its entirety, is a reprint of the peer-reviewed publication as it appears in Marine Ecology Progress Series 2014. Citation: Wright, Alexandra K.; Ponganis, Katherine V.; McDonald, Birgitte I.; Ponganis, Paul J. 2014. Heart rates of emperor penguins diving at sea: implications for oxygen store management. *Marine Ecology*

Progress Series 496: 85 – 98. http://dx.doi.org/10.3354/meps10592. The dissertation author was the primary investigator and author of this publication.

Chapter 2, in its entirety, is a reprint of the peer-reviewed publication as it appears in Brain Structure and Function 2016. Citation: Wright, Alexandra; Scadeng, Miriam; Stec, Dominik; Dubowitz, Rebecca; Ridgway, Sam; St. Leger, Judy. 2016. Neuroanatomy of the killer whale (*Orcinus orca*): a magnetic resonance imaging investigation of structure with insights on function and evolution. *Brain Structure & Function*, 1–20. doi:10.1007/s00429-016-1225-x. The dissertation author was the primary investigator and author of this publication.

Chapter 3, in its entirety, has been submitted for publication as it may appear in Brain Structure and Function 2016. Wright, Alexandra K.; Theilmann, Rebecca J.; Ridgway, Sam H., Scadeng, Miriam. (*in review*). Diffusion tractography reveals pervasive asymmetry of cerebral white matter tracts in the bottlenose dolphin (*Tursiops truncatus*). The dissertation author was the primary investigator and author of this publication.

VITA

2007	Research Assistant, University of Alaska, Anchorage
2010	Bachelor of Science, University of Miami
2016	Doctor of Philosophy, University of California, San Diego

PUBLICATIONS

Wright, AK, Ponganis, KV, McDonald, BI, Ponganis, PJ. 2014. Heart rates of emperor penguins diving at sea: implications for oxygen store management. *Marine Ecology Progress Series* 496: 85 – 98. http://dx.doi.org/10.3354/meps10592.

Wright, A, Scadeng, M, Stec, D, Dubowitz, R, Ridgway, S, St. Leger, J. 2016. Neuroanatomy of the killer whale (*Orcinus orca*): a magnetic resonance imaging investigation of structure with insights on function and evolution. *Brain Structure & Function*, 1–20. doi:10.1007/s00429-016-1225-x.

Wright, AK, Theilmann, RJ, Ridgway, SH, Scadeng, M. (*in review*). Diffusion tractography reveals pervasive asymmetry of cerebral white matter tracts in the bottlenose dolphin (*Tursiops truncatus*).

ABSTRACT OF THE DISSERTATION

Adaptation to the aquatic environment: from penguin heart rates to cetacean brain morphology

by

Alexandra Katharine Wright

Doctor of Philosophy in Marine Biology

University of California, San Diego, 2016

Paul Ponganis, Chair

The evolutionary process of adaptation to the aquatic environment has dramatically modified the anatomy and physiology of secondarily-aquatic, air-breathing seabirds and marine mammals to address oxygen constraints and unique sensorimotor conditions. As taxa that have arguably undergone significant evolutionary transformations, deep-diving sphenisciforms (penguins) and obligatorily aquatic cetaceans (whales, dolphins, and porpoises) provide an excellent opportunity to study such physiological and anatomical adaptation. Investigation of heart rates of free-ranging emperor penguins (*Aptenodytes forsteri*) equipped with digital electrocardiogram

recorders and time depth recorders revealed a phenomenal dive capacity extending to 431 m as well as extreme bradycardia, reaching heart rates as low as 10 beats min^{-1} during deep dives to promote oxygen conservation. The organization and potential function of the cetacean brain were examined with structural magnetic resonance imaging and diffusion tensor imaging of post-mortem killer whale (*Orcinus orca*) and bottlenose dolphin (*Tursiops truncatus*) brains. Structural images were acquired for an *O. orca* brain *in situ* and underwent manual segmentation to obtain volumetric measurements of neuroanatomy including gray and white matter, constituent neural regions (i.e., cerebrum, brainstem, and cerebellum), and subcortical and midbrain structures. This *O. orca* had one of the largest forebrains studied to date with cerebral volume comprising 81.51% of the total brain volume. Moreover, the cerebral white matter of *O. orca* and other delphinoids exhibited isometric scaling unlike other mammals suggesting that this divergent morphology may have evolved in response to the sensorimotor demands of the aquatic environment. Examination of *T. truncatus* cerebral white matter with diffusion tractography revealed widespread structural asymmetries potentially attributable to brain enlargement and isometrically-scaled white matter. Moreover, these structural asymmetries may underpin previously reported observations of functional and behavioral lateralization in cetaceans. These studies of cetacean anatomy and sphenisciform physiology provide insight into and promote our understanding of the evolution of arguably the most ocean-adapted seabirds and marine mammals.

Chapter 1. Heart rates of emperor penguins diving at sea: implications for oxygen store management

Vol. 496: 85–98, 2014
doi: 10.3354/meps10592

MARINE ECOLOGY PROGRESS SERIES
Mar Ecol Prog Ser

Published January 27

Contribution to the Theme Section 'Tracking fitness in marine vertebrates'

Heart rates of emperor penguins diving at sea: implications for oxygen store management

Alexandra K. Wright*, Katherine V. Ponganis, Birgitte I. McDonald, Paul J. Ponganis

Center for Marine Biotechnology and Biomedicine, Scripps Institution of Oceanography, University of California San Diego, La Jolla, California 92093-0204, USA

ABSTRACT: Heart rate (f_H) contributes to control of blood oxygen (O_2) depletion through regulation of the magnitude of pulmonary gas exchange and of peripheral blood flow in diving vertebrates such as penguins. Therefore, we measured f_H during foraging trip dives of emperor penguins *Aptenodytes forsteri* equipped with digital electrocardiogram (ECG) recorders and time depth recorders (TDRs). Median dive f_H (total heartbeats/duration, 64 beats min^{-1}) was higher than resting f_H (56 beats min^{-1}) and was negatively related to dive duration. Median dive f_H in dives greater than the 5.6 min aerobic dive limit (ADL; dive duration associated with the onset of a net accumulation of lactic acid above resting levels) was significantly less than the median dive f_H of dives less than the ADL (58 vs. 66 beats min^{-1}). f_H profile patterns differed between shallow (<50 m) and deep dives (>250 m), with values usually declining to levels near resting f_H in shallow, short-duration dives, and to levels as low as 10 beats min^{-1} during the deepest segments of deep dives. The total number of heartbeats in a dive was variable in shallow dives and consistently high in deep dives. A true bradycardia (f_H below resting levels) during segments of 31% of shallow and deep dives of emperor penguins is consistent with reliance on myoglobin-bound O_2 stores for aerobic muscle metabolism that is especially accentuated during the severe bradycardias of deep dives. Although f_H is low during the deepest segments of deep dives, the total number and distribution of heartbeats in deep, long dives suggest that pulmonary gas exchange and peripheral blood flow primarily occur at shallow depths.

KEY WORDS: Aerobic dive limit · Diving physiology · Electrocardiogram · ECG · Emperor penguin · Gas exchange · Heart rate · Oxygen store management · Peripheral perfusion

Resale or republication not permitted without written consent of the publisher

INTRODUCTION

Regulation of heart rate (f_H) underlies the oxygen store management and dive capacity of seabirds and marine mammals. The reduction in cardiac output associated with a decline in f_H during forced submersion results in: (1) decreased organ blood flow and perfusion-dependent O_2 consumption, (2) decreased blood flow to locomotory muscle and a decline in blood-to-muscle O_2 transfer, and (3) decreased pulmonary blood flow and blood oxygen uptake from the lung (Scholander 1940, Irving et al. 1941, Ponganis et al. 2011). The decrease in peripheral blood flow associated with a diving bradycardia conserves the blood O_2 store and maximizes breath-hold capacity (Scholander 1940, Irving et al. 1941). A decrease in pulmonary flow similarly conserves the respiratory O_2 store and additionally preserves the respiratory O_2 fraction, which, in turn, optimizes oxygenation of any blood passing through the lung, thus maintaining arterial oxygen saturation longer and maximizing breath-hold capacity (Andersson et al. 2002).

Although severe bradycardia occurs in forced submersions (the classic dive response), the diving f_H response in free-ranging animals is often less intense and more variable. For example, f_H decreases from pre-dive levels during dives of king penguins *Aptenodytes patagonicus* and macaroni penguins *Eudyptes chrysolophus* at sea, but it does not decline below resting levels on land, nor does it approach levels

*Corresponding author: awright@ucsd.edu

© Inter-Research 2014 · www.int-res.com

observed in simulated dives (Kooyman et al. 1973, Ponganis et al. 1997, 1999a, Green et al. 2003, Froget et al. 2004). In terms of muscle blood flow and oxygen delivery, this f_H pattern during the penguin's dive has been considered a trade-off between the classic dive response of forced submersions and the exercise response of flighted birds and terrestrial mammals (Butler 1988, Green et al. 2003). Higher f_H in diving king and macaroni penguins than in forced submersions should also enhance pulmonary blood flow and lung-to-blood O_2 transfer, thus contributing to rapid utilization of the respiratory O_2 store.

In contrast, in emperor penguins *Aptenodytes forsteri* diving at an isolated dive hole, dive f_H often declined below levels of birds resting on ice and even reached levels recorded during simulated dives, especially in dives beyond the previously measured 5.6-min aerobic dive limit (ADL; dive duration associated with the onset of a net accumulation of lactic acid above resting levels) (Kooyman 1989, Ponganis et al. 1997, 1999a, Meir et al. 2008). These lower f_H values, especially in longer dives, imply a greater reliance on muscle O_2 stores in emperor penguins than in other penguin species. Indeed, myoglobin desaturation profiles in diving emperor penguins revealed that the large muscle O_2 store is utilized and often depleted, although at variable rates and in variable patterns (Williams et al. 2011). The low f_H values observed in emperor penguins diving at an isolated dive hole likely contributed to the slow venous O_2 depletion observed in dives as long as 22 min and to maintenance of arterial oxygen saturation during most of the dive, including dives as long as 10 min (Meir & Ponganis 2009).

Regarding O_2 store management of emperor penguins at sea, especially during their long, deep dives, the question remains as to whether a trade-off occurs, analogous to that of king and macaroni penguins, between elevated f_H values characteristic of the exercise response and depressed f_H values specific to the classic dive response. Or does a classic dive response with more extreme bradycardia predominate, as with emperor penguins at the isolated dive hole? Lower f_H values would conserve respiratory and blood O_2 at the potential expense of muscle O_2 depletion and the subsequent onset of glycolysis, while higher f_H values could lead to longer maintenance of aerobic muscle metabolism but more rapid depletion of respiratory and blood O_2 stores.

We investigated f_H responses during dives of emperor penguins making foraging trips to sea during the chick-rearing period. Specifically, we used an electrocardiogram (ECG) recorder to measure f_H and a time depth recorder (TDR) to record the dive profile in order to: (1) examine the relationship between dive f_H (total heartbeats during the dive/dive duration) and dive duration, (2) investigate how f_H fluctuated throughout the course of dives of varying depths, and (3) examine the f_H profile of dives of different depths to evaluate the potential for variation in the number of heartbeats, an index of cumulative cardiac output, during different segments of these dives.

We suspected that, because both the diving air volume and the total number of wing strokes during a dive increased with maximum dive depth in emperor penguins (Sato et al. 2011), the total number of heartbeats during early descent and throughout the course of the dive would increase in deeper dives despite an overall lower dive f_H in order to accommodate greater pulmonary gas exchange. A greater number of heartbeats, especially during the gradual decline in f_H typical of descent, could also potentially increase muscle O_2 delivery during that segment of the dive. Therefore, we hypothesized that: (1) dive f_H would negatively correlate with dive duration, (2) dive f_H of dives >ADL would be less than resting f_H, and (3) the total number of heartbeats would be greater in deeper dives throughout the total dive and during the gradual decline in f_H during descent.

MATERIALS AND METHODS

In November 2010 and 2011, emperor penguins were captured at the sea-ice edge as they departed on foraging trips from the Cape Washington breeding colony (74° 40′ S, 165° 28′ E), equipped with ECG recorders, TDRs, and VHF transmitters, and then released. Upon return from foraging trips, penguins were recaptured to recover the devices. All procedures were approved under a University of California San Diego Animal Subjects Committee Protocol (S02153) and a US Antarctic Treaty Permit (2011–016).

Instrument deployments

Under 0.5% bupivacaine local anesthetic (3–5 ml per bird), 2 subcutaneous ECG electrodes were inserted dorsally, with one right of midline at the level of the axilla and the other left of midline above the pelvis in manually restrained, hooded emperor penguins. The electrodes were connected to a custom-built digital ECG recorder (3991 BioLog, UFI) in

an underwater cylindrical housing (215 g, 16 × 3 cm), secured to the feathers of the mid-back with 5 min epoxy glue (Loctite; Henkel Corp.) and steel cable ties. ECG signals were recorded for 48 h at a sampling rate of 50 Hz. ECG recording was programmed to start 4 d after deployment of the recorder in order to collect data during the mid-portion of the foraging trip. Additionally, all birds were equipped with an Mk9 TDR (Wildlife Computers; sensitive to 0.5 m, 30 g, 6.7 × 1.7 × 1.7 cm) to record depth at a sampling rate of 1 Hz, and a VHF transmitter (Model MM130, ATS) to facilitate recapture.

Data processing and statistics

The f_H and dive data were processed, graphed, and statistically analyzed using Origin (ver. 8.6, OriginLab), Microsoft Excel, R software (R Development Core Team 2012), MATLAB (The MathWorks), and JMP (ver. 10.0.2, SAS Institute). TDR data were analyzed in MATLAB using a custom-written dive analysis program (IKNOS; Y. Tremblay unpubl.) and Instrument Helper (Wildlife Computers), which calculated a zero offset correction at the surface and identified dives on the basis of a minimum depth and duration. Dives were defined as submergences of ≥5 m and ≥1 min. Dive depth categories were designated as shallow (<50 m), intermediate (50–250 m), and deep (>250 m). ECG and TDR data were synchronized and a custom peak detection program (K. Ponganis) was utilized to mark R-wave peaks from the digital ECG records and calculate R-R intervals in Origin. All peaks were visually confirmed in order to ensure marking accuracy. The number of dives analyzed for individual birds was dictated by the clarity of the ECG signal. Portions of the ECG record that were difficult to decipher were omitted (n = 48 dives with f_H data gaps; all gap durations were <5% of dive duration).

A custom R script was used to determine dive f_H and total dive heartbeats. Dive f_H for each dive was calculated from the total number of heartbeats for each dive divided by the dive duration. In dives with a gap in the ECG record (<5% of dive duration), the gap duration was subtracted from the dive duration in the calculation of the overall dive f_H. Pre- and post-dive f_H values were calculated from the total number of heartbeats during the final and initial minute prior to and following a dive, respectively. Lowest resting f_H values were determined for individual birds over a period of 1 h. Resting periods were selected during long surface intervals at least 1 h after or before a dive bout, when the birds were presumably at rest.

Total number of heartbeats during a dive and the number of heartbeats from the start of a dive to the time that instantaneous f_H was consistently below resting f_H were determined through visual inspection of f_H profiles for each dive. Dives with f_H data gaps resulting from brief periods of indecipherable ECG signals were omitted from this analysis.

Mean f_H values at 30 s intervals were also analyzed by dividing depth profiles of dives into 7 categories of dive depth (0–25, >25–50, >50–100, >100–150, >150–250, >250–400, and >400 m). Instantaneous f_H for 30 s periods was determined using a custom R script and calculated as the mean of all instantaneous f_H values within a 30 s period. Dives with f_H data gaps resulting from brief periods of indecipherable ECG signals were excluded from this analysis.

Linear mixed-effects models (JMP) were used to examine the relationships of dive duration with dive f_H, dive depth with total dive heartbeats, and dive duration with total dive heartbeats. One model was fitted with dive f_H as a response variable, dive duration as a fixed effect, and individual as a random effect to account for repeated measures. A second model was fitted with total dive heartbeats as a response variable, dive depth as a fixed effect, and individual as a random effect. A third model was fitted with total dive heartbeats as a response variable, dive duration as a fixed effect, and individual as a random effect. An additional model was constructed to assess whether dive f_H values for dives with durations less than or greater than ADL (5.6 min) (Ponganis et al. 1997) were significantly different, with dive f_H as a response variable, dive duration category (< or >ADL) as a fixed effect, and individual as a random effect. Corrected Akaike's information criterion (AIC_c) was used to select the most parsimonious model. All means and medians are listed as means ± SE and median (range).

RESULTS

Data recovery

The ECG signal was indecipherable in 2 of 6 birds, due to obfuscation of the signal by muscle artifact and possibly movement of ECG electrodes or mechanical malfunction. Consequently, simultaneous measurements of instantaneous f_H and depth were recorded from 4 birds (24.6 ± 0.4 kg), resulting

Table 1. *Aptenodytes forsteri*. Individual and pooled heart rate (f_H) data of emperor penguins diving at Cape Washington. The number of dives for each bird was dictated by the clarity of the ECG signal. Maximum depth, dive duration and dive f_H are presented as means ± SE and medians (range)

Penguin	Body mass (kg)	No. of dives	Resting f_H (beats min^{-1})	Maximum depth (m)	Dive duration (min)	Dive f_H (beats min^{-1})
1	25.0	87	55	127.0 ± 8.2 126.0 (15.0–340.0)	5.10 ± 0.17 5.18 (1.32–8.77)	67 ± 1 68 (38–90)
2	24.0	54	71	96.0 ± 7.3 100.3 (5.0–246.0)	5.04 ± 0.20 5.23 (1.32–7.22)	68 ± 1 67 (53–91)
5	25.5	247	50	44.1 ± 4.3 19.0 (6.0–422.5)	2.88 ± 0.11 2.23 (1.00–9.22)	61 ± 1 62 (9–117)
7	24.0	4	64	299.8 ± 89.9 364.5 (39.0–431.0)	6.96 ± 1.52 7.82 (2.80–9.42)	64 ± 6 64 (52–76)
Grand mean[a]	24.6 ± 0.4		56 ± 4[b]	72.3 ± 4.1	3.71 ± 0.10	64 ± 1
Grand median (range)[a]	24.5 (24–25.5)		55 (50–64)[b]	32.5 (5.0–431.0)	3.08 (1.00–9.42)	64 (9–117)

[a]Pooled data (n = 4 birds, 392 dives); [b]Penguin 2 was excluded from resting f_H grand mean and median

in f_H and depth records for 392 dives ≥1 min in duration.

Resting heart rate profiles

Resting f_H ranged from 50 to 71 beats min^{-1} (n = 4 birds; Table 1). However, it is unknown whether the lowest resting f_H calculated for Penguin 2 was the minimum resting f_H over a 1 h period because of a dearth of resting hours with high signal clarity. Excluding Penguin 2, resting f_H ranged from 50 to 64 beats min^{-1}, with a mean of 56 ± 4 beats min^{-1} (n = 3 birds; Table 1). For this study, 56 ± 4 beats min^{-1} was selected as a conservative estimate of resting f_H for free-ranging emperor penguins.

General description of dive behavior

Dive durations from all dives ranged from 1 to 9.42 min, with a grand median of 3.08 min (Table 1). Sixty-one percent of dives were shorter than 4 min (Fig. 1A). Twenty-one percent of dives in the study were greater in duration than the previously

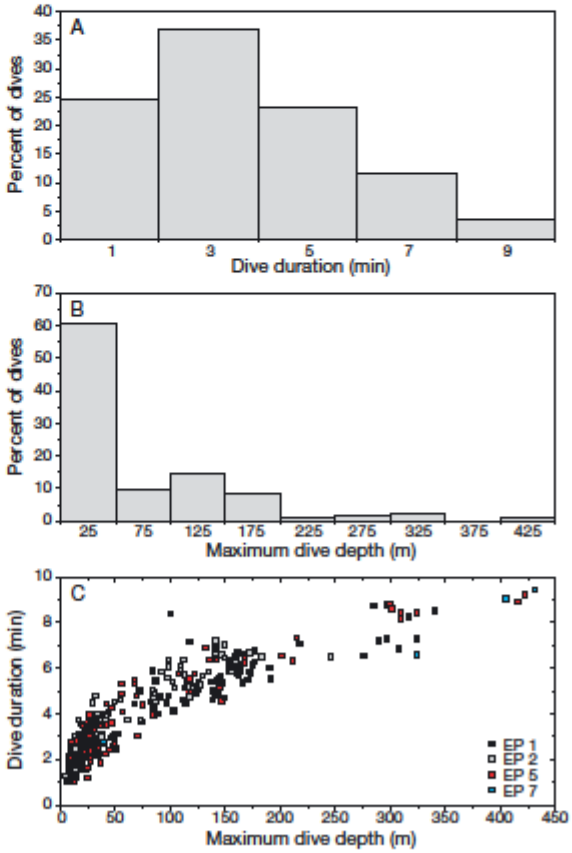

Fig. 1. *Aptenodytes forsteri*. Distributions of (A) dive duration and (B) maximum dive depth, and (C) dive duration versus maximum dive depth of dives from emperor penguins (EP) at sea. In (C), individual birds are denoted by color (n = 4 birds, 392 dives)

measured ADL of 5.6 min, and 4% of dives were greater than 8 min. Maximum depth of all dives ranged from 5 to 431 m, with a grand median of 32.5 m. The maximum dive depth for each bird ranged from 246 to 431 m (Table 1). Most dives were shallower than 100 m; however, 30% of dives were deeper than 100 m, and 5% of dives were deeper than 250 m (Fig. 1B).

Heart rate profiles during diving

All dives exhibited a characteristic pattern of f_H, with a pre- and post-dive tachycardia during surface intervals, reduced f_H upon submersion and throughout dives, and anticipatory tachycardia (increase in f_H coinciding with ascent) prior to surfacing. The pre-dive tachycardia (median = 202 beats min^{-1}, range = 109–231 beats min^{-1}) and post-dive tachycardia (median = 200 beats min^{-1}, range = 145–226 beats min^{-1}) were both >f_H at rest (56 beats min^{-1}). Instantaneous f_H profiles in 3 dives of varying depth are shown in Fig. 2. The f_H response was characterized by: (1) pre- and post-dive tachycardia, (2) an abrupt partial decline from pre-dive levels (usually with a transient decrease to below resting levels), (3) a progressive, gradual decline in f_H during early descent, sometimes to below resting levels, (4) a continuation of lower f_H values during the bottom phase of the dive, and (5) a gradual increase in f_H during ascent (Fig. 2, 3). In 27% of dives, dive f_H was below the resting level of 56 beats min^{-1} (Table 2).

Diving heart rate and dive duration

The median dive f_H was 64 beats min^{-1} (range = 9–117 beats min^{-1}) for all dives (Table 1). The median dive f_H for dives shorter than the ADL (79% of the dives in this study; 66 beats min^{-1}, range = 9–117 beats min^{-1}) was significantly greater than the median dive f_H of 58 beats min^{-1} (range = 38–76 beats min^{-1}) for dives longer than the ADL (21% of the dives in this study; Tables 2, 3). Eighteen percent of dives below the ADL had dive f_H values less than the resting level of 56 beats min^{-1}, while 45% of dives above the ADL had dive f_H values less than 56 beats min^{-1} (Table 2). For the previously reported f_H at rest of 73 beats min^{-1} (Meir et al. 2008) in emperor penguins at the isolated dive hole, dive f_H was less than resting f_H in 76% of dives shorter than the ADL and in 98% of dives longer than the ADL.

In dives ≥1 min in duration, there was a significant negative relationship between dive duration and dive f_H (Fig. 4, Table 3). However, dive f_H of dives

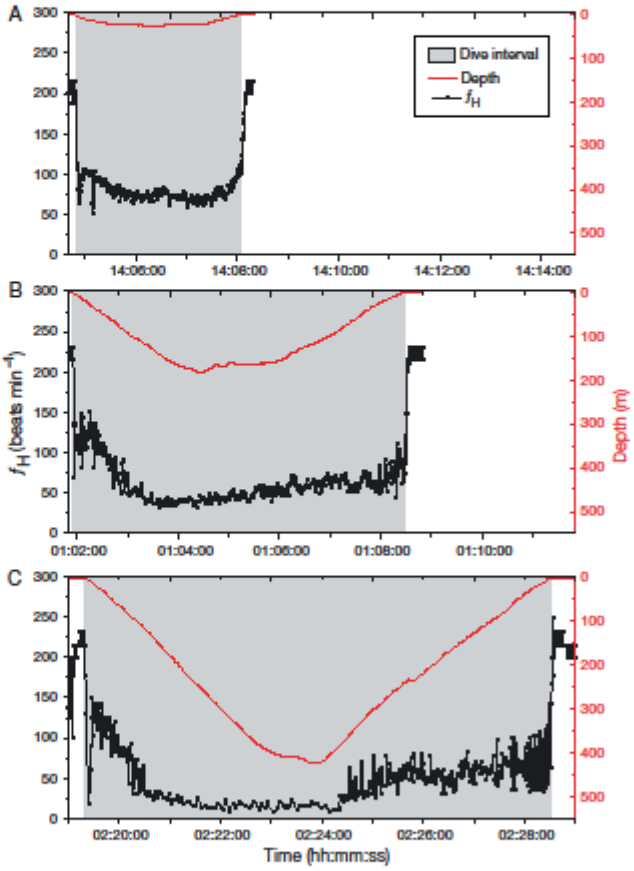

Fig. 2. *Aptenodytes forsteri*. Instantaneous heart rate (f_H) and dive depth profiles from (A) a shallow (27 m, <aerobic dive limit [ADL]) dive of Emperor Penguin 1, (B) an intermediate (183 m, >ADL) dive of Emperor Penguin 2, and (C) the deepest (423 m, >ADL) dive of Emperor Penguin 5. In (A), f_H reaches a minimum of 52 beats min^{-1}. In (B), f_H reaches a minimum of 33 beats min^{-1}. In (C), mean f_H is 17 beats min^{-1} for over 3 min, reaching a minimum of 8 beats min^{-1}

Mar Ecol Prog Ser 496: 85–98, 2014

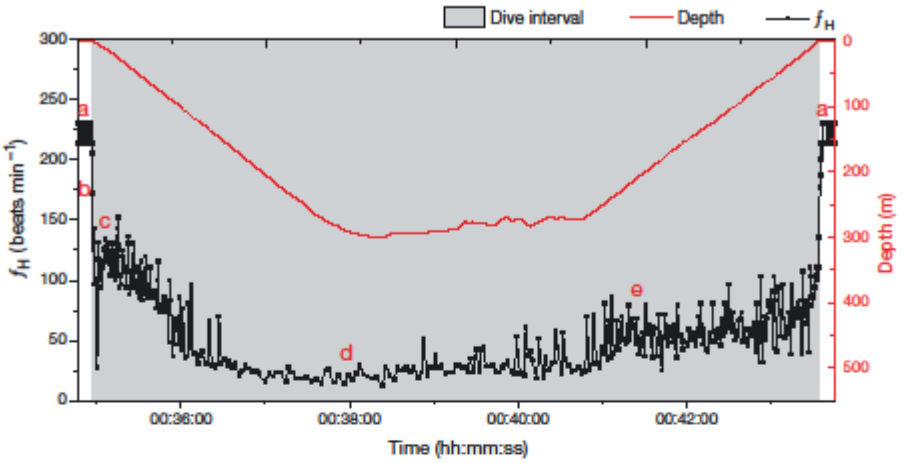

Fig. 3. *Aptenodytes forsteri*. Instantaneous heart rate (f_H) and dive depth profiles from a deep (301 m) dive of Emperor Penguin 5 with prominent features typical of the dive f_H profile: a, surface interval tachycardia (pre- and post-dive); b, initial sharp partial decline in f_H, immediately upon submersion, often with transient decrease to below resting levels; c, gradual decline in elevated f_H during early descent; d, prolonged severe bradycardia during latter descent and near maximum dive depth; e, slow increase in f_H during ascent

less than 2 min in duration or less than 50 m in depth varied considerably (Fig. 4).

In the analysis of dive f_H, 12% of dives had a data gap in the f_H profile. Eighty-one percent of gaps were ≤5 s and 75% of all gaps occurred at the start of the dive when wing movement, and thus the potential for muscle artifact, was greatest. Gaps of short duration should not significantly affect the results or interpretation of the data. For example, a dive with a 6 s gap and dive f_H of 100 beats min^{-1} would only have an increase in dive f_H by 2 beats min^{-1} for a 5 min dive.

Heart rate within dives

For all dives at sea with a complete ECG record (without a f_H data gap; 344 dives), total number of dive heartbeats was in the same range as total heartbeats for dives of equivalent duration performed at the isolated dive hole (Meir et al. 2008) (Fig. 5). For dives near 5–7 min in duration, total dive heartbeats ranged between 250 and 400 heartbeats (Fig. 5).

In dives ≥1 min in duration, there was a significant relationship between dive depth and total number of dive heartbeats (Fig. 6A, Table 3). Total dive heartbeats was variable but increased until 150 m maximum depth, after which total dive heartbeats began to level off and remained high (Fig. 6A). A significant relationship was also observed between dive duration and total number of dive heartbeats (Fig. 6B, Table 3).

Instantaneous f_H reached values consistently below resting f_H in 31% of dives (dives without gaps in the f_H profile). The number of heartbeats prior to

Table 2. *Aptenodytes forsteri*. Heart rate (f_H) data for dives shorter and longer than the aerobic dive limit (ADL; 5.6 min). Maximum depth, dive duration and dive f_H are presented as means ± SE and medians (range)

	No. dives	Maximum depth (m)	Dive duration (min)	Dive f_H (beats min^{-1})	% dives with dive f_H below resting f_H
All dives	392	72.3 ± 4.1 32.5 (5.0–431.0)	3.71 ± 0.10 3.08 (1.00–9.42)	64 ± 1 64 (9–117)	27
Dives < ADL	310	40.4 ± 2.3 23.5 (5.0–191.5)	2.91 ± 0.07 2.58 (1.00–5.57)	65 ± 1 66 (9–117)	18
Dives > ADL	82	192.9 ± 9.3 160.5 (83.5–431.0)	6.74 ± 0.11 6.43 (5.63–9.42)	57 ± 1 58 (38–76)	45

Table 3. Data from mixed-effect models examining the relationships between dive duration and dive heart rate (f_{Hi}), aerobic dive limit (ADL) and dive f_{Hi}, dive depth and total dive heartbeats, and dive duration and total dive heartbeats. The corrected Akaike's information criteria (AIC_c) for all models are reported. The fixed effects and intraclass correlation coefficient (ICC) are presented for the superior model(s) (indicated in **bold**). Dive duration, dive duration category (<ADL, >ADL), and dive depth were fixed effects in corresponding models, and individual penguin was the random effect (with random intercept or random intercept and slope) in all models

Model	Model variables		AIC_c	Fixed effect						Random effect
	Fixed effect	Random effect		Coefficient	Error	df	t	p	*F*-ratio	p	ICC (%)
Duration vs. dive f_H	Duration		3066.6								
	Duration	**Penguin ID (intercept)**	**2959.3**	−4.12307	0.31506	390	−13.09	<0.0001	171.2628	<0.0001	39.5
	Duration	**Penguin ID (intercept + slope)**	**2958.3**	−4.05915	0.73629	2	−5.5	0.0251	30.2284	0.0251	39.2
		Penguin ID (intercept)	3097.0								
ADL vs. dive f_H	ADL		3061.2								
	ADL	**Penguin ID (intercept)**	**3034.3**	−6.37484	0.76622	390	−8.32	<0.0001	69.2198	<0.0001	17.5
	ADL	**Penguin ID (intercept + slope)**	**3035.0**	−6.11369	1.33275	2	−4.59	0.0390	21.0431	0.0390	16.4
		Penguin ID (intercept)	3097.0								
Depth vs. total dive heartbeats	Depth		3834.2								
	Depth	Penguin ID (intercept)	3575.2								
	Depth	**Penguin ID (intercept + slope)**	**3557.4**	0.95637	0.15875	3	6.02	0.0108	36.2917	0.0108	62.4
		Penguin ID (intercept)	3949.4								
Duration vs. total dive heartbeats	Duration		3539.4								
	Duration	Penguin ID (intercept)	3332.6								
	Duration	**Penguin ID (intercept + slope)**	**3310.0**	44.79090	4.53256	3	9.88	0.0019	97.6545	0.0019	59.8
		Penguin ID (intercept)	3949.4								

reaching resting f_H (56 beats min^{-1}) was variable (2–164 heartbeats), but as depth of dive increased, variability decreased, and values leveled off and remained between 100 and 120 heartbeats in most dives (Fig. 7A). A similar relationship was observed between the dive depth and the number of heartbeats prior to reaching the previously reported resting f_H (Meir et al. 2008) (Fig. 7B).

The profiles of mean instantaneous f_H at 30 s intervals of dives in 7 dive depth categories (Fig. 8) reflected instantaneous f_H profiles. Deeper dives had higher initial 30 s values, but then had lower f_H values throughout the middle portions of dives.

DISCUSSION

Resting heart rate

The resting f_H for free-ranging emperor penguins (56 ± 4 beats min^{-1}) was significantly less than the resting f_H determined for emperor penguins at the isolated dive hole (Meir et al. 2008). Differences in surrounding conditions can affect baseline f_H and may account for the large disparity of resting f_H values observed in free-ranging and captive emperor penguins (Halsey et al. 2008). Resting f_H for emperor penguins at the isolated dive hole may have been elevated due to stress associated with captivity, interactions with other birds, differences in dive and prey types, and longer diving recovery periods. In addition, the lower resting f_H values of emperor penguins at sea were the minimum 1 h resting f_H values found during prolonged surface intervals. These lower f_H values may occur during sleep and reflect a lower metabolic rate induced by sleep (Stahel et al. 1984, Dewasmes et al. 1989, Halsey et al. 2008). Thus, in our analyses of dive f_H, we consider the resting f_H of 73 and 56 beats min^{-1} to represent the upper and lower limits of resting f_H, respectively (Fig. 7), and, consequently, the upper and lower thresholds for f_H associated with a resting level of muscle blood flow.

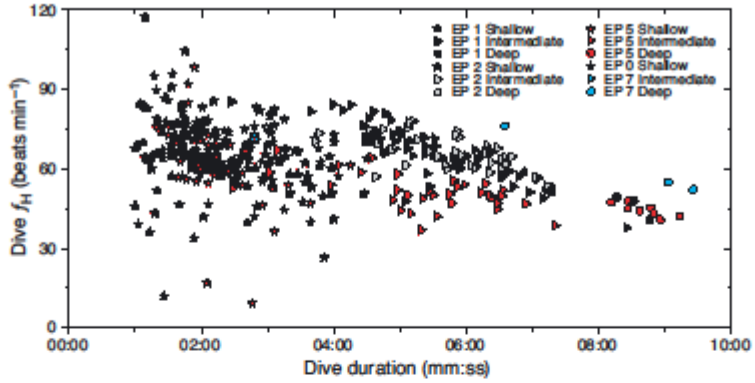

Fig. 4. *Aptenodytes forsteri*. Dive heart rate (f_H) (total number of heartbeats/dive duration) versus dive duration for emperor penguins (EP) at sea. Individual birds are denoted by color; dive depth categories (shallow: <50 m; intermediate: 50–250 m; deep: >250 m) are denoted by symbols (see key; n = 4 birds, 392 dives)

Dive behavior

Dive durations and maximum depths of dives of emperor penguins in this study (Fig. 1A,B) were typical of those reported in previous studies of free-ranging emperor penguins on foraging trips to sea during the chick-rearing period (Kooyman & Kooyman 1995, Kirkwood & Robertson 1997, Wienecke et al. 2007, Sato et al. 2011, Williams et al. 2012) and of dive durations of emperor penguins at the isolated dive hole (Ponganis et al. 2001, 2007, Meir et al. 2008, Sato et al. 2011, Williams et al. 2011). The tightly coupled positive relationship between dive duration and maximum dive depth (Fig. 1C) during foraging trips to sea was similar to results from prior studies of free-ranging emperor penguins (Kooyman & Kooyman 1995, Sato et al. 2011). Despite the exclusion of dives less than 1 min in duration, the grand median dive duration was 3.08 min (range = 1.00–9.42 min; Table 1), below the ADL of 5.6 min.

Heart rate profiles during dives

Examination of individual f_H profile patterns revealed notable differences between shallow (<50 m) and deep (>250 m) dives. In shallow, short-duration dives, the overall f_H pattern was similar to that

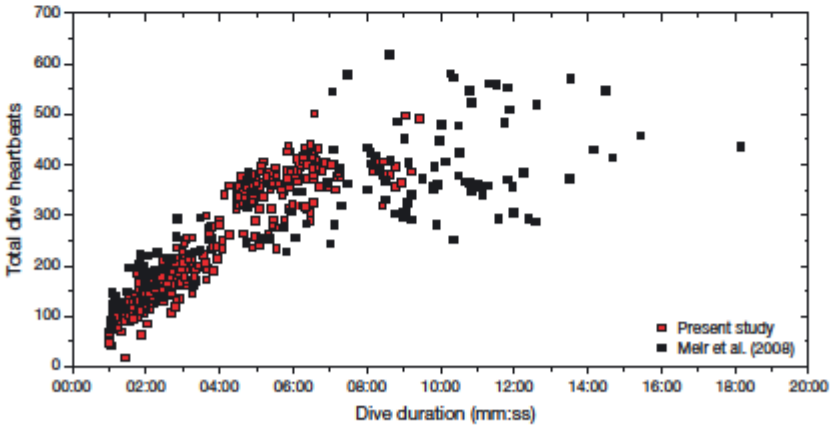

Fig. 5. *Aptenodytes forsteri*. Total dive heartbeats versus dive duration for the present study of emperor penguins diving at sea (n = 4 birds, 344 dives) and the Meir et al. (2008) study of emperor penguins diving at an isolated dive hole (n = 9 birds, 125 dives)

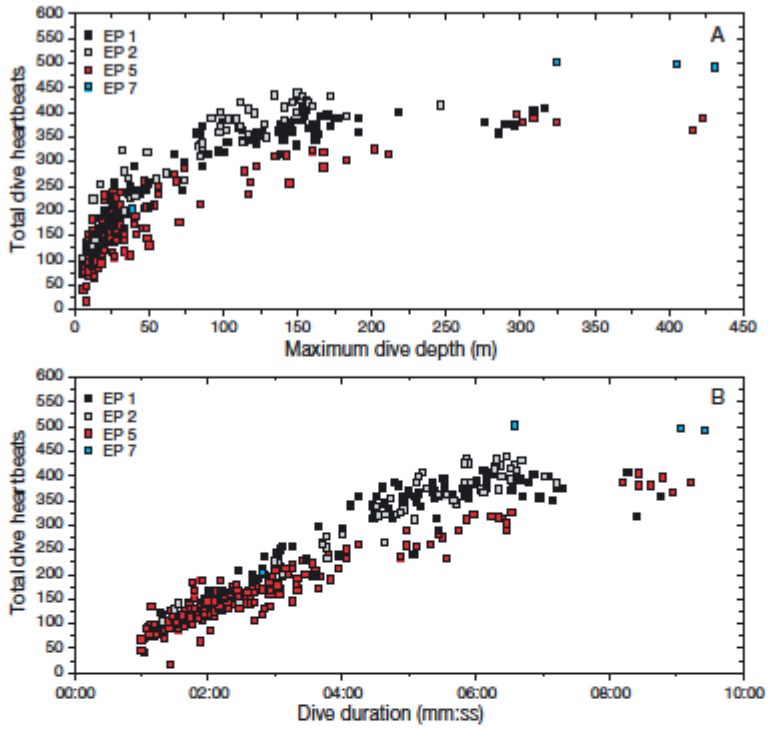

Fig. 6. *Aptenodytes forsteri*. Total dive heartbeats versus (A) maximum dive depth and (B) dive duration for emperor penguins (EP) at sea. Individual birds are denoted by color (see key; n = 4 birds, 344 dives)

observed in other free-ranging penguin species (Green et al. 2003, Froget et al. 2004) and in emperor penguins making short dives at an isolated dive hole (Meir et al. 2008). The f_H profile pattern of these dives was characterized by an initial rapid decrease in f_H from pre-dive values, followed by a gradual decline in f_H throughout the dive to a level sometimes below that at rest, and lastly, an increase in f_H during ascent (Fig. 2A). Although shallow, short-duration dives of emperor penguins had f_H profile patterns similar in shape to those of free-ranging birds of other penguin species, the f_H values during these shallow dives were much lower in emperor penguins than in the other species. Instantaneous f_H and overall dive f_H of these shallow dives were lower on both an absolute and a relative-to-resting basis than in the other 2 penguin species. Therefore, if there is a trade-off between the elevated f_H of the exercise response and the depressed f_H of the classic dive response in emperor penguins, the response of the emperor penguin is much closer to the classic dive response than those of other penguins.

In contrast to shallow dive profiles of emperor penguins (both at sea and at an isolated dive hole) and all dive profiles of free-ranging king and macaroni penguins, the f_H profile pattern of emperor penguins in deep, long-duration dives differed in that the gradual decline in f_H during early descent culminated in a severe bradycardia to as low as 10 beats min^{-1} during late descent and during the bottom phase of the dive (Figs. 2C, 3, 8). Dives to intermediate depths had less-intense bradycardias than the deep dives, but rates were lower than during shallow dives (Figs. 2B, 8).

The extremely low f_H during late descent or near the greatest depth of deep dives may serve to limit pulmonary gas exchange as well as peripheral perfusion during this segment of the dive. In addition to conserving respiratory O_2 for potential use later in the dive, the extreme bradycardia should also limit nitrogen absorption at maximal depths of deep dives,

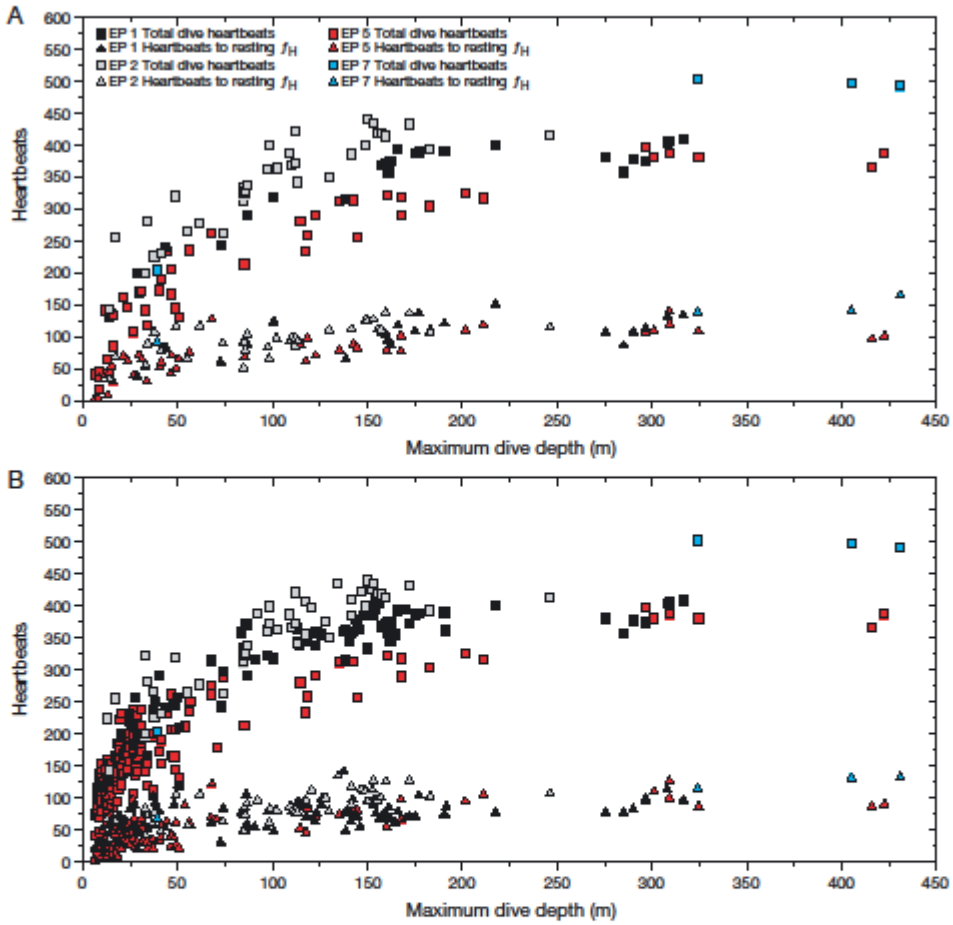

Fig. 7. *Aptenodytes forsteri*. Total dive heartbeats (squares) and heartbeats to reach resting heart rate (f_H; triangles); (A) 56 beats min^{-1} (present study) and (B) 73 beats min^{-1} (Meir et al. 2008) versus maximum dive depth for emperor penguins (EP) at sea. Individual birds are denoted by color (see key; n = 4 birds, 105 dives in A, 301 dives in B)

a potential advantage in avoidance of decompression sickness. The decrease in cardiac output associated with a bradycardia of 10–20 beats min^{-1} would also limit perfusion of central organs and muscle, decreasing the rate at which blood O_2 is consumed and isolating muscle from the circulation. During this bottom phase of deep dives, stroke rates are highest (Williams et al. 2012), so the locomotory muscle, isolated from the circulation, is most probably dependent on myoglobin-bound O_2 for maintenance of aerobic metabolism.

Heart rate and the potential for muscle blood flow during dives

In 27% of all dives, the dive f_H was less than the lower limit of f_H at rest (56 beats min^{-1}). In 45% of dives greater than the ADL and 18% of dives shorter than the ADL, dive f_H demonstrated a true bradycardia across a range of dive depths at sea (Table 2). Additionally, the degree of bradycardia during dives increased with dive duration (Fig. 4). Such low f_H values (even relative to surface f_H or resting f_H) have not

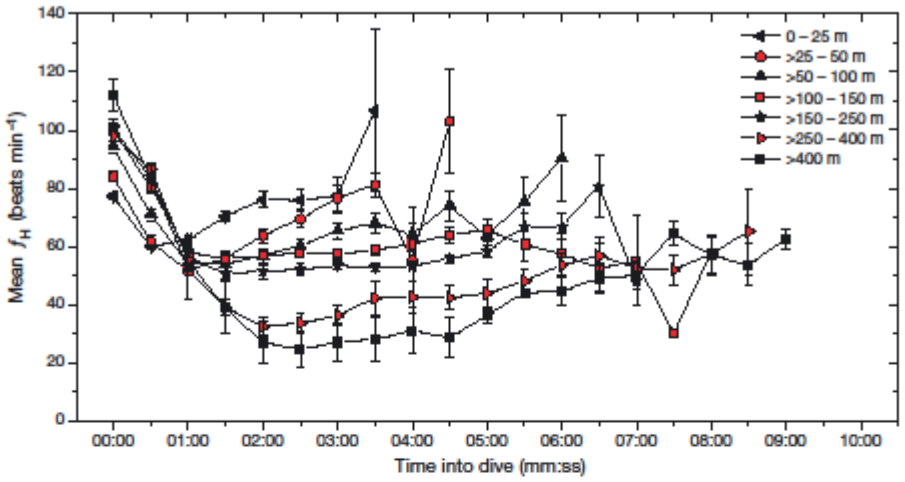

Fig. 8. *Aptenodytes forsteri*. Profiles of mean heart rate (f_H) at 30 s intervals of dives for 7 depth categories (0–25, >25–50, >50–100, >100–150, >150–250, >250–400, and >400 m). Standard error bars shown (n = 4 birds, 344 dives)

been reported in free-ranging macaroni and king penguins (Green et al. 2003, Froget et al. 2004). Lower dive f_H of emperor penguins at sea suggests relatively lower organ blood flow and lower muscle blood flow than in other penguin species, with slow depletion of blood O_2 and greater dependence of aerobic muscle metabolism on the higher O_2 content of muscle in emperor penguins (Ponganis et al. 2010, 2011). The myoglobin concentration of emperor penguin locomotory muscle is about 1.5 to 2 times greater than in other penguin species (Weber et al. 1974, Baldwin et al. 1984, Ponganis et al. 1999b). Thus, while the distribution of O_2 stores is similar in emperor and king penguins, emperor penguins have higher muscle myoglobin concentrations and greater muscle O_2 stores (Ponganis et al. 2010, 2011). Consequently, in regard to muscle metabolism, emperor penguins would be more tolerant of muscle ischemia and depressed f_H than other penguin species. In addition, due to their large size, the locomotory effort of the emperor penguin is potentially less than that of other penguin species, leading to a lower muscle metabolic rate and myoglobin desaturation rate (Sato et al. 2010). Thus, both larger muscle O_2 stores and less locomotory effort in emperor penguins probably make them more tolerant than other penguin species of lower f_H and less muscle perfusion during both shallow and deep dives.

It is also notable, in regard to potential restriction of muscle blood flow during dives at sea, that the total number of heartbeats in dives of equivalent duration were similar in emperor penguins at sea and at the isolated dive hole (Fig. 5). Given that the number of wing strokes for dives of equivalent duration was greater at sea than at the isolated dive hole (Sato et al. 2011), the similarity between total heartbeats for dives of equivalent duration at sea and at the isolated dive hole suggests that the relationship of muscle work effort and f_H (i.e. muscle blood flow and O_2 delivery) is even more restricted at sea than at the isolated dive hole, resulting in greater dependence on myoglobin-bound O_2. Alternatively, one might propose that selective dilatation of the locomotory muscle vascular bed as demonstrated in diving ducks may also occur in penguins (Bevan & Butler 1992). Such dilatation during dives at sea could then account for a greater distribution of cardiac output to muscle and, thus, allow more muscle blood flow per heartbeat. However, this has not been investigated in diving penguins. In addition, f_H of the diving duck is much higher, even on a relative basis (Bevan & Butler 1992), than that of diving emperor penguins.

Comparison of the relationships of total number of heartbeats and total number of wing strokes with dive duration offers additional support for a reduction in muscle blood flow in prolonged dives of free-ranging emperor penguins. The total number of heartbeats in a dive leveled off at approximately 6 min duration (Fig. 6B); in addition, for dives between 6 and 10 min of individual birds, the total number of heartbeats is within the same range. In contrast, the total number of

strokes during dives of emperor penguins at sea increased linearly with dive duration, with 10 min dives having nearly twice the number of strokes as 6 min dives (Sato et al. 2011). Despite a 2-fold increase in the total number of strokes between 6 min and 10 min dives, there is no increase in the total number of heartbeats, which again would suggest a greater reliance on muscle myoglobin and less muscle blood flow relative to stroke rate for longer dives.

Although myoglobin desaturation profiles of diving emperor penguins have demonstrated that muscle blood flow may occur during dives (Williams et al. 2011), the findings of the present study do not offer any evidence that there is a coupling of stroke rate (muscle workload) and f_H, as in a classic exercise f_H response or even as in the exercise-modified dive response suggested in other penguin species and, more recently, in dolphins and seals (Butler 1988, Green et al. 2003, Davis & Williams 2012). The lack of coupling of f_H and stroke rate is reflected, especially in deeper dives, by the fact that the lowest f_H values in the deepest dives of emperor penguins (Fig. 8) occurs at a time when previously measured stroke rates are near maximal levels (Williams et al. 2012). Similarly, although muscle blood flow may be enhanced by increasing f_H during ascent (Figs. 2, 3, 8), stroke rate is declining during this period (Williams et al. 2012). The same conclusion of a lack of coupling of stroke rate and f_H was also reached from f_H and stroke rate analyses during dives of emperor penguins at an isolated dive hole (Meir et al. 2008).

In contrast, because f_H and stroke rate during dives at sea are always highest during initial descent (Figs. 2 & 8) (Williams et al. 2012), it could be argued that muscle blood flow matches work effort at least during this period of the dive. However, during this time, at least in dives at the isolated dive hole, venous partial pressure of O_2 (P_{O2}) and hemoglobin saturation are usually increasing, sometimes to arterial levels (Meir & Ponganis 2009). With increasing venous saturations it is unlikely that there is muscle blood flow and muscle O_2 extraction; if there were such flow to exercising muscle, venous saturation should decrease. Indeed, it has been suggested that arterialized venous blood O_2 levels early in the dive are consistent with flow-through peripheral arterio-venous shunts (Ponganis et al. 2009). Thus, the regulation of muscle blood flow during dives of emperor penguins at sea still requires further investigation.

It should be noted that in shorter, shallower dives, emperor penguins exhibit a range of f_H responses in relation to resting f_H limits, and therefore the muscle blood flow response may be variable during these dives. For a large proportion of short, shallow dives, the f_H response of emperor penguins resembles that of other penguin species with a high potential for muscle blood flow and reduced dependence on myoglobin. However, when dive f_H exceeds resting f_H in shallow dives, it is still unknown whether diving emperor penguins perfuse muscle or possibly utilize peripheral arterio-venous shunts to enhance blood O_2 levels (Ponganis et al. 2009, Williams et al. 2011).

Heart rate and the potential for pulmonary blood flow during dives

The higher f_H values during short-duration, shallow dives imply more pulmonary blood flow, greater potential for gas exchange and more rapid utilization of the respiratory O_2 store than during deep dives. Although overall f_H is slower in longer dives (Fig. 4), the total number of heartbeats is maximal during these deeper dives secondary to (1) the duration of the dive, (2) the greater number of beats during early descent, and (3) the gradual increase in f_H during long ascents (Figs. 2, 3, 8). Thus, despite an overall low dive f_H and extreme bradycardia during the late descent and bottom phases of the deepest dives, the cumulative potential for pulmonary blood flow and gas exchange is maximized during these dives, consistent with the increased diving air volumes determined in deeper dives of emperor penguins (Sato et al. 2011). Overall utilization of the respiratory O_2 store should be slower under such circumstances, although gas exchange is probably greatest early in the dive, when f_H values are high (Figs. 2, 3, 6–8) and when air movement through the parabronchi of the lung is increased by high wing stroke rates (Boggs et al. 2001). Higher f_H values and a maximal number of strokes during this phase of deep dives (Figs. 6–8) support this suggestion. As already discussed, the severe bradycardias during the late descent and bottom phases of deep dives would limit gas exchange at great depths, a potential advantage for limiting nitrogen absorption as well as conserving respiratory O_2 for utilization during the increased f_H periods during ascent, as recently proposed for deep-diving sea lions (McDonald & Ponganis 2012).

Heart rate variability: a multi-factored response

Although the greater part of this discussion has been devoted to variations in f_H and implications for pulmonary gas exchange and muscle blood flow, individual dive f_H variability is also likely influenced

by an assortment of endogenous and exogenous factors. In short, shallow dives, physiological variability has been documented not only in f_H responses but also in levels and rates of blood O_2 depletion and in diving air volumes (Meir & Ponganis 2009, Sato et al. 2011). f_H and other physiological responses are clearly dependent on the nature and circumstances of individual dives (Furilla & Jones 1987, Jones et al. 1988, Noren et al. 2012). For example, extremely low dive f_H (range = 9–17 beats min^{-1}) in a few short-duration dives in this study corresponded to dives with very short surface intervals (descent following a limited post-dive surface interval of ≤5 s). After such short surface intervals, low dive f_H in the subsequent dive may function to conserve partially loaded O_2 reserves resulting from the abbreviated surface interval and may also reflect uncertainty about the timing of the next surface period. Future f_H studies of free-ranging emperor penguins should aid in the interpretation of dive responses in relation to specific behaviors and circumstances of individual dives (i.e. hunting, prey capture, travelling, and escape).

In summary, we have investigated the diving f_H response of emperor penguins during foraging trips at sea. We confirmed that: (1) dive f_H varies inversely with dive duration; (2) a significant proportion of dives have dive f_H values that are less than the value at rest, and dive f_H of dives greater than the ADL is lower than dive f_H of dives less than the ADL; (3) the total number of heartbeats in dives of equivalent duration at sea was similar to that of birds diving at an isolated dive hole, but dive profiles, especially in deeper dives, had different f_H patterns; (4) a profound bradycardia occurs during deep dives; and (5) the total number of heartbeats, and thus the cumulative cardiac output, is maximized in deep dives due to (a) the duration of the dive, (b) higher instantaneous f_H and a maximized number of heartbeats during early descent, and (c) the increase in f_H during the long ascent.

f_H values below resting rates during long-duration, deep dives at sea are consistent with conservation of blood and respiratory O_2 stores and with significant reliance on myoglobin-bound O_2 for aerobic muscle metabolism. Our findings suggest that adjustments to diving f_H preserve blood and pulmonary O_2 stores during deep dives by: (1) maintaining higher f_H to promote gas exchange during early descent and, perhaps, ascent periods, (2) lowering f_H to decrease gas exchange during deep portions of dives, and (3) limiting muscle blood flow. In contrast, f_H values during short-duration, shallow dives are usually higher, implying a greater potential for muscle perfusion, and perhaps also arterio-venous shunting.

Acknowledgements. We thank G. L. Kooyman, G. Marshall, J. Goldbogen, M. Tift, and M. Fowler for assistance in the field, and J. U. Meir for use of f_H data from the isolated dive hole study. We greatly appreciate the support of the United States Antarctic Program and McMurdo Station staff, and in particular, the efforts of the Berg Field Center, Fixed Wing Operations, and the pilots/crew of Ken Borek Air. This work was supported by National Science Foundation grant 09-44220. A.K.W. was supported by the NSF Graduate Research Fellowship Program.

LITERATURE CITED

Andersson JP, Linér MH, Rünow E, Schagatay E (2002) Diving response and arterial oxygen saturation during apnea and exercise in breath-hold divers. J Appl Physiol 93:882–886

Baldwin J, Jardel JP, Montague T, Tomkin R (1984) Energy metabolism in penguin swimming muscles. Mol Physiol 6:33–41

Bevan R, Butler P (1992) Cardiac output and blood flow distribution during swimming and voluntary diving of the tufted duck (*Aythya fuligula*). J Exp Biol 168:199–217

Boggs DF, Baudinette RV, Frappell PB, Butler P (2001) The influence of locomotion on air-sac pressures in little penguins. J Exp Biol 204:3581–3586

Butler P (1988) The exercise response and the 'classical' diving response during natural submersion in birds and mammals. Can J Zool 66:29–39

Davis RW, Williams TM (2012) The marine mammal dive response is exercise modulated to maximize aerobic dive duration. J Comp Physiol A 198:583–591

Dewasmes G, Buchet C, Geloen A, Le Maho Y (1989) Sleep changes in emperor penguins during fasting. Am J Physiol 256:R476–R480

Froget G, Butler P, Woakes A, Fahlman A, Kuntz G, Le Maho Y, Handrich Y (2004) Heart rate and energetics of free-ranging king penguins (*Aptenodytes patagonicus*). J Exp Biol 207:3917–3926

Furilla R, Jones D (1987) The relationship between dive and pre-dive heart rates in restrained and free dives by diving ducks. J Exp Biol 127:333–348

Green JA, Butler PJ, Woakes AJ, Boyd IL (2003) Energetics of diving in macaroni penguins. J Exp Biol 206:43–57

Halsey LJ, Butler PJ, Fahlman A, Woakes AJ, Handrich Y (2008) Behavioral and physiological significance of minimum resting metabolic rate in king penguins. Physiol Biochem Zool 81:74–86

Irving L, Scholander P, Grinnell S (1941) Significance of the heart rate to the diving ability of seals. J Cell Comp Physiol 18:283–297

Jones D, Furilla R, Heieis M, Gabbott G, Smith F (1988) Forced and voluntary diving in ducks: cardiovascular adjustments and their control. Can J Zool 66:75–83

Kirkwood R, Robertson G (1997) Seasonal change in the foraging ecology of emperor penguins on the Mawson Coast, Antarctica. Mar Ecol Prog Ser 156:205–223

Kooyman GL (1989) Diverse divers: physiology and behavior. Springer-Verlag, Berlin

Kooyman GL, Kooyman TG (1995) Diving behavior of emperor penguins nurturing chicks at Coulman Island, Antarctica. Condor 97:536–549

Kooyman GL, Schroeder JP, Greene DG, Smith VA (1973) Gas exchange in penguins during simulated dives to 30 and 68 m. Am J Physiol 225:1467–1471

McDonald BI, Ponganis PJ (2012) Lung collapse in the diving sea lion: hold the nitrogen and save the oxygen. Biol Lett 8:1047–1049
Meir JU, Ponganis PJ (2009) High-affinity hemoglobin and blood oxygen saturation in diving emperor penguins. J Exp Biol 212:3330–3338
Meir JU, Stockard TK, Williams CL, Ponganis KV, Ponganis PJ (2008) Heart rate regulation and extreme bradycardia in diving emperor penguins. J Exp Biol 211:1169–1179
Noren SR, Kendall T, Cuccurullo V, Williams TM (2012) The dive response redefined: underwater behavior influences cardiac variability in freely diving dolphins. J Exp Biol 215:2735–2741
Ponganis PJ, Kooyman GL, Starke LN, Kooyman CA, Kooyman TG (1997) Post-dive blood lactate concentrations in emperor penguins, *Aptenodytes forsteri*. J Exp Biol 200: 1623–1626
Ponganis PJ, Kooyman GL, Van Dam R, LeMaho Y (1999a) Physiological responses of king penguins during simulated diving to 136 m depth. J Exp Biol 202:2819–2822
Ponganis PJ, Starke LN, Horning M, Kooyman GL (1999b) Development of diving capacity in emperor penguins. J Exp Biol 202:781–786
Ponganis PJ, Van Dam RP, Knower T, Levenson DH (2001) Temperature regulation in emperor penguins foraging under sea ice. Comp Biochem Physiol A 129:811–820
Ponganis PJ, Stockard TK, Meir JU, Williams CL, Ponganis KV, Van Dam RP, Howard R (2007) Returning on empty: extreme blood O_2 depletion underlies dive capacity of emperor penguins. J Exp Biol 210:4279–4285
Ponganis PJ, Stockard TK, Meir JU, Williams CL, Ponganis KV, Howard R (2009) O_2 store management in diving emperor penguins. J Exp Biol 212:217–224
Ponganis PJ, Meir JU, Williams CL (2010) Oxygen store depletion and the aerobic dive limit in emperor penguins. Aquat Biol 8:237–245
Ponganis PJ, Meir JU, Williams CL (2011) In pursuit of Irving and Scholander: a review of oxygen store management in seals and penguins. J Exp Biol 214: 3325–3339
R Development Core Team (2012) R: A language and environment for statistical computing. R Foundation for Statistical Computing, Vienna
Sato K, Shiomi K, Watanabe Y, Watanuki Y, Takahashi A, Ponganis PJ (2010) Scaling of swim speed and stroke frequency in geometrically similar penguins: They swim optimally to minimize cost of transport. Proc R Soc B 277: 707–714
Sato K, Shiomi K, Marshall G, Kooyman GL, Ponganis PJ (2011) Stroke rates and diving air volumes of emperor penguins: implications for dive performance. J Exp Biol 214:2854–2863
Scholander PF (1940) Experimental investigations on the respiratory function in diving mammals and birds. Hvalrad Skr 22:1–131
Stahel C, Megirian D, Nicol S (1984) Sleep and metabolic rate in the little penguin, *Eudyptula minor*. J Comp Physiol B 154:487–494
Weber RE, Hemmingsen EA, Johansen K (1974) Functional and biochemical studies of penguin myoglobin. Comp Biochem Physiol B 49:197–214
Wienecke B, Robertson G, Kirkwood R, Lawton K (2007) Extreme dives by free-ranging emperor penguins. Polar Biol 30:133–142
Williams CL, Meir JU, Ponganis PJ (2011) What triggers the aerobic dive limit? Patterns of muscle oxygen depletion during dives of emperor penguins. J Exp Biol 214: 1802–1812
Williams CL, Sato K, Shiomi K, Ponganis PJ (2012) Muscle energy stores and stroke rates of emperor penguins: implications for muscle metabolism and dive performance. Physiol Biochem Zool 85:120–133

Submitted: February 15, 2013; Accepted: October 9, 2013

Proofs received from author(s): January 21, 2014

Acknowledgements

Chapter 1, in its entirety, is a reprint of the peer-reviewed publication as it appears in Marine Ecology Progress Series 2014. Citation: Wright, Alexandra K.; Ponganis, Katherine V.; McDonald, Birgitte I.; Ponganis, Paul J. 2014. Heart rates of emperor penguins diving at sea: implications for oxygen store management. *Marine Ecology Progress Series* 496: 85 – 98. http://dx.doi.org/10.3354/meps10592. The dissertation author was the primary investigator and author of this publication.

Chapter 2. Neuroanatomy of the killer whale (*Orcinus orca*): a magnetic resonance imaging investigation of structure with insights on function and evolution

Brain Struct Funct
DOI 10.1007/s00429-016-1225-x

ORIGINAL ARTICLE

Neuroanatomy of the killer whale (*Orcinus orca*): a magnetic resonance imaging investigation of structure with insights on function and evolution

Alexandra Wright[1] · Miriam Scadeng[2] · Dominik Stec[2] · Rebecca Dubowitz[2] · Sam Ridgway[3] · Judy St. Leger[4]

Received: 1 August 2015 / Accepted: 7 April 2016
© Springer-Verlag Berlin Heidelberg 2016

Abstract The evolutionary process of adaptation to an obligatory aquatic existence dramatically modified cetacean brain structure and function. The brain of the killer whale (*Orcinus orca*) may be the largest of all taxa supporting a panoply of cognitive, sensory, and sensorimotor abilities. Despite this, examination of the *O. orca* brain has been limited in scope resulting in significant deficits in knowledge concerning its structure and function. The present study aims to describe the neural organization and potential function of the *O. orca* brain while linking these traits to potential evolutionary drivers. Magnetic resonance imaging was used for volumetric analysis and three-dimensional reconstruction of an in situ postmortem *O. orca* brain. Measurements were determined for cortical gray and cerebral white matter, subcortical nuclei, cerebellar gray and white matter, corpus callosum, hippocampi, superior and inferior colliculi, and neuroendocrine structures. With cerebral volume comprising 81.51 % of the total brain volume, this *O. orca* brain is one of the most corticalized mammalian brains studied to date. *O. orca* and other delphinoid cetaceans exhibit isometric scaling of cerebral white matter with increasing brain size, a trait that violates an otherwise evolutionarily conserved cerebral scaling law. Using comparative neurobiology, it is argued that the divergent cerebral morphology of delphinoid cetaceans compared to other mammalian taxa may have evolved in response to the sensorimotor demands of the aquatic environment. Furthermore, selective pressures associated with the evolution of echolocation and unihemispheric sleep are implicated in substructure morphology and function. This neuroanatomical dataset, heretofore absent from the literature, provides important quantitative data to test hypotheses regarding brain structure, function, and evolution within Cetacea and across Mammalia.

Keywords Cetacea · Delphinoidea · Killer whale (*Orcinus orca*) · Magnetic resonance imaging (MRI) · Neuroanatomy · Cerebral scaling

Electronic supplementary material The online version of this article (doi:10.1007/s00429-016-1225-x) contains supplementary material, which is available to authorized users.

✉ Alexandra Wright
awright@ucsd.edu; alexandrakwright@gmail.com

[1] Center for Marine Biotechnology and Biomedicine, Scripps Institution of Oceanography, University of California, San Diego, La Jolla, CA 92093, USA

[2] Center for Functional MRI, Department of Radiology, University of California, San Diego, La Jolla, CA 92093, USA

[3] National Marine Mammal Foundation, San Diego, CA 92106, USA

[4] SeaWorld San Diego, 500 SeaWorld Drive, San Diego, CA 92109, USA

Introduction

Many species of Cetacea (whales, dolphins, and porpoises) possess exceptionally large brains characterized by distinct structural and diverse neuronal morphology (Oelschläger and Oelschläger 2009; Butti et al. 2014a), unique cortical topography (Ladygina et al. 1978), and unparalleled gyrencephaly (Manger et al. 2012). Cetacean species of the superfamily Delphinoidea, a group comprising the Delphinidae and their relatives, attain some of the largest relative brain sizes among extant mammals, which are comparable to and in some cases surpass that of nonhuman anthropoid primates (Marino 1998; Marino et al. 2004a;

Published online: 27 April 2016

Ridgway and Brownson 1984). Delphinoid brain size evolution may be driven by developmental prolongation, increased information-processing demands imposed by complex social systems, or obligate existence within the marine environment. Global enlargement of the delphinoid brain may be associated with protracted pre- and postnatal development periods (Charvet and Finlay 2012; Whitehead and Mann 2000) characterized by prolonged maternal investment (i.e., gestation and lactation phases; Barton and Capellini 2011; Whitehead and Mann 2000) that serve to extend the duration of neuronal and glial cell production (Charvet et al. 2011). Selection for enhanced social cognition permitting behavioral flexibility to negotiate interactions with conspecifics may also be associated with delphinoid encephalization (Connor 2007; Dunbar 1998; Shultz and Dunbar 2006). Alternatively, or additionally, the large size of the delphinoid brain may be attributed to hypertrophy of neural structures that mediate acoustic processing of echolocation and communication signals and acousticomotor integration (Ridgway 1986, 1990, 2000; Oelschläger 2008; Hanson et al. 2013). The ability of delphinoid cetaceans to rapidly integrate and process auditory stimuli is critical for prey detection, predator avoidance, navigation, and communication with conspecifics in the marine environment, where sound transmission is considerably faster than in air and alternate reliable sensory input is limited (Oelschläger 2008; Au and Nachtigall 1997; Tyack 1999; Wartzok and Ketten 1999).

Quantitative examination of the hypertrophy, regression, or loss of neural structures using magnetic resonance imaging (MRI) may provide functional and evolutionary insights into delphinoid neuroanatomy. MRI has been used to examine the neuroanatomy of an assortment of delphinoids, including the Atlantic white-sided dolphin (*Lagenorhynchus acutus*; Montie et al. 2007, 2008), beluga whale (*Delphinapterus leucas*; Marino et al. 2001a; Ridgway et al. 2002), bottlenose dolphin (*Tursiops truncatus*; Hanson et al. 2013; Ridgway et al. 2006; Marino et al. 2001c, 2004d), common dolphin (*Delphinus delphis*; Alonso-Farré et al. 2014; Haddad et al. 2012; Marino et al. 2001b, 2002; Berns et al. 2015; Oelschläger et al. 2007), harbor porpoise (*Phocoena phocoena*; Marino et al. 2003), killer whale (*Orcinus orca*; Marino et al. 2004b), pantropical spotted dolphin (*Stenella attenuata*; Haddad et al. 2012; Berns et al. 2015), spinner dolphin (*Stenella longirostris orientalis*; Marino et al. 2004c), and striped dolphin (*Stenella coeruleoalba*; Alonso-Farré et al. 2014). Also, studies implementing MRI for quantitative analysis and three-dimensional (3D) reconstruction of neuroanatomical structures have been performed in a range of delphinoid species of varying ontogeny (Hanson et al. 2013; Montie et al. 2008; Marino et al. 2001b, c, 2002, 2004c, d). However, detailed morphometric analysis of the neuroanatomy of *O. orca*, the largest delphinoid cetacean, with possibly the most voluminous brain of all mammals (Ridgway and Hanson 2014), has not been conducted. To date, neuroanatomical assessments of *O. orca* have been limited in scope, encompassing descriptive studies of gross morphology (Marino et al. 2004b) and brain stem anatomy (De Graaf 1967) in addition to measurements of mass relationships (Ridgway and Brownson 1984; Ridgway and Hanson 2014; Ridgway and Tarpley 1996; Pilleri and Gihr 1970), mid-sagittal area of the corpus callosum (Tarpley and Ridgway 1994; Keogh and Ridgway 2008), callosal fiber composition (Keogh and Ridgway 2008), neuron number per cortical unit (Poth et al. 2005), and von Economo neurons (Hof and Van Der Gucht 2007). Consequently, acquisition of MRI-derived neuroanatomical measurements and a global 3D atlas of *O. orca* neuromorphology are important for expanding knowledge of *O. orca* brain structure and potential function, making cross-species comparisons within the Cetacea, and examining mammalian brain evolution.

Therefore, in this study, MRI-based measurements and 3D reconstructions of an *O. orca* brain, acquired while intact within the neurocranium, are presented. MR images were manually segmented into regions of interest (ROIs) for quantitative analysis and 3D volume rendering. ROIs encompass: (1) cortical gray and cerebral white matter, (2) subcortical nuclei (i.e., caudate nuclei, putamina, globi pallidi, and thalamic nuclei), (3) cerebellar gray and white matter, (4) corpus callosum, (5) hippocampi, (6) superior and inferior colliculi, and (7) neuroendocrine structures (i.e., pineal and pituitary glands). *O. orca* neuroanatomy is discussed as it relates to the evolutionary adaptations of delphinoid cetaceans to the marine environment and mammalian brain evolution with comparisons across taxa.

Materials and methods

Specimen

The specimen examined in this study was the in situ postmortem brain of a male 544 cm, 2368 kg *O. orca* aged 12 years. This *O. orca* was not yet physically mature compared to conspecifics in this population. The cause of death was acute intestinal volvulus (Begeman et al. 2012) and non-neurological in nature. On necropsy examination, the head was separated from the body at the atlanto-occipital joint (Fig. 1). The specimen was prepared for insertion into the 3 Tesla MR scanner bore (diameter: 60 cm) by removing soft tissues (i.e., cranial blubber, acoustic fat, muscle, and connective tissue) and reducing cranial bone by repeated cuts (Fig. 1). MRI was performed within 30 h of death.

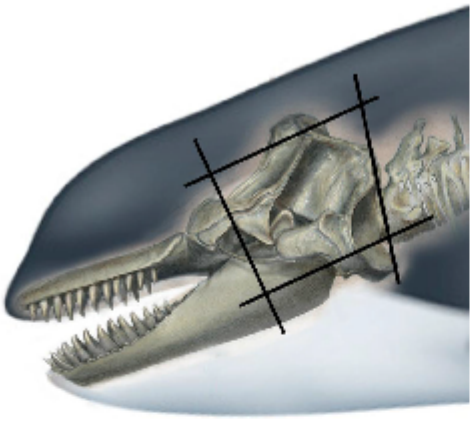

Fig. 1 *O. orca* head with superimposed cranium extending a few vertebrae beyond the atlanto-occipital joint. *Lines* indicate where cuts were made in preparing the specimen for MRI. Illustration by Sharon Birzer

Ethics statement

No live animals were used for this study. The *O. orca* specimen was examined opportunistically during post-mortem investigation.

MRI protocol

The size of the specimen (width = 30.5 cm × height = 24.0 cm × anteroposterior length = 22.6 cm) was at the upper limits of the imaging capability of the body gradient coil of the MRI scanner, while allowing data collection as a single acquisition. MR images were acquired in the frontal plane with a 3 Tesla General Electric (GE) scanner (GE Medical Systems, Milwaukee, WI, USA) at the University of California, San Diego Center for Functional MRI. T2-weighted images were acquired using a 2D fast spin echo (FSE-XL) imaging sequence with the following protocol parameters: echo time (TE) = 48 ms; repetition time (TR) = 6000 ms; inversion time (TI) = 450 ms; 10 averages; field of view = 48 × 48 cm; in-plane matrix = 512 × 512; in-plane resolution = 0.93 mm; slice thickness = 1 mm. Total imaging time was 1 h 57 min.

ROI delineation, quantitative analysis, and 3D reconstruction

ROIs were delineated by manual image segmentation (Fig. 2) of the MRI dataset using AMIRA software (FEI Visualization Sciences Group, Burlington, MA, USA). Segmentation was based on image grayscale intensity and a priori knowledge of derived neural features characteristic of odontocete cetaceans (toothed whales, dolphins, and porpoises) and general mammalian neuroanatomy, spatial relationships, and external landmarks. Thresholding for signal intensity was used where possible; however, due to the large size of the specimen relative to the MR scanner bore, there was signal inhomogeneity across the tissue, rendering automatic segmentation ineffective. However, given the 1 mm isotropic resolution of the dataset, accurate parcellation of many complex structures was possible.

To accurately delineate gray and white matter within the total brain, cerebrum, brainstem, and cerebellum, exclusion of neurocranial adnexa such as the meninges, cerebral falx, cerebellar tentorium, cerebrospinal fluid (CSF), and retia mirabilia was undertaken. The final delineated cerebrum included the cortical gray matter (neocortex and allocortex) and cerebral white matter. Subcortical nuclei parcellated were the head of the caudate nuclei, composite structures of the putamina and globi pallidi, and thalamic nuclei. Basal ganglia nuclei that could not be reliably visualized and delineated were included with cerebral white matter. The delineated brainstem comprised both gray and white matter structures of the midbrain, pons, emergent cerebellar peduncles, and medulla oblongata anterior to the foramen magnum. The cerebellum was separated from the brainstem consistent with the guidelines described by Pierson et al. (2002). The final delineated cerebellum included the cerebellar hemispheres and vermis. Cerebellar nuclei could not be reliably parcellated and were consequently included with cerebellar white matter.

The corpus callosum was delineated through identification of anterior–posterior, dorsal-ventral, and lateral boundaries. The callosal sulcus and cingulate gyrus served as the anterior, dorsal, and ventral boundaries of the corpus callosum. The lateral ventricles and caudate nuclei formed the posterior boundary of the corpus callosum. In frontal view, the lateral extent of the corpus callosum was delimited by tracing a straight horizontal line from the posterior-most boundary of the cingulum to the ipsilateral lateral ventricle or caudate nucleus. This protocol permitted the delineation of the genu, truncus, and splenium of the corpus callosum while endeavoring to exclude the callosal radiations (forceps minor, tapetum, and forceps major) to surrounding white matter. Within the midline sagittal section, the outer contour of the corpus callosum was segmented.

The studies of *T. truncatus* neuroanatomy by Jacobs et al. (1979) and McFarland et al. (1969) aided identification of anatomical landmarks and hippocampal boundaries, and were essential to the development of the hippocampal segmentation protocol for the present study. Moreover, *Homo sapiens* hippocampal protocols (Morey et al. 2009; McHugh et al. 2007; Knoops et al. 2010) were adapted for

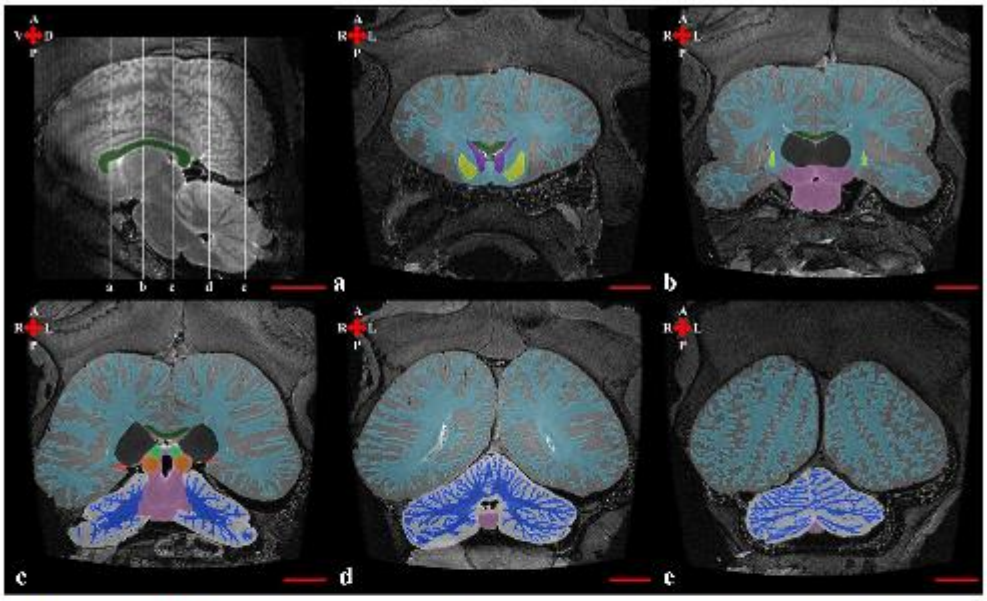

Fig. 2 Pilot parasagittal MR image and corresponding frontal MR images of the *O. orca* brain with representative manual parcellation of regions of interest (ROIs). *Parallel vertical lines* (*a*–*e*) on the parasagittal MR image represent the frontal planes of section. ROIs include cortical gray matter (*dark gray*), cerebral white matter (*light blue*), cerebellar gray matter (*light gray*), cerebellar white matter (*dark blue*), brainstem (*pink*), corpus callosum (*dark green*), hippocampi (*red*), superior colliculi (*light green*), inferior colliculi (*orange*), thalamic nuclei (*black*), putamina and globi pallidi (*yellow*), and caudate nuclei (*purple*). Anatomical directions: *A* (anterior), *P* (posterior), *D* (dorsal), *V* (ventral), *R* (right), and *L* (*left*). *Scale bar* ≈5 cm

O. orca hippocampus delineation. The ventral-anterior boundary of the hippocampus was demarcated by both the alveus, a thin white matter tract that separates the amygdala and hippocampus, and ventricular CSF. Continuing dorsally, CSF, choroid plexus, and the pulvinar thalami defined the anterior boundary of the hippocampus. The most dorsal boundary of the hippocampus was measured where the total length of the fornix was discernible. The white matter of the temporal lobe served as the posterior boundary of the hippocampus. Lateral and medial hippocampal boundaries were formed by the CSF of the lateral ventricles and subarachnoid space, respectively. The term hippocampus refers to a complex of subfields including the dentate gyrus, hippocampus proper, and subiculum. These hippocampal subfields were visually indistinguishable in this dataset and were consequently delineated as a singular complex and collectively designated as hippocampus.

The neuroendocrine structures of the pineal gland, anterior pituitary (adenohypophysis), and posterior pituitary (neurohypophysis) were also delineated.

Following image segmentation, ROI areas, volumes, and three-dimensional reconstructions were generated. Neuroanatomical measurements included the total brain volume, total gray and white matter volumes, total cerebrum volume, cortical gray and cerebral white matter volumes, aggregate subcortical nuclei volume, caudate nuclei volume, putamina and globi pallidi volume, thalamic nuclei volume, total brainstem volume, total cerebellar volume, cerebellar gray and white matter volumes, corpus callosum volume and mid-sagittal area, hippocampal volumes, superior and inferior colliculi volumes and maximal cross-sectional areas, and neuroendocrine structure volumes. Total brain volume was multiplied by the specific gravity of brain tissue [1.036 g/cm^3; Gompertz 1902; Stephan 1960] to calculate brain mass. The percentage of the total brain occupied by a ROI was determined for each structure. The ratios of white matter volume relative to gray matter volume were derived for the total brain, cerebrum, and cerebellum. Callosal mid-sagittal area to calculated brain mass (CCA:BM), cortical gray matter volume to callosal mid-sagittal area, inferior colliculi volume to superior colliculi volume, and inferior colliculi cross-sectional area to superior colliculi cross-sectional area ratios were also calculated. To control for dimensional

inconsistency (Smith 2005), the ratios of the mid-sagittal corpus callosum area to the calculated brain mass (1) and the cortical gray matter volume to the callosal mid-sagittal area (2) were determined with the following equations:

$$\left\{\frac{\left[\sqrt{\text{callosal mid} - \text{sagittal area } (\text{cm}^2)}\right]}{\left[\sqrt[3]{\text{calculated brain mass } (\text{g})}\right]}\right\} \quad (1)$$

$$\left\{\frac{\left[\sqrt[3]{\text{cortical gray matter volume } (\text{cm}^3)}\right]}{\left[\sqrt{\text{callosal mid} - \text{sagittal area } (\text{cm}^2)}\right]}\right\} \quad (2)$$

To determine scaling relationships between cortical gray matter, cerebral white matter, and cerebrum volumes in relation to total brain volume, bivariate reduced major axis (RMA) regression of $\log_{10}$-transformed volumetric data was performed with RMA for JAVA 1.21 (Bohonak and van der Linde 2004) to calculate scaling exponents (α). RMA regression was applied because both variables were subject to natural variation or measurement error, rendering ordinary linear regression inappropriate (Hofman et al. 1986). A *t* test was performed according to McArdle (1988) to test for the deviation of scaling exponents from isometry (α = unity).

Annotated MR images

Annotated MR images of the *O. orca* brain are provided in Online Resource 1.

Results and discussion

Gray and white matter: total brain

The total brain volume for this *O. orca* was 6211.30 cm^3 (Table 1; Fig. 3). Total gray matter volume was 3676.74 cm^3 (Table 1; Fig. 3), while total white matter volume was 2374.88 cm^3 (excluding the neurohypophysis and brainstem gray and white matter structures; Table 1; Fig. 3). In this *O. orca*, the gray matter volume relative to total brain volume was 59.19 %, whereas relative white matter volume was 38.23 %, constituting nearly the remainder of brain volume. With 37.58 % of total brain volume occupied by white matter, the relative white matter extent of *L. acutus*, a small delphinid, is comparable to the much larger *O. orca* with a brain volume 5 times the size of that of *L. acutus* (Montie et al. 2008). In contrast, the proportion of total gray matter in *O. orca* is larger than that of *L. acutus* (55.47 %; Montie et al. 2008). Similar to *L. acutus*, the brain volume of *H. sapiens* is 5 times less than this *O. orca* with a relative gray matter volume of 55.38 % (data from Walhovd et al. 2011; Pakkenberg and Gundersen 1997; Rilling and Insel 1999b). The amount of white matter relative to total brain size in *H. sapiens* is relatively large (42.65 %) compared to both *O. orca* and *L. acutus*. This finding suggests that the architecture of the delphinid brain emphasizes high local connectivity that minimizes conduction delay and increases computational power (Wen and Chklovskii 2005). This rapid processing power would appear to be necessary for the evolution of echolocation in delphinids such as *O. orca* and *L. acutus* living obligately within an aquatic environment that increases sound velocity.

Gray and white matter: cerebrum

The expansive cortical gray matter of this *O. orca* exhibited dramatic gyrification and sulcation, consistent with prior reports of cortical features in cetaceans (Ridgway and Brownson 1984; Hof et al. 2005; Manger et al. 2012). The cortical gray matter volume was 2999.52 cm^3 (Table 1; Figs. 3, 4), comprising nearly 50 % of the total brain volume. The volumes of the cerebral white matter (Table 1; Fig. 3), aggregate subcortical nuclei (Table 1; Fig. 4), and neuroendocrine structures (Table 1; Figs. 3, 5) expressed as percentages of total brain volume were 33.26, 2.08, and 0.04 %, respectively. The pineal gland (Fig. 5), while previously elusive in other cetacean species (for review, Panin et al. 2012), was presumably identified in this *O. orca*; however, histological evaluation is required for confirmation, but was not possible for the present study due to alteration of the specimen following MRI.

The cerebrum (cortical gray matter and cerebral white matter, excluding the hippocampus) of *O. orca* constitutes 81.51 % of the total brain volume (Table 2). The profound corticalization of this *O. orca* (Fig. 3) may only be exceeded by the sperm whale (*Physeter macrocephalus*; Ridgway and Hanson 2014), the largest odontocete cetacean, and is unsurpassed compared to other mammalian taxa (Table 2; Clark et al. 2001), including *H. sapiens* for which the cerebrum occupies 76.18 % of the total brain volume (Table 2; data from Walhovd et al. 2011; Pakkenberg and Gundersen 1997; Rilling and Insel 1999b). These results are consistent with previous research concerning *O. orca* cortical surface area (Ridgway and Brownson 1984). Voluminous cerebra are characteristic of delphinoid cetaceans with relative sizes ranging from 70.39 to 73.40 % of total brain size (Table 2) in five species (*P. phocoena*, *T. truncatus*, *Globicephala macrorhynchus*, *Grampus griseus*, and *S. coeruleoalba*) of varying brain size (Haug 1970; Hofman 1985, 1988). Mammalian cortical enlargement has been associated with prolonged maternal investment (Barton and Capellini 2011) and developmental period (Joffe 1997), sociality (Dunbar 1998; Shultz and Dunbar 2006), and sensory specialization

Table 1 Measurements of neural regions of interest (ROIs) for *O. orca* and literature review of neuroanatomical data available for odontocete cetaceans

ROI measurement	Wright et al.	Literature review	
	O. orca	*O. orca*[a]	Odontoceti[a,b]
Brain mass (g)	–	(4500.00–9300.00)[1,2]	(205.00–9200.00)[1,2,3,4,5,6,7]
Calculated brain mass (g)[c]	6434.91	–	–
Brain volume (cm^3)	6211.30	–	(483.00–3650.00)[7,8,9,10,11]
WM[d]	2374.88	–	(467.04–475.83)[7]
GM[e]	3676.74	–	(673.31–718.55)[7]
WM:GM[f]	0.65	–	(0.66–0.71)[7]
Cerebrum volume (cm^3)	5065.55	–	(340.00–2045.00)[8,9,10]
Cerebral WM[d]	2066.03	–	(135.00–868.00)[8,9,10]
Cortical GM[e,g]	2999.52	–	(205.00–1177.00)[8,9,10]
WM:GM[f]	0.69	–	(0.66–0.81)[8,9,10]
% of brain[h]	81.55	–	(70.39–73.40)[8,9,10]
Subcortical nuclei volume (cm^3)	129.14	–	–
% of brain[h]	2.08	–	–
Caudate nuclei	10.19	–	–
Globi pallidi + putamina	14.09	–	–
Thalamic nuclei	104.86	–	(18.00–52.50)[8]
Neuroendocrine volume (cm^3)	2.65	–	–
% of brain[h]	0.04	–	–
Adenohypophysis	2.20	–	(0.17–1.50)[4,12,13,14,15,16]
Neurohypophysis	0.25	–	(0.21)[12]
Pineal gland	0.20	–	–
Brainstem volume (cm^3)	157.02	–	(21.00–209.00)[8]
% of brain[h]	2.53	–	(4.35–6.83)[8]
Cerebellum volume (cm^3)	856.93	(727.00–1544.00)[2]	(92.66–656.00)[2,7,11]
WM[d]	308.85	–	(53.17–61.71)[7]
GM[e]	548.08	–	(110.42–113.67)[7]
WM:GM[f]	0.56	–	(0.47–0.56)[7]
% of brain[h]	13.80	(11.80–17.20)[2]	(5.00–18.20)[2,4,7,11]
Corpus callosum volume (cm^3)	27.19	–	–
% of brain[h]	0.44	–	–
Corpus callosum mid-sagittal area (cm^2)	4.29	(4.47–8.29)[17,18]	(1.04–4.63)[7,17,18]
CCA:BM[i]	0.11	(0.12–0.15)[17,18]	(0.11–0.17)[7,17,18]
Cortical GM:CCA[j]	6.96	–	(4.71–5.87)[10,17,18]
Hippocampus volume (cm^3)	2.46	–	(0.60–1.90)[7,19]
% of brain[h]	0.04	–	(0.07–0.15)[7,19]
Left	1.10	–	(0.87–1.04)[7]
Right	1.35	–	(0.74–0.86)[7]
Superior colliculus volume (cm^3)	2.40	–	–
% of brain[h]	0.04	–	–
Left	1.11	–	–
Right	1.29	–	–
Superior colliculus maximal cross-sectional area (mm^2)[k]	235.52	–	(6.00–118.80)[4,20]
Left	108.42	–	–
Right	127.11	–	–

Table 1 continued

ROI measurement	Wright et al.	Literature review	
Inferior colliculus volume (cm^3)	6.07	–	–
% of brain[b]	0.10	–	–
Left	2.94	–	–
Right	3.13	–	–
Inferior colliculus maximal cross-sectional area (mm^2)[k]	530.86	–	(75.40–296.10)[1,4,20,21]
Left	246.27	–	–
Right	284.59	–	–
IC volume:SC volume[l]	2.53	–	–
IC cross-sectional area:SC cross-sectional area[m]	2.25	–	(2.20–28.30)[1,4,20]

[a] Range of ROI measurement from data in cited literature; [b] excluding *O. orca*; [c] calculated brain mass (g) = brain volume (cm^3) × brain tissue specific gravity [1.036 g/cm^3; Gompertz (1902); Stephan (1960)]; [d] *WM* white matter; [e] *GM* gray matter; [f] WM:GM = white matter volume (cm^3)/gray matter volume (cm^3); [g] including hippocampus; [h] percentage of total brain comprised by ROI; [i] CCA:BM = [corpus callosum mid-sagittal area (cm^2)]$^{1/2}$/[calculated brain mass (g)]$^{1/3}$; [j] Cortical GM:CCA = [cortical gray matter volume (cm^3)]$^{1/3}$/[corpus callosum mid-sagittal area (cm^2)]$^{1/2}$; [k] collicular cross-sectional area (mm^2) = [length (mm) × width (mm) × π]/4; [l] IC volume:SC volume = inferior colliculi volume (cm^3)/superior colliculi volume (cm^3); [m] IC cross-sectional area:SC cross-sectional area = inferior colliculi cross-sectional area (mm^2)/superior colliculi cross-sectional area (mm^2)

[1] Pilleri and Gihr (1970); [2] Ridgway and Hanson (2014); [3] Jacobs and Jensen (1964); [4] Pilleri (1972); [5] Ridgway and Brownson (1984); [6] Ridgway and Tarpley (1996); [7] Montie et al (2008); [8] Haug (1970); [9] Hofman (1985); [10] Hofman (1988); [11] Marino et al. (2000); [12] Wislocki (1929); [13] Gihr and Pilleri(1969); [14] Pilleri and Gihr (1969); [15] Gruenberger (1970); [16] Pilleri and Gihr (1972); [17] Tarpley and Ridgway (1994); [18] Keogh and Ridgway (2008); [19] Patzke et al. (2013); [20] Chen (1979); [21] Oelschläger et al. (2010)

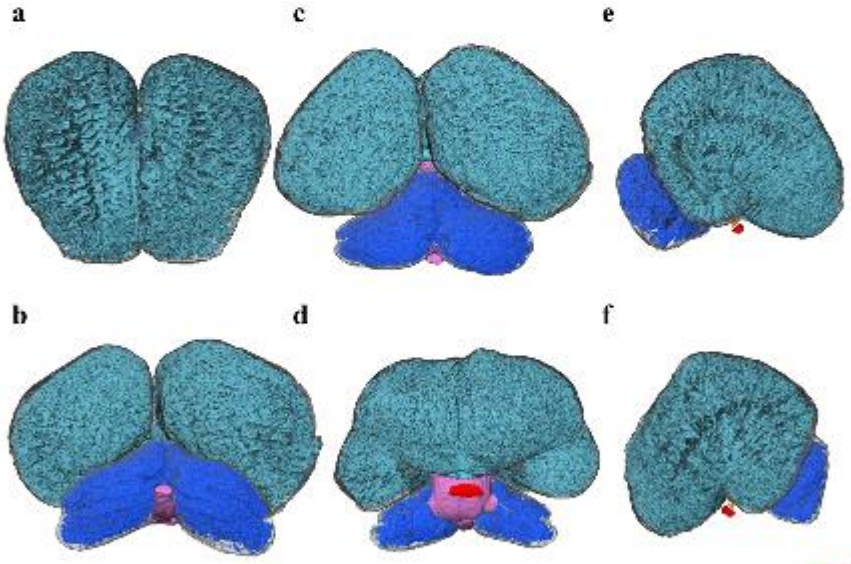

Fig. 3 **a** Anterior, **b** posterior, **c** dorsal, **d** ventral, **e** right parasagittal, and **f** left parasagittal views of the *O. orca* brain segmented into cortical gray matter (*translucent dark gray*), cerebral white matter (*light blue*), adenohypophysis (*red*), neurohypophysis (*orange*), brainstem (*pink*), cerebellar gray matter (*translucent light gray*), and cerebellar white matter (*dark blue*). *Scale bar* ≈ 5 cm

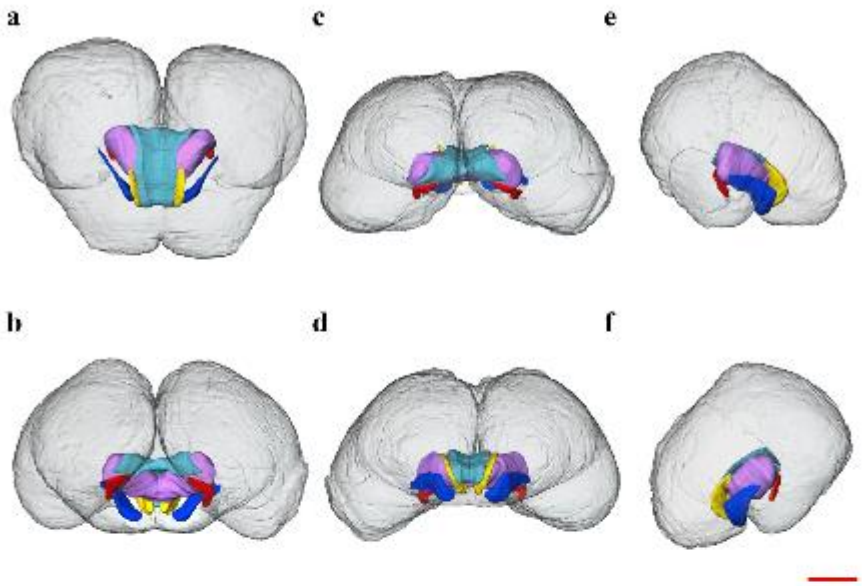

Fig. 4 **a** Anterior, **b** posterior, **c** dorsal, **d** ventral, **e** right parasagittal, and **f** left parasagittal views of the *O. orca* cerebrum segmented into cortical gray matter (*translucent dark gray*), corpus callosum (*light blue*), hippocampi (*red*), caudate nuclei (*yellow*), putamina and globi pallidi (*dark blue*), and thalamic nuclei (*purple*). *Scale bar* ≈ 5 cm

(Barton 1998, 2006) which are traits common to delphinoids, and the wider Odontoceti. Moreover, cortical size has been suggested as a good predictor of cognitive ability (Reader and Laland 2002; Byrne and Bates 2007). However, recent studies propose that absolute neuron number, irrespective of body size, may be a better determinant of cognitive performance (Herculano-Houzel 2011; Roth and Dicke 2005). A limited number of studies using unbiased stereological methods have estimated the total cortical neuron number of cetaceans. *P. phocoena* and *Globicephala melas* both have high numbers of cortical neurons; moreover, *G. melas* has almost twice as many neurons as *H. sapiens* (Mortensen et al. 2014; Walløe et al. 2010). Considering the corpus of research on the cognitive abilities of delphinoid cetaceans (for review, Herman 2010; Würsig 2009, but cf. Manger 2013), it will be of great interest to determine the absolute neuron number of the highly corticalized *O. orca*, thus offering an opportunity to explore the intersection of delphinoid brain and cognitive evolution.

A distinctive feature of delphinoid brain evolution is the deviation from allometric scaling relationships between cortical gray and white matter volumes that are otherwise evolutionarily conserved. Typical mammalian brain allometry exhibits hyperscaling of cortical white matter with increasing brain size (Barton and Harvey 2000; Zhang and Sejnowski 2000). It has been proposed that larger brains require thicker, more abundant, and heavily-myelinated long-range axonal connections between different brain regions to minimize conduction delay, resulting in a disproportionate expansion of cortical white matter (Wen and Chklovskii 2005; Zhang and Sejnowski 2000; Changizi 2001). Curiously, the cerebral white matter of *O. orca*, with possibly the largest brain in the animal kingdom (Ridgway and Hanson 2014), and of the delphinoids examined (data from Haug 1970; Hofman 1988) scales isometrically with total brain volume, rendering a scaling exponent of $\alpha = 1.059$ [t test, degrees of freedom (df) = 3, $P = 0.88$] and extending previous findings by Hofman (1989). Furthermore, overall cerebral volume (cortical gray matter and cerebral white matter) and cortical gray matter volume did not depart from isometry [($\alpha = 1.045$, t test, $df = 4$, $P = 0.85$ and $\alpha = 1.05$, t test, $df = 3$, $P = 0.71$, respectively; data from Haug 1970; Hofman 1985, 1988]. In other words, cortical proportionality is relatively fixed across delphinoid species thus far examined with the proportion of cortical gray matter and cerebral white matter minimally altered with brain enlargement. As a consequence, despite a nearly 13-fold difference in brain size between *O. orca* and *P. phocoena*, relative cortical gray matter and cerebral

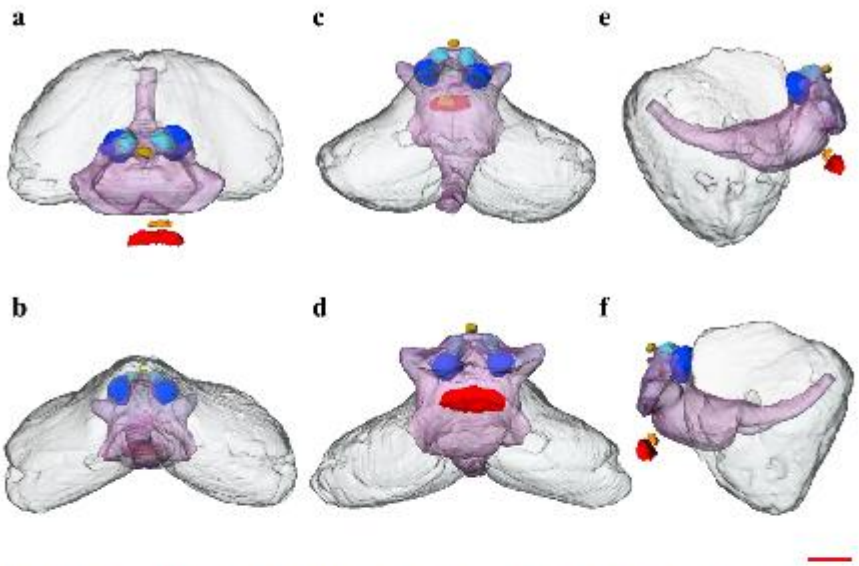

Fig. 5 **a** Anterior, **b** posterior, **c** dorsal, **d** ventral, **e** right parasagittal, and **f** left parasagittal views of the *O. orca* adenohypophysis (*red*), neurohypophysis (*orange*), pineal gland (*gold*), brainstem (*translucent pink*), superior colliculi (*light blue*), inferior colliculi (*dark blue*), and cerebellar gray matter (*translucent light gray*). *Scale bar* ≈ 3 cm

Table 2 Brain, cerebrum (cortical GM and cerebral WM), cortical GM, and cerebral WM volumes and percentage of total brain occupied by these volumes in *O. orca* and other mammals

	Brain (cm^3)	Cerebrum (cm^3)[a]	Cortical GM (cm^3)[a,b]	Cerebral WM (cm^3)[c]	% Cerebrum	% Cortical GM	% Cerebral WM
O. orca	6211.30	5063.10	2997.07	2066.03	81.51	48.25	33.26
Delphinoid cetaceans[d,1,2,3]	483.00–2786.00	340.00–2045.00	205.00–1177.00	135.00–868.00	70.39–73.40	39.29–42.44	27.95–31.68
Artiodactyls[3,4,5]	105.00–486.00	71.60–337.00	51.80–226.00	19.80–111.00	60.22–69.34	46.50–49.33	18.86–22.84
Sirenians[6,7]	223.00–439.19	127.46–283.01	–	–	57.16–67.25	–	–
Proboscideans[2,8]	3886.70–4148.00	2460.10–2491.00	1378.70–1402.00	1081.40–1089.00	60.05–63.30	33.80–35.47	26.25–27.82
Anthropoid primates[9,10,11]	23.10–1225.38	16.50–933.54	11.70–506.88	4.80–426.66	62.14–76.18	38.43–50.65	19.70–34.82

[a] Excluding hippocampus volume; [b] *GM* gray matter; [c] *WM* white matter; [d] excluding *O. orca*

[1] Haug (1970); [2] Hofman (1985); [3] Hofman (1988); [4] Schleniska (1974); [5] Meyer (1981); [6] Pirlot and Kamiya (1985); [7] Reep and O'Shea (1990); [8] Hakeem et al. 2005; [9] Pakkenberg and Gundersen (1997); [10] Rilling and Insel (1999b); [11] Walhovd et al. (2011)

white matter volumes exhibit limited ranges of 39.29–48.25 and 27.95–33.26 %, respectively, across delphinoids (Table 2). Further cross-species studies are needed to determine whether isometric scaling of cerebral tissues is a trait that is widespread within, or unique to, the Delphinoidea, or that characterizes the wider Odontoceti or Mysticeti (baleen whales), more generally. Studies demonstrating callosal isometry in a range of cetacean species (Gilissen 2006; Manger et al. 2010) tentatively suggest that the isometric cerebral scaling observed in the delphinoids studied to date may be a defining neuroanatomical feature of Cetacea.

The absence of cerebral white matter hyperscaling in delphinoid cetaceans suggests that conduction velocity is either compromised or optimized by alternative mechanisms. Studies of auditory brainstem response in delphinids measured latencies that were shorter than predicted on the basis of brain size, indicating a higher conduction velocity

compared to other mammals (Ridgway et al. 1981). Conduction velocity along mammalian myelinated axons increases with axon diameter (Hursh 1939), degree of myelination (Waxman 1980), and neuron-glia interactions (Yamazaki et al. 2007). The cranial nerves of delphinoid cetaceans have the largest axon diameters reported for all mammals (Gao and Zhou 1991, 1992; Dawson et al. 1982). The cochlear nerve of *Neophocaena phocaenoides*, the finless porpoise, contains giant axons as thick as 54.9 µm (Gao and Zhou 1991). The significant proportion of giant axons within the cochlear nerve indicates specialization for rapid transmission of acoustic stimuli in delphinoids (Gao and Zhou 1992). While delphinoid cranial nerves contain the highest percentages of large-diameter axons compared to other mammals, they exhibit the lowest axonal densities (Gao and Zhou 1992). The low axonal densities observed across delphinoid species may account for the absence of white matter hyperscaling in these taxa. Moreover, low axonal density suggests a relatively high proportion of neuroglia—astrocytes, oligodendrocytes, NG2-glia, and microglia—within white matter (Herculano-Houzel 2014). Though glial subpopulations have not yet been quantified in cetaceans, one study identified high astroglial content within the optic nerves of *S. coeruleoalba* (suborder Odontoceti) and *Balaenoptera physalus* (suborder Mysticeti; Mazzatenta et al. 2001). Oligodendrocytes support neuronal function by producing axon-ensheathing myelin that allows for faster signal propagation (Verkhratsky and Butt 2013). Furthermore, depolarization of oligodendrocytes has been demonstrated to directly increase the conduction velocity of action potentials (Yamazaki et al. 2007). Thus, conduction velocity could be optimized in delphinoids through amplifying interactions between axons and ancillary oligodendrocytes. Axonal gigantism, low axonal densities, and potentially high numbers of white matter glial cells per axon in the large brains of delphinoid cetaceans indicate that different mechanisms to white matter hyperscaling evolved to support rapid information processing across greater transmission distances in this taxon.

The evolutionary process of adaptation to an obligatory aquatic existence dramatically modified cetacean brain morphology and function. Isometric scaling of cerebral tissues with brain volume may have arisen due to rigid constraints imposed by the marine environment on delphinoids. Indeed, interhemispheric connectivity (Gilissen 2006; Manger et al. 2010), cortical surface area (Ridgway and Brownson 1984) and gyrencephaly (Manger et al. 2012) also scale isometrically in the Odontoceti. Moreover, odontocete middle ear bones exhibit isometric scaling indicating that these echolocating mammals were under considerable selective pressure for the preservation of certain auditory structure dimensions (Nummela et al. 1999) that conceivably enhanced underwater hearing ability. Considering the unique cerebral isometry of delphinoids, it may be suggested that significant advantages were gained from the restriction of cerebral white matter hyperscaling. The volume of cortical gray matter expressed as a percentage of cerebral volume was 59.19 % for this *O. orca* and averaged 57.84 % across delphinoids (data from Haug 1970; Hofman 1988), comprising the majority of cerebral space. Within the cerebrum of delphinoid cetaceans, the proportion of cortical gray matter appears to be larger than that of *H. sapiens* (54.30 %; data from Walhovd et al. 2011; Pakkenberg and Gundersen 1997; Rilling and Insel 1999b) and the African elephant (*Loxodonta africana*; 56.16 %; data from Hofman 1985; Hakeem et al. 2005), a mammal with the largest brain among extant and extinct terrestrial mammals. Conversely, the volume of cerebral white matter relative to the total cerebrum averaged 42.16 % across the delphinoids examined, compared to 45.70 % in *H. sapiens* (data from Walhovd et al. 2011; Pakkenberg and Gundersen 1997; Rilling and Insel 1999b) and 43.84 % in *L. africana* (Hofman 1985; Hakeem et al. 2005). Delphinoids may have evolved this divergent cortical morphology in response to the sensorimotor demands of the aquatic environment. Cortical gray matter contains networks of neurons that in large brains exhibit dense clustering, high local connectivity, and sparse global connectivity, resembling a 'small-world' network (Bassett and Bullmore 2006; Watts and Strogatz 1998). These 'small-world' properties are thought to play a central role in cortical information processing by minimizing conduction delay and enhancing computational power (Wen and Chklovskii 2005). Thus, in the aquatic environment, where sound velocity is accelerated compared to air, increased local connectivity (gray matter) at the expense of global connectivity (white matter) in the cerebrum of delphinoid cetaceans could potentially support rapid auditory analysis and reduce motor response latencies to acoustic stimuli. Selection for high local connectivity and short conduction delay in the delphinoid cortex is suggested by increased cortical gray matter volume, unparalleled gyrencephaly (Manger et al. 2012; Hofman 2012), unique cortical topography (Ladygina et al. 1978), commissural deficit (Tarpley and Ridgway 1994), hemispheric asymmetry (Ridgway and Brownson 1984), and functional lateralization (MacNeilage 2013; Ringo 1991).

Though delphinoid cortical gray matter is expansive and contains large numbers of neurons, neuronal density is low resulting in increased numbers of glial cells per neuron (Mortensen et al. 2014; Walløe et al. 2010; Herculano-Houzel 2014). The cortical glial cell to cortical neuron ratios of *G. melas* and *P. phocoena* are higher than that in *H. sapiens* (1.4:1) at 3.4:1 and 2.3:1, respectively (Pakkenberg and Gundersen 1997; Mortensen et al. 2014;

Walløe et al. 2010). Moreover, *Balaenoptera acutorostrata*, the minke whale, has one of the highest ratios of cortical glial cells to cortical neurons (7.7:1) studied to date (Eriksen and Pakkenberg 2007). An increased number of glial cells per neuron may be advantageous for species inhabiting the aquatic environment by enhancing neuronal signaling and conferring neuroprotective benefits; however, an alternative hypothesis on the potential thermogenetic function of cetacean glia has been proposed previously (Manger 2006), albeit controversial and as yet unsupported quantitatively (Marino et al. 2008; Maximino 2009a, b). High numbers of astrocytes and oligodendrocytes could potentially support rapid processing of acoustic information by regulating synaptogenesis (Ullian et al. 2001), enhancing synaptic efficacy (Pfrieger and Barres 1997), and increasing conduction velocity (Yamazaki et al. 2007). Astrocytes are relatively resistant to hypoxic conditions (Swanson et al. 1997), and afford neuroprotective benefits to adjacent neurons that are more vulnerable to hypoxic insult. During hypoxia, astrocytes can augment glycolytic capacity (Marrif and Juurlink 1999), downregulate synaptic activity (Martín et al. 2007), and upregulate erythropoietin to potentially inhibit hypoxia-induced apoptosis (Ruscher et al. 2002). Thus, astrocyte-mediated neuroprotection may serve a critical role for cetaceans which spend the majority of their time underwater and are reliant on limited oxygen stores at depth. Moreover, higher glial content per neuron may have permitted the ancestors of extant cetaceans to successfully invade the aquatic environment by enhancing hypoxia tolerance and limiting conduction delay. In support of this hypothesis, a recent study of cellular composition within the cerebral cortex of artiodactyls, the closest phylogenetic relatives of cetaceans (Gatesy et al. 2013), found high numbers of non-neuronal (presumably mostly glial) cells per neuron (Kazu et al. 2014). High non-neuronal cell to neuron ratios have also been measured in *L. africana* (Herculano-Houzel et al. 2014), one of the closest phylogenetic relatives to obligately aquatic sirenians (dugongs and manatees; Seiffert 2007), suggesting that increased numbers of glial cells per neuron may have been necessary to facilitate the evolutionary transition from terrestrial to obligatory aquatic existence.

Gray and white matter: brainstem

The brainstem of this *O. orca* occupied 2.53 % of the total brain volume at 157.02 cm^3 (Table 1; Figs. 3, 5). The relative volume of the brainstem in this *O. orca* compared to other delphinoids is considerably small. The relative size of the brainstem in *P. phocoena, T. truncatus, and G. macrorhynchus* is 4.35, 4.38, and 6.83 %, respectively (Haug 1970). The divergence in relative brainstem volumes across these species may reflect the greater corticalization of *O. orca* in comparison to other delphinoids. These discrepant measurements may also arise from sampling error, dissimilar methodology, or differential shrinkage of heterogeneous brain tissues in fixative (Kretschmann et al. 1982; Quester and Schröder 1997). The relative volume of the brainstem in *O. orca* is larger than that of *H. sapiens* (1.97 %; Walhovd et al. 2011). This increased relative size may be ascribed to hypertrophy of various components of the auditory, trigeminal, and motor systems (for review, Oelschläger 2008).

Gray and white matter: cerebellum

The cerebellum of *O. orca* was voluminous, constituting 13.80 % of the total brain size. Total cerebellar volume was 856.93 cm^3 (Table 1; Figs. 3, 5), consisting of gray and white matter volumes that were 548.08 and 308.85 cm^3, respectively (Table 1). The large cerebellum in *O. orca* is consistent with previous measurements of cerebellar size in *O. orca* (Ridgway and Hanson 2014), and other odontocete cetaceans (Montie et al. 2008; Ridgway and Tarpley 1996; Marino et al. 2000; Pilleri 1972). The large cerebella relative to total brain size observed in delphinoid cetaceans may signal an integral role for the cerebellum in acoustic processing and potentially higher-order cognitive functions such as learning and memory. The paraflocculus, an auditory-associated cerebellar region, is particularly expanded in odontocetes and echolocating bats (Hanson et al. 2013; Larsell 1970) and may be vital for acousticomotor processing related to sound production and navigation (Oelschläger 2008). Moreover, anatomical and functional MRI studies have implicated the paraflocculus in verbal working memory (lobules VIIIa, VIIIb, and IX; Cooper et al. 2012) and episodic memory retrieval (lobule IX; Habas et al. 2009).

Corpus callosum

The volume of this *O. orca* corpus callosum was 27.19 cm^3 occupying 0.44 % of the total brain volume and 1.32 % of cerebral white matter volume (Table 1; Fig. 4). The small volume of the *O. orca* corpus callosum is consistent with previous measurements of callosal extent in other odontocete species (Montie et al. 2008; Tarpley and Ridgway 1994; Keogh and Ridgway 2008). The mid-sagittal corpus callosum area of this *O. orca* was 4.29 cm^2 (Tables 1, 3). The ratio of the square root of the corpus callosum mid-sagittal area (cm^2) to the cube root of the calculated brain mass (g) [CCA:BM] was 0.11 (Tables 1, 3), illustrating the diminutive size of the *O. orca* corpus callosum relative to brain mass. Although this value fell below the range of CCA:BM ratios (0.12–0.15) calculated from previously

Table 3 Brain mass (BM), callosal mid-sagittal area (CCA), CCA:BM, and cortical GM:CCA in *O. orca* and other mammals

	BM (g)	CCA (cm^2)	CCA:BM[a]	Cortical GM:CCA[b]
O. orca[1]	6434.91	4.29	0.11	6.96
O. orca[c,2,3]	5667.00–7100.00	4.47–8.29	0.12–0.15	–
Odontocete cetaceans[d,2,3,4,5]	514.00–4739.00	1.04–4.63	0.11–0.17	4.71–5.87
Artiodactyls[6,7,8]	244.00–530.00	1.17–1.93	0.16–0.22	–
Sirenians[2,6,7]	188.00–302.00	0.90–2.50	0.17–0.24	–
Proboscideans[6,7,9,10]	4026.62–5250.00	8.09–12.57	0.17–0.22	3.11
Pinnipeds[2,6,7]	345.00–1250.00	1.01–1.89	0.13–0.17	–
Anthropoid primates[11,12,13]	23.93–1345.66	0.44–6.90	0.21–0.24	3.16–3.61

[a] CCA:BM = [corpus callosum mid-sagittal area $(cm^2)]^{1/2}$/[calculated brain mass (g)]$^{1/3}$; [b] Cortical GM:CCA = [cortical gray matter volume $(cm^3)]^{1/3}$/[corpus callosum mid-sagittal area $(cm^2)]^{1/2}$; [c] excluding *O. orca* data from Wright et al; [d] excluding *O. orca*

[1] Wright et al.; [2] Tarpley and Ridgway (1994); [3] Keogh and Ridgway (2008); [4] Hofman (1988); [5] Montie et al. (2008); [6] Anthony (1938); [7] Manger et al. (2010); [8] Butti et al. (2014b); [9] Hakeem et al. (2005); [10] Shoshani et al. (2006); [11] Rilling and Insel (1999a); [12] Rilling and Insel (1999b); [13] Fears et al (2009)

reported callosal data for *O. orca* (Tables 1, 3; Tarpley and Ridgway 1994; Keogh and Ridgway 2008), it lies within the range of CCA:BM ratios (0.11–0.17) calculated for wider Odontoceti (Tables 1, 3; Montie et al. 2008; Tarpley and Ridgway 1994; Keogh and Ridgway 2008). The slight departure of this specimen from the CCA:BM ratio range established for *O. orca* (Tarpley and Ridgway 1994; Keogh and Ridgway 2008) may reflect discrepancies in measurement arising from comparison of fresh versus fixed tissues (shrinkage artifact; Schulz et al. 2011), or alternatively, sampling error or divergent methodology. Despite these comparative limitations, it is apparent that this *O. orca* along with conspecifics and wider Odontoceti, exhibit lower interhemispheric connectivity compared to most other mammals, except for the semi-aquatic Pinnipedia (seals, sea lions, and walruses; Table 3; Manger et al. 2010).

The ratio of the cube root of cortical gray matter volume (cm^3) to the square root of callosal mid-sagittal area (cm^2) in *O. orca* (6.96; Tables 1, 3) was larger than the ratios for the delphinids, *G. griseus* (5.87), *G. macrorhynchus* (5.21), and *T. truncatus* (4.71; delphinid data from Haug 1970; Hofman 1988; Tarpley and Ridgway 1994; Keogh and Ridgway 2008), as well as the large-brained terrestrial mammals, *H. sapiens* (3.18; Rilling & Insel 1999a) and *L. africana* (3.11; Hakeem et al. 2005). Thus, the callosal area per unit volume of cortical gray matter in other delphinids, *H. sapiens*, and *L. africana* was 1.32, 2.19, and 2.24 times larger than that of this *O. orca*.

As the major commissural linkage between the cerebral hemispheres, the relatively small callosal size of *O. orca* and other odontocete cetaceans presumably supports greater hemispheric independence than in other mammalian orders (Ridgway 1990). Indeed, odontocete unihemispheric slow wave sleep (USWS), a state of interhemispheric asymmetry in which one cerebral hemisphere produces sleeping electroencephalograms (EEGs) while the opposite hemisphere produces waking EEGs (for review, Lyamin et al. 2008), is likely associated with reduced interhemispheric communication via the small corpus callosum. USWS is proposed to support locomotion required for surface respiration as well as environmental monitoring for detection of conspecifics, predators, and prey (Lyamin et al. 2008; Goley 1999; Rattenborg et al. 2000). Additionally, USWS facilitated by reduced callosal linkage, may also limit cerebral O_2 metabolism through unihemispheric vasoconstriction and reduction in cerebral blood flow and glucose consumption (Ridgway et al. 2006).

Hippocampus

The hippocampus is a limbic structure subserving learning, memory, and spatial navigation (Burgess et al. 2002). The cetacean hippocampus is widely recognized as diminutive, both in absolute size and relative to the size of the brain as a whole (Table 4; Morgane et al. 1982; Jacobs et al. 1979; Patzke et al. 2013). The hippocampi of *O. orca* are no exception, with hippocampal volume measuring 2.46 cm^3, constituting 0.04 % of the total brain volume (Tables 1, 4; Fig. 4). The left and right hippocampi of *O. orca* were 1.10 and 1.35 cm^3 (Table 1), respectively, exhibiting an asymmetry of hippocampal size similar to that observed in *L. acutus* (Montie et al. 2008). The percentage of the total brain occupied by the hippocampus in cetaceans varies from 0.04 to 0.15 % (Table 4), with *O. orca* representing the lower boundary of the range. The relative hippocampal volumes of cetaceans are the smallest of all mammals examined (Table 4). Interestingly, the relative hippocampal volume of the large-brained *L. africana* (0.21–0.23 %; data from Patzke et al. 2013) more closely approaches this measure in cetaceans than do the relative hippocampal

Table 4 Brain and hippocampal volumes and percentage of total brain occupied by the hippocampus in *O. orca* and other mammals

	Brain volume (cm^3)	Hippocampal volume (cm^3)	% Hippocampus
O. orca	6211.30	2.46	0.04
Cetaceans[a,1,2]	469.11–2799.23	0.60–1.90	0.05–0.15
Artiodactyls[2,3,4]	77.70–559.27	2.67–8.58	0.92–3.44
Sirenians[2,3,5]	223.00–337.84	2.07–3.63	0.93–1.07
Proboscideans[2]	4666.99–5067.57	10.57–11.21	0.21–0.23
Pinnipeds[2,3]	265.44–638.27	1.95–3.53	0.55–0.79
Anthropoid primates[6]	4.34–1283.78	0.13–10.29	0.80–3.27

[a] Excluding *O. orca*

[1] Montie et al. (2008); [2] Patzke et al. (2013); [3] Reep et al. (2007); [4] Butti et al. (2014b); [5] Pirlot and Kamiya (1985); [6] Stephan (1981)

volumes of obligatorily aquatic sirenians (0.93–1.07 %; data from Patzke et al. 2013; Reep et al. 2007; Pirlot and Kamiya 1985), or semi-aquatic pinnipeds (0.55–0.79 %; data from Patzke et al. 2013; Reep et al. 2007).

The poor development of the cetacean hippocampus compared to other mammals (Table 4; Patzke et al. 2013) and its apparent lack of adult neurogenesis (Patzke et al. 2013) is enigmatic, given the high cognitive function (for review, Herman 2010; Würsig 2009; but cf. Manger 2013) and navigational prowess (Block et al. 2011; Durban and Pitman 2012) observed in Cetacea. Patzke et al. (2013) proposed that the unusual cetacean hippocampal morphology and apparent absence of hippocampal neurogenesis may be related to their mammalian-atypical sleep physiology [i.e., limited or potentially absent rapid eye movement (REM) sleep; for review, Lyamin et al. 2008]. However, the presence of well-developed hippocampi and hippocampal neurogenesis in obligatorily aquatic sirenians and semi-aquatic pinnipeds (Patzke et al. 2013) along with observations of reduced REM sleep in these taxa (for review, Lyamin et al. 2008) would not seem to support this hypothesis. Therefore, it is posited that the small size of the cetacean hippocampus may arise from a suite of phenomena related to sensory function, rather than sleep physiology.

The dominant sensory mode of odontocete cetaceans is echolocation, a high resolution sensing system that relies on the rapid production of click trains, or sequences of discrete clicks, to create an "acoustic image" of the environment from returning echoes. Odontocetes can emit high-intensity ultrasonic echolocation signals with maximum source levels exceeding 220 dB (Au 1993; Møhl et al. 2003), produce click trains consisting of up to several hundred clicks per second (Herzing 1996), and echolocate continuously (Branstetter et al. 2012). Numerous studies have demonstrated that sound overstimulation induces neural plasticity in the hippocampus and impairs hippocampal function (for review, Kraus and Canlon 2012). High-intensity sound exposure has been associated with alterations in hippocampal place cell activity (Goble et al. 2009), chronic suppression of hippocampal neurogenesis (Kraus et al. 2010), and even apoptosis of hippocampal neurons (Säljö et al. 2002). The mammalian hippocampus appears to be particularly vulnerable to auditory insult; thus, the routine exposure of odontocete cetaceans to high-intensity sounds during echolocation and communication may impact the development, structural integrity, and neurogenic capacity of their hippocampi selecting for an overall small size. The potentially significant influence of echolocation on hippocampal volume is further supported by findings that echolocating bats have smaller hippocampi than non-echolocating bats (Hutcheon et al. 2002). Furthermore, the Mysticeti also have diminutive hippocampi (Hof and Van Der Gucht 2007; Patzke et al. 2013) and produce high-intensity, low-frequency acoustic signals (Širović et al. 2007; Tyack 2000) associated with reproductive advertisement displays (Tyack and Clark 2000), as well as for long-range communication with conspecifics (Payne and Webb 1971; Clark and Ellison 2004), and potentially for orientation and navigation (Clark and Ellison 2004). Similar to mysticetes, *L. africana* produces high-intensity infrasonic signals for long-distance communication (Poole et al. 1988; Garstang 2010). Moreover, *L. africana* has the lowest relative hippocampal volume apart from cetaceans (Table 4). However, unlike cetaceans, *L. africana* exhibits hippocampal neurogenesis (Patzke et al. 2013). This suggests that both the production of high-intensity acoustic signals and the type of sound propagating medium (i.e., water or air) in which those signals are generated, each impact upon hippocampal morphology and function. Perhaps, the generation of high-intensity sound, whether ultra- or infrasonic, by cetaceans within a dense medium that accelerates and amplifies acoustic signals, is incompatible with sound-sensitive hippocampal tissue, potentially eliminating neurogenic capacity. This, in turn, may have necessitated an overall reduction of the cetacean hippocampus and indicates transfer of memory, learning, and navigational functions to neural structures less prone to acoustic injury, such as the entorhinal cortex or cerebellum.

Poor development of the odontocete hippocampus may also be associated with its potentially diminished function as a site of association and integration of multimodal (visual, auditory, olfactory, tactile, vestibular) sensory information (Mayes et al. 2007; Sweatt 2003). For odontocete cetaceans, olfactory input is absent, vestibular input is limited, and visual input is reduced. The most consistent and detailed spatial information available to odontocetes is acquired through audition. Odontocetes may not require spatial representations that integrate extensive information from multiple sensory stimuli to support navigation; instead, relying predominantly on acoustic information for spatial memory and orientation. Moreover, since odontocetes must attempt to localize mobile and patchily distributed prey species in a seemingly featureless aquatic environment, the utility of the hippocampus as a spatial mapping structure may be diminished. Ultimately, the role of the hippocampus as a multimodal association and integration site may no longer be of such utility in the odontocetes, potentially leading to the diminutive hippocampal size observed in this suborder.

Superior and inferior colliculi

In *O. orca*, the volume of the superior colliculi was 2.40 cm^3 comprising 0.04 % of the total brain volume (Table 1; Fig. 5). The inferior colliculi volume was 2.53 times larger than the volume of the superior colliculi, measuring 6.07 cm^3 and occupying 0.10 % of the total brain volume (Table 1; Fig. 5). A similar spatial relationship was observed for the maximal cross-sectional areas of the superior and inferior colliculi, with the maximal cross-sectional area of the inferior colliculi 2.25 times greater than that of the superior colliculi.

The superior and inferior colliculi are major sensory processing nodes within the midbrain. The inferior colliculus integrates acoustic information from various structures along the ascending and descending acoustic pathways (Casseday et al. 2002). Whereas, the superficial laminae of the superior colliculus are involved in visual processing (May 2006; Meredith and Stein 1986). The deep laminae of the superior colliculus integrate visual, auditory, and somatosensory inputs and mediate orientation responses toward sensory stimuli (Meredith and Stein 1986; Stein et al. 1989). The enlarged size of the inferior colliculi relative to the superior colliculi in *O. orca* is representative of the strong development of various components of the auditory system (for review, Oelschläger 2008) in the echolocating Odontoceti. In odontocete cetaceans, ratios of the maximal cross-sectional area of the inferior colliculi to superior colliculi range from 2:1 to 28:1 (Table 1). While in most non-echolocating Mysticeti, the superior colliculi are larger or approximately the same size as the inferior colliculi (Oelschläger and Oelschläger 2009). Remarkably, in absolute terms, the inferior colliculi of *O. orca* are 6.46 times as large as those of *D. delphis*, the common dolphin, and nearly 80 times larger than the inferior colliculi of *H. sapiens* (Bullock and Gurevich 1979).

The dominant role of audition in the sensory repertoire of echolocating mammals is also apparent in the colliculi of microchiropteran bats which have hypertrophied inferior colliculi that exceed the superior colliculi in size (Covey and Casseday 1995; Hu et al. 2006). However, anatomical and neurophysiological studies of the microchiropteran superior colliculus suggest that this structure has evolved to function as a major auditory rather than visual sensorimotor interface, linking echoic spatial information to orienting behaviors (Covey et al. 1987; Valentine and Moss 1997; Sinha and Moss 2007). Though the extent of the superior colliculi of odontocete cetaceans is surpassed by that of the inferior colliculi, the potential evolution of acoustic specializations in the odontocete superior colliculi as observed in echolocating bats may ultimately confer to this structure greater relevance within the auditory system. While the odontocete superior colliculus may allocate considerable functional capacity to acoustic orientation by echolocation, behavioral evidence for cross-modal perception in *T. truncatus* (Pack and Herman 1995; Herman et al. 1998) suggests that the superior colliculus may also be an important site of multisensory integration in the Odontoceti.

A slight size asymmetry was observed between contralateral superior and inferior colliculi (Fig. 5). The volumes and maximal cross-sectional areas of the right superior (1.29 cm^3; 127.11 mm^2) and inferior (3.13 cm^3; 284.59 mm^2) colliculi were larger than the measurements for the left superior (1.11 cm^3; 108.42 mm^2) and inferior (2.94 cm^3; 246.27 mm^2) colliculi (Table 1). The asymmetry of the inferior colliculi in *O. orca* may be related to asymmetric cranial morphology, differential acoustic signaling mechanisms, and cerebral lateralization of function. Most odontocete crania exhibit varying degrees of asymmetry (Ness 1967; Dahlheim and Heyning 1999) potentially linked to the development of directional hearing in water (Fahlke et al. 2011). Furthermore, delphinids actively control acoustic signal dynamics through beam-steering (Moore et al. 2008) as well as preferentially utilize the right pair of phonic lips for generation of echolocation signals (clicks), and the left pair of phonic lips for production of communication signals (whistles; Madsen et al. 2013). The asymmetries of the inferior colliculi may reflect lateralized processing of behaviorally distinct acoustic stimuli as well as binaurally and spectrotemporally variant acoustic information arising from cranial asymmetry and active modification of cranial soft tissues. Evidence for neural circuit asymmetries in the perception of acoustic cues has

been collected for various mammalian species, including sea lions (Böye et al. 2005) and echolocating bats (Kanwal 2012; Washington and Kanwal 2012). Though studies of auditory lateralization have yet to be performed in odontocete cetaceans, there is an accumulating body of behavioral evidence for lateralized processing of social (Karenina et al. 2013a, b) and non-social (Yaman et al. 2003; von Fersen et al. 2000; Kilian et al. 2000) visual stimuli. Though the ubiquity and potential functional implications of collicular asymmetry in the Odontoceti awaits future investigation, it may be speculated that the size asymmetries observed in the superior and inferior colliculi of *O. orca* reflect lateralized processing of social and non-social acoustic information (e.g., communication whistles and echolocation clicks). Moreover, such functional asymmetry may bear some relevance to the detailed auditory localization ability demonstrated in *T. truncatus* by Renaud and Popper (1975).

Conclusions

There are some acknowledged limitations of the present study. Given the rarity of *O. orca* specimens, only one brain was available for morphometric analysis. While it is not suspected that the brain of this *O. orca* was anomalous for the species (i.e., this specimen is within the size range reported for adult male *O. orca*; Ridgway and Hanson 2014), due to the limited sample size of this study, future quantitative research examining *O. orca* specimens of varying sex, ontogenetic stage, and ecotype is required to increase the confidence of the present results and conclusions.

Volumetric measurements of neuroanatomy can be subject to error associated with postmortem processes, MRI, and segmentation. In the present study, volume deformation of the gray and white matter structures of this *O. orca* brain was likely mitigated by short postmortem interval (Montie et al. 2010) and imaging fresh, unfixed tissue within the neurocranium. However, limited local deformation was evident where cranial bone was cut to the dura mater. Additionally, CSF leakage from the neurocranium allowed for some positional shift of the brain. MRI acquisition artifacts, such as intensity inhomogeneity and partial-volume effect (i.e., multiple tissue types within a single voxel), may have contributed to error in gray and white matter tissue classification and substructure (e.g., subcortical nuclei and hippocampi) delineation. The very high resolution of this dataset limited partial-volume error due to the lower percentage of total voxels at the gray-white matter interface; however, volumetric overestimation and underestimation were still possible. Acquisition of ultra-high resolution 7 Tesla MRI data in future quantitative cetacean brain studies would mitigate such measurement errors and allow for neuroanatomical measurements of greater accuracy to be obtained. Lastly, manual segmentation of neuroanatomical structures is subjective. Segmentation error was reduced through consultation of various cetacean-specific and mammalian neuroanatomical atlases to determine structure boundaries and landmarks.

The present study, with its acknowledged caveats, has shown the potential for using MRI to examine cetacean neuroanatomy, and potential brain function and evolution. A unique neuroanatomical dataset for *O. orca*, heretofore absent from the literature, has resulted from this study. It is, therefore, particularly important for interspecific comparisons, and furnishes data which may be used to test hypotheses regarding cetacean brain structure, function, and evolution. This *O. orca* brain is one of the most corticalized (81.51 %, cerebrum volume occupying total brain volume) mammalian brains reported to date, and is representative of a species which may have the largest brain of all extant and extinct taxa (Ridgway and Hanson 2014). The divergent cerebral morphology of delphinoid cetaceans compared to other mammalian taxa may have evolved in response to the sensorimotor demands of the aquatic environment and may confer significant advantages for obligatory aquatic existence. Furthermore, environmental selective pressures associated with the evolution of echolocation and unihemispheric sleep have ostensibly altered substructure morphology and function. The delphinoid brain with its distinctive morphological features, cerebral scaling, and functional capacities offers fertile ground for future research concerning mammalian brain structure, function, and evolution. Moreover, the methodology of high resolution in situ MR imaging described in this study offers great promise for future investigation of cetacean brains.

Acknowledgments The authors sincerely thank Erika Nilson for preparation of the specimen, Sharon Birzer for illustration, and Paul Ponganis for valuable manuscript feedback. The authors also thank Hauke Bartsch for improved visualization of MR images (Fig. 2 and Online Resource 1) through MR image preprocessing to remove intensity non-uniformity using the Non-parametric Non-uniform intensity Normalization (N3) algorithm as implemented in ITK (http://github.com/HaukeBartsch/itkN3). AW was supported by the National Science Foundation Graduate Research Fellowship Program. The funder had no role in the study design, data collection, analysis, or interpretation, preparation of the manuscript, or decision to publish.

Compliance with ethical standards

Conflict of interest AW, MS, DS, RD, and SR declare that they have no conflict of interest. JSL is a paid employee of SeaWorld Parks and Entertainment. No live animals were used for this study. The *O. orca* specimen was examined opportunistically during postmortem investigation.

References

Alonso-Farré J, Gonzalo-Orden M, Barreiro-Vázquez J, Barreiro-Lois A, André M, Morell M, Llarena-Reino M, Monreal-Pawlowsky T, Degollada E (2014) Cross-sectional anatomy, computed tomography and magnetic resonance imaging of the head of common dolphin (*Delphinus delphis*) and Striped Dolphin (*Stenella coeruleoalba*). Anat Histol Embryol 44(1):13–21

Anthony R (1938) Essai de recherche d'une expression anatomique approximative du degré d'organisation cérébrale, autre que le poids de l'encéphale comparé au poids du corps. B Mem Soc Anthro Par 9(1):17–67

Au W (1993) Characteristics of dolphin sonar signals. The sonar of dolphins. Springer, New York, pp 115–139

Au W, Nachtigall P (1997) Acoustics of echolocating dolphins and small whales. Mar Freshw Behav Phys 29(1–4):127–162

Barton R (1998) Visual specialization and brain evolution in primates. Philos Roy Soc B 265(1409):1933–1937

Barton R (2006) Primate brain evolution: integrating comparative, neurophysiological, and ethological data. Evol Anthropol 15(6):224–236

Barton R, Capellini I (2011) Maternal investment, life histories, and the costs of brain growth in mammals. P Natl Acad Sci 108(15):6169–6174

Barton R, Harvey P (2000) Mosaic evolution of brain structure in mammals. Nature 405(6790):1055–1058

Bassett D, Bullmore E (2006) Small-world brain networks. Neuroscientist 12(6):512–523

Begeman L, St. Leger J, Blyde D, Jauniaux T, Lair S, Lovewell G, Raverty S, Seibel H, Siebert U, Staggs S (2012) Intestinal volvulus in cetaceans. Vet Pathol 50(4):590–596

Berns G, Cook P, Foxley S, Jbabdi S, Miller K, Marino L (2015) Diffusion tensor imaging of dolphin brains reveals direct auditory pathway to temporal lobe. Proc R Soc B 282:20151203

Block B, Jonsen I, Jorgensen S, Winship A, Shaffer S, Bograd S, Hazen E, Foley D, Breed G, Harrison A (2011) Tracking apex marine predator movements in a dynamic ocean. Nature 475(7354):86–90

Bohonak A, van der Linde K (2004) RMA: software for reduced major axis regression. http://www.bio.sdsu.edu/pub/andy/rma.html. Accessed 10 Feb 2015

Böye M, Güntürkün O, Vauclair J (2005) Right ear advantage for conspecific calls in adults and subadults, but not infants, California sea lions (*Zalophus californianus*): hemispheric specialization for communication? Eur J Neurosci 21(6):1727–1732

Branstetter B, Finneran J, Fletcher E, Weisman B, Ridgway S (2012) Dolphins can maintain vigilant behavior through echolocation for 15 days without interruption or cognitive impairment. PLoS One 7(10):e47478

Bullock T, Gurevich V (1979) Soviet literature on the nervous system and psychobiology of Cetacea. Int Rev Neurobiol 21:47–127

Burgess N, Maguire E, O'Keefe J (2002) The human hippocampus and spatial and episodic memory. Neuron 35(4):625–641

Butti C, Janeway C, Townshend C, Wicinski B, Reidenberg J, Ridgway S, Sherwood C, Hof P, Jacobs B (2014a) The neocortex of cetartiodactyls: I. A comparative Golgi analysis of neuronal morphology in the bottlenose dolphin (*Tursiops truncatus*), the minke whale (*Balaenoptera acutorostrata*), and the humpback whale (*Megaptera novaeangliae*). Brain Struct Funct 220(6):3339–3368

Butti C, Raghanti M, Gu X, Bonar C, Wicinski B, Wong E, Roman J, Brake A, Eaves E, Spocter M (2014b) The cerebral cortex of the pygmy hippopotamus, *Hexaprotodon liberiensis* (Cetartiodactyla, Hippopotamidae): MRI, cytoarchitecture, and neuronal morphology. Anat Rec 297(4):670–700

Byrne R, Bates L (2007) Sociality, evolution and cognition. Curr Biol 17(16):R714–R723

Casseday J, Fremouw T, Covey E (2002) The inferior colliculus: a hub for the central auditory system. Integrative functions in the mammalian auditory pathway. Springer, Berlin, pp 238–318

Changizi M (2001) Principles underlying mammalian neocortical scaling. Biol Cybern 84(3):207–215

Charvet C, Finlay B (2012) Embracing covariation in brain evolution: large brains, extended development, and flexible primate social systems. Prog Brain Res 195:71–87

Charvet C, Striedter G, Finlay B (2011) Evo-devo and brain scaling: candidate developmental mechanisms for variation and constancy in vertebrate brain evolution. Brain Behav Evol 78(3):248–257

Chen Y (1979) On the cerebral anatomy of the Chinese river dolphin, *Lipotes vexillifer* Miller. Acta Hydrob Sin 4:365–372

Clark C, Ellison W (2004) Potential use of low-frequency sounds by baleen whales for probing the environment: evidence from models and empirical measurements. In: Thomas J, Moss C, Vater M (eds) Echolocation in bats and dolphins. The University of Chicago Press, Chicago, pp 564–582

Clark D, Mitra P, Wang S (2001) Scalable architecture in mammalian brains. Nature 411(6834):189–193

Connor R (2007) Dolphin social intelligence: complex alliance relationships in bottlenose dolphins and a consideration of selective environments for extreme brain size evolution in mammals. Philos Trans R Soc B 362:587–602

Cooper F, Grube M, Von Kriegstein K, Kumar S, English P, Kelly T, Chinnery P, Griffiths T (2012) Distinct critical cerebellar subregions for components of verbal working memory. Neuropsychologia 50(1):189–197

Covey E, Casseday J (1995) The lower brainstem auditory pathways. Hearing by bats. Springer, New York, pp 235–295

Covey E, Hall W, Kobler J (1987) Subcortical connections of the superior colliculus in the mustache bat, *Pteronotus parnellii*. J Comp Neurol 263(2):179–197

Dahlheim M, Heyning J (1999) Killer Whale— *Orcinus orca* (Linnaeus, 1758). In: Ridgway S, Harrison R (eds) Handbook of marine mammals: the second book of dolphins and porpoises, vol 6. Academic Press, London

Dawson W, Hawthorne M, Jenkins R, Goldston R (1982) Giant neural systems in the inner retina and optic nerve of small whales. J Comp Neurol 205(1):1–7

De Graaf A (1967) Anatomical aspects of the cetacean brain stem, vol 5. Royal VanGorcum Ltd., The Netherlands

Dunbar R (1998) The social brain hypothesis. Brain 9:178–190

Durban J, Pitman R (2012) Antarctic killer whales make rapid, round-trip movements to subtropical waters: evidence for physiological maintenance migrations? Biol Lett 8(2):274–277

Eriksen N, Pakkenberg B (2007) Total neocortical cell number in the mysticete brain. Anat Rec 290(1):83–95

Fahlke J, Gingerich P, Welsh R, Wood A (2011) Cranial asymmetry in *Eocene archaeocete* whales and the evolution of directional hearing in water. Proc Natl Acad Sci 108(35):14545–14548

Fears S, Melega W, Lee C, Chen K, Tu Z, Jorgensen M, Fairbanks L, Cantor R, Freimer N, Woods R (2009) Identifying heritable brain phenotypes in an extended pedigree of vervet monkeys. J Neurosci 29(9):2867–2875

Gao G, Zhou K (1991) The number of fibers and range of fiber diameters in the cochlear nerve of three odontocete species. Can J Zool 69(9):2360–2364

Gao G, Zhou K (1992) Fiber analysis of the optic and cochlear nerves of small cetaceans. Marine mammal sensory systems. Springer, Berlin, pp 39–52

Garstang M (2010) Elephant infrasounds: long-range communication. In: Brudzynski S (ed) Handbook of mammalian vocalization—

References

Alonso-Farré J, Gonzalo-Orden M, Barreiro-Vázquez J, Barreiro-Lois A, André M, Morell M, Llarena-Reino M, Monreal-Pawlowsky T, Degollada E (2014) Cross-sectional anatomy, computed tomography and magnetic resonance imaging of the head of common dolphin (*Delphinus delphis*) and Striped Dolphin (*Stenella coeruleoalba*). Anat Histol Embryol 44(1):13–21

Anthony R (1938) Essai de recherche d'une expression anatomique approximative du degré d'organisation cérébrale, autre que le poids de l'encéphale comparé au poids du corps. B Mem Soc Anthro Par 9(1):17–67

Au W (1993) Characteristics of dolphin sonar signals. The sonar of dolphins. Springer, New York, pp 115–139

Au W, Nachtigall P (1997) Acoustics of echolocating dolphins and small whales. Mar Freshw Behav Phys 29(1–4):127–162

Barton R (1998) Visual specialization and brain evolution in primates. Philos Roy Soc B 265(1409):1933–1937

Barton R (2006) Primate brain evolution: integrating comparative, neurophysiological, and ethological data. Evol Anthropol 15(6):224–236

Barton R, Capellini I (2011) Maternal investment, life histories, and the costs of brain growth in mammals. P Natl Acad Sci 108(15):6169–6174

Barton R, Harvey P (2000) Mosaic evolution of brain structure in mammals. Nature 405(6790):1055–1058

Bassett D, Bullmore E (2006) Small-world brain networks. Neuroscientist 12(6):512–523

Begeman L, St. Leger J, Blyde D, Jauniaux T, Lair S, Lovewell G, Raverty S, Seibel H, Siebert U, Staggs S (2012) Intestinal volvulus in cetaceans. Vet Pathol 50(4):590–596

Berns G, Cook P, Foxley S, Jbabdi S, Miller K, Marino L (2015) Diffusion tensor imaging of dolphin brains reveals direct auditory pathway to temporal lobe. Proc R Soc B 282:20151203

Block B, Jonsen I, Jorgensen S, Winship A, Shaffer S, Bograd S, Hazen E, Foley D, Breed G, Harrison A (2011) Tracking apex marine predator movements in a dynamic ocean. Nature 475(7354):86–90

Bohonak A, van der Linde K (2004) RMA: software for reduced major axis regression. http://www.bio.sdsu.edu/pub/andy/rma.html. Accessed 10 Feb 2015

Böye M, Güntürkün O, Vauclair J (2005) Right ear advantage for conspecific calls in adults and subadults, but not infants, California sea lions (*Zalophus californianus*): hemispheric specialization for communication? Eur J Neurosci 21(6):1727–1732

Branstetter B, Finneran J, Fletcher E, Weisman B, Ridgway S (2012) Dolphins can maintain vigilant behavior through echolocation for 15 days without interruption or cognitive impairment. PLoS One 7(10):e47478

Bullock T, Gurevich V (1979) Soviet literature on the nervous system and psychobiology of Cetacea. Int Rev Neurobiol 21:47–127

Burgess N, Maguire E, O'Keefe J (2002) The human hippocampus and spatial and episodic memory. Neuron 35(4):625–641

Butti C, Janeway C, Townshend C, Wicinski B, Reidenberg J, Ridgway S, Sherwood C, Hof P, Jacobs B (2014a) The neocortex of cetartiodactyls: I. A comparative Golgi analysis of neuronal morphology in the bottlenose dolphin (*Tursiops truncatus*), the minke whale (*Balaenoptera acutorostrata*), and the humpback whale (*Megaptera novaeangliae*). Brain Struct Funct 220(6):3339–3368

Butti C, Raghanti M, Gu X, Bonar C, Wicinski B, Wong E, Roman J, Brake A, Eaves E, Spocter M (2014b) The cerebral cortex of the pygmy hippopotamus, *Hexaprotodon liberiensis* (Cetartiodactyla, Hippopotamidae): MRI, cytoarchitecture, and neuronal morphology. Anat Rec 297(4):670–700

Byrne R, Bates L (2007) Sociality, evolution and cognition. Curr Biol 17(16):R714–R723

Casseday J, Fremouw T, Covey E (2002) The inferior colliculus: a hub for the central auditory system. Integrative functions in the mammalian auditory pathway. Springer, Berlin, pp 238–318

Changizi M (2001) Principles underlying mammalian neocortical scaling. Biol Cybern 84(3):207–215

Charvet C, Finlay B (2012) Embracing covariation in brain evolution: large brains, extended development, and flexible primate social systems. Prog Brain Res 195:71–87

Charvet C, Striedter G, Finlay B (2011) Evo-devo and brain scaling: candidate developmental mechanisms for variation and constancy in vertebrate brain evolution. Brain Behav Evol 78(3):248–257

Chen Y (1979) On the cerebral anatomy of the Chinese river dolphin, *Lipotes vexillifer* Miller. Acta Hydrob Sin 4:365–372

Clark C, Ellison W (2004) Potential use of low-frequency sounds by baleen whales for probing the environment: evidence from models and empirical measurements. In: Thomas J, Moss C, Vater M (eds) Echolocation in bats and dolphins. The University of Chicago Press, Chicago, pp 564–582

Clark D, Mitra P, Wang S (2001) Scalable architecture in mammalian brains. Nature 411(6834):189–193

Connor R (2007) Dolphin social intelligence: complex alliance relationships in bottlenose dolphins and a consideration of selective environments for extreme brain size evolution in mammals. Philos Trans R Soc B 362:587–602

Cooper F, Grube M, Von Kriegstein K, Kumar S, English P, Kelly T, Chinnery P, Griffiths T (2012) Distinct critical cerebellar subregions for components of verbal working memory. Neuropsychologia 50(1):189–197

Covey E, Casseday J (1995) The lower brainstem auditory pathways. Hearing by bats. Springer, New York, pp 235–295

Covey E, Hall W, Kobler J (1987) Subcortical connections of the superior colliculus in the mustache bat, *Pteronotus parnellii*. J Comp Neurol 263(2):179–197

Dahlheim M, Heyning J (1999) Killer Whale— *Orcinus orca* (Linnaeus, 1758). In: Ridgway S, Harrison R (eds) Handbook of marine mammals: the second book of dolphins and porpoises, vol 6. Academic Press, London

Dawson W, Hawthorne M, Jenkins R, Goldston R (1982) Giant neural systems in the inner retina and optic nerve of small whales. J Comp Neurol 205(1):1–7

De Graaf A (1967) Anatomical aspects of the cetacean brain stem, vol 5. Royal VanGorcum Ltd., The Netherlands

Dunbar R (1998) The social brain hypothesis. Brain 9:178–190

Durban J, Pitman R (2012) Antarctic killer whales make rapid, round-trip movements to subtropical waters: evidence for physiological maintenance migrations? Biol Lett 8(2):274–277

Eriksen N, Pakkenberg B (2007) Total neocortical cell number in the mysticete brain. Anat Rec 290(1):83–95

Fahlke J, Gingerich P, Welsh R, Wood A (2011) Cranial asymmetry in *Eocene archaeocete* whales and the evolution of directional hearing in water. Proc Natl Acad Sci 108(35):14545–14548

Fears S, Melega W, Lee C, Chen K, Tu Z, Jorgensen M, Fairbanks L, Cantor R, Freimer N, Woods R (2009) Identifying heritable brain phenotypes in an extended pedigree of vervet monkeys. J Neurosci 29(9):2867–2875

Gao G, Zhou K (1991) The number of fibers and range of fiber diameters in the cochlear nerve of three odontocete species. Can J Zool 69(9):2360–2364

Gao G, Zhou K (1992) Fiber analysis of the optic and cochlear nerves of small cetaceans. Marine mammal sensory systems. Springer, Berlin, pp 39–52

Garstang M (2010) Elephant infrasounds: long-range communication. In: Brudzynski S (ed) Handbook of mammalian vocalization—

an integrative neuroscience approach, vol 19. Elsevier, Oxford, pp 57–67
Gatesy J, Geisler J, Chang J, Buell C, Berta A, Meredith R, Springer M, McGowen M (2013) A phylogenetic blueprint for a modern whale. Mol Phylogenet Evol 66(2):479–506
Gihr M, Pilleri G (1969) On the anatomy and biometry of *Stenella styx* Gray and *Delphinus delphis* L. (*Cetacea*, Delphinidae) of the western Mediterranean. Investig Cetacea 1:15–65
Gilissen E (2006) Scaling patterns of interhemispheric connectivity in eutherian mammals. Behav Brain Sci 29:16–17
Goble T, Møller A, Thompson L (2009) Acute high-intensity sound exposure alters responses of place cells in hippocampus. Hear Res 253(1):52–59
Goley P (1999) Behavioral aspects of sleep in Pacific White-Sided Dolphins (*Lagenorhynchus obliquidens*, Gill 1865). Mar Mamm Sci 15(4):1054–1064
Gompertz R (1902) Specific gravity of the brain. J Physiol 27(6):459–462
Gruenberger H (1970) On the cerebral anatomy of the Amazon dolphin, *Inia geoffrensis*. Investig Cetacea 2:129–144
Habas C, Kamdar N, Nguyen D, Prater K, Beckmann C, Menon V, Greicius M (2009) Distinct cerebellar contributions to intrinsic connectivity networks. J Neurosci 29(26):8586–8594
Haddad D, Huggenberger S, Haas-Rioth M, Kossatz L, Oelschläger H, Haase A (2012) Magnetic resonance microscopy of prenatal dolphins (Mammalia, Odontoceti, Delphinidae)—ontogenetic and phylogenetic implications. Zool Anz 251(2):115–130
Hakeem A, Hof P, Sherwood C, Switzer R, Rasmussen L, Allman J (2005) Brain of the African elephant (*Loxodonta africana*): neuroanatomy from magnetic resonance images. Anat Rec A 287(1):1117–1127
Hanson A, Grisham W, Sheh C, Annese J, Ridgway S (2013) Quantitative examination of the bottlenose dolphin cerebellum. Anat Rec 296:1215–1228
Haug H (1970) Der makroskopische Aufbau des Großhirns: qualitative und quantitative Untersuchungen an den Gehirnen des Menschen, der Delphinoidene und des Elefanten. ERG ANAT ENTW, vol 43(4). Springer, Berlin. Accessed 17 Feb 2015
Herculano-Houzel S (2011) Brains matter, bodies maybe not: the case for examining neuron numbers irrespective of body size. Ann NY Acad Sci 1225(1):191–199
Herculano-Houzel S (2014) The glia/neuron ratio: how it varies uniformly across brain structures and species and what that means for brain physiology and evolution. Glia 62(9):1377–1391
Herculano-Houzel S, Avelino-de-Souza K, Neves K, Porfírio J, Messeder D, Feijó L, Maldonado J, Manger P (2014) The elephant brain in numbers. Front Neuroanat 8:46. Accessed 30 Sep 2015
Herman L (2010) What laboratory research has told us about dolphin cognition. Int J Comp Psychol 23(3):310–330
Herman L, Pack A, Hoffmann-Kuhnt M (1998) Seeing through sound: Dolphins (*Tursiops truncatus*) perceive the spatial structure of objects through echolocation. J Comp Psychol 112(3):292–305
Herzing D (1996) Vocalizations and associated underwater behavior of free-ranging Atlantic spotted dolphins, *Stenella frontalis* and bottlenose dolphins, *Tursiops truncatus*. Aquat Mamm 22:61–80
Hof P, Van Der Gucht E (2007) Structure of the cerebral cortex of the humpback whale, *Megaptera novaeangliae* (Cetacea, Mysticeti, Balaenopteridae). Anat Rec 290(1):1–31
Hof P, Chanis R, Marino L (2005) Cortical complexity in cetacean brains. Anat Rec A 287(1):1142–1152
Hofman M (1985) Size and shape of the cerebral cortex in mammals: I. The cortical surface. Brain Behav Evol 27(1):28–40
Hofman M (1988) Size and shape of the cerebral cortex in mammals. Brain Behav Evol 32(1):17–26
Hofman M (1989) On the evolution and geometry of the brain in mammals. Prog Neurobiol 32(2):137–158
Hofman M (2012) Design principles of the human brain: an evolutionary perspective. Prog Brain Res 195:373–390
Hofman M, Laan A, Uylings H (1986) Bivariate linear models in neurobiology: problems of concept and methodology. J Neurosci Methods 18(1):103–114
Hu K, Li Y, Gu X, Lei H, Zhang S (2006) Brain structures of echolocating and nonecholocating bats, derived in vivo from magnetic resonance images. Neuroreport 17(16):1743–1746
Hursh J (1939) Conduction velocity and diameter of nerve fibers. Am J Physiol 127:131–139
Hutcheon J, Kirsch J, Garland T (2002) A comparative analysis of brain size in relation to foraging ecology and phylogeny in the chiroptera. Brain Behav Evol 60(3):165–180
Jacobs M, Jensen A (1964) Gross aspects of the brain and a fiber analysis of cranial nerves in the great whale. J Comp Neurol 123(1):55–71
Jacobs M, McFarland W, Morgane P (1979) The anatomy of the brain of the bottlenose dolphin (*Tursiops truncatus*). Rhinic lobe (rhinencephalon): the archicortex. Brain Res Bull 4(1):1–108
Joffe T (1997) Social pressures have selected for an extended juvenile period in primates. J Hum Evol 32(6):593–605
Kanwal J (2012) Right-left asymmetry in the cortical processing of sounds for social communication vs. navigation in mustached bats. Eur J Neurosci 35(2):257–270
Kazenina K, Giljov A, Glazov D, Malashichev Y (2013a) Social laterality in wild beluga whale infants: comparisons between locations, escort conditions, and ages. Behav Ecol Sociobiol 67(7):1195–1204
Kazenina K, Giljov A, Ivkovich T, Burdin A, Malashichev Y (2013b) Lateralization of spatial relationships between wild mother and infant orcas, *Orcinus orca*. Anim Behav 86(6):1225–1231
Kazu R, Maldonado J, Mota B, Manger P, Herculano-Houzel S (2014) Cellular scaling rules for the brain of Artiodactyla include a highly folded cortex with few neurons. Front Neuroanat 8:128. Accessed 7 Oct 2015
Keogh M, Ridgway S (2008) Neuronal fiber composition of the corpus callosum within some odontocetes. Anat Rec 291(7):781–789
Kilian A, von Fersen L, Güntürkün O (2000) Lateralization of visuospatial processing in the bottlenose dolphin (*Tursiops truncatus*). Behav Brain Res 116(2):211–215
Knoops A, Gerritsen L, van der Graaf Y, Mali W, Geerlings M (2010) Basal hypothalamic pituitary adrenal axis activity and hippocampal volumes: the SMART-Medea study. Biol Psychiatr 67(12):1191–1198
Kraus K, Canlon B (2012) Neuronal connectivity and interactions between the auditory and limbic systems. Effects of noise and tinnitus. Hear Res 288(1):34–46
Kraus K, Mitra S, Jimenez Z, Hinduja S, Ding D, Jiang H, Gray L, Lobarinas E, Sun W, Salvi R (2010) Noise trauma impairs neurogenesis in the rat hippocampus. Neurosci 167(4):1216–1226
Kretschmann H, Tafesse U, Herrmann A (1982) Different volume changes of cerebral cortex and white matter during histological preparation. Microsc Acta 86(1):13–24
Ladygina T, Mass A, Supin A (1978) Multiple sensory projections in the dolphin cerebral cortex. Zh Vyssh Nerv Deyat 28(5):1047–1053
Larsell O (1970) The comparative anatomy and histology of the cerebellum: from monotremes through apes, vol 2. University Of Minnesota Press, Minneapolis
Lyamin O, Manger P, Ridgway S, Mukhametov L, Siegel J (2008) Cetacean sleep: an unusual form of mammalian sleep. Neurosci Biobehav Rev 32(8):1451–1484

MacNeilage P (2013) Vertebrate whole-body-action asymmetries and the evolution of right handedness: a comparison between humans and marine mammals. Dev Psychobiol 55(6):577–587

Madsen P, Lammers M, Wisniewska D, Beedholm K (2013) Nasal sound production in echolocating delphinids (*Tursiops truncatus* and *Pseudorca crassidens*) is dynamic, but unilateral: clicking on the right side and whistling on the left side. J Exp Biol 216(21):4091–4102

Manger P (2006) An examination of cetacean brain structure with a novel hypothesis correlating thermogenesis to the evolution of a big brain. Biol Rev 81(02):293–338

Manger P (2013) Questioning the interpretations of behavioral observations of cetaceans: is there really support for a special intellectual status for this mammalian order? Neurosci 250:664–696

Manger P, Hemingway J, Haagensen M, Gilissen E (2010) Cross-sectional area of the elephant corpus callosum: comparison to other eutherian mammals. Neuroscience 167(3):815–824

Manger P, Prowse M, Haagensen M, Hemingway J (2012) Quantitative analysis of neocortical gyrencephaly in African elephants (*Loxodonta africana*) and six species of cetaceans: comparison with other mammals. J Comp Neurol 520(11):2430–2439

Marino L (1998) A comparison of encephalization between odontocete cetaceans and anthropoid primates. Brain Behav Evol 51(4):230–238

Marino L, Rilling J, Lin S, Ridgway S (2000) Relative volume of the cerebellum in dolphins and comparison with anthropoid primates. Brain Behav Evol 56(4):204–211

Marino L, Murphy T, Deweerd A, Morris J, Fobbs A, Humblot N, Ridgway S, Johnson J (2001a) Anatomy and three-dimensional reconstructions of the brain of the white whale (*Delphinapterus leucas*) from magnetic resonance images. Anat Rec 262(4):429–439

Marino L, Murphy T, Gozal L, Johnson J (2001b) Magnetic resonance imaging and three-dimensional reconstructions of the brain of a fetal common dolphin, *Delphinus delphis*. Anat Embryol 203(5):393–402

Marino L, Sudheimer K, Murphy T, Davis K, Pabst D, McLellan W, Rilling J, Johnson J (2001c) Anatomy and three-dimensional reconstructions of the brain of a bottlenose dolphin (*Tursiops truncatus*) from magnetic resonance images. Anat Rec 264(4):397–414

Marino L, Sudheimer K, Pabst D, Mclellan W, Filsoof D, Johnson J (2002) Neuroanatomy of the common dolphin (*Delphinus delphis*) as revealed by magnetic resonance imaging (MRI). Anat Rec 268(4):411–429

Marino L, Sudheimer K, Sarko D, Sirpenski G, Johnson J (2003) Neuroanatomy of the harbor porpoise (*Phocoena phocoena*) from magnetic resonance images. J Morphol 257(3):308–347

Marino L, McShea D, Uhen M (2004a) Origin and evolution of large brains in toothed whales. Anat Rec A 281(2):1247–1255

Marino L, Sherwood C, Delman B, Tang C, Naidich T, Hof P (2004b) Neuroanatomy of the killer whale (*Orcinus orca*) from magnetic resonance images. Anat Rec A 281(2):1256–1263

Marino L, Sudheimer K, Mclellan W, Johnson J (2004c) Neuroanatomical structure of the spinner dolphin (*Stenella longirostris orientalis*) brain from magnetic resonance images. Anat Rec A 279(1):601–610

Marino L, Sudheimer K, Pabst D, McLellan W, Arshad S, Naini G, Johnson J (2004d) Anatomical description of an infant bottlenose dolphin (*Tursiops truncatus*) brain from magnetic resonance images. Aquat Mamm 30(2):315–326

Marino L, Butti C, Connor R, Fordyce R, Herman L, Hof P, Lefebvre L, Lusseau D, McCowan B, Nimchinsky E (2008) A claim in search of evidence: reply to Manger's thermogenesis hypothesis of cetacean brain structure. Biol Rev 83(4):417–440

Marrif H, Juurlink B (1999) Astrocytes respond to hypoxia by increasing glycolytic capacity. J Neurosci Res 57(2):255–260

Martín E, Fernández M, Perea G, Pascual O, Haydon P, Araque A, Ceña V (2007) Adenosine released by astrocytes contributes to hypoxia-induced modulation of synaptic transmission. Glia 55(1):36–45

Maximino C (2009a) A quantitative test of the thermogenesis hypothesis of cetacean brain evolution, using phylogenetic comparative methods. Mar Freshw Behav Phy 42(1):1–17

Maximino C (2009b) Reply to Manger's Commentary on "A quantitative test of the thermogenesis hypothesis of cetacean brain evolution, using phylogenetic comparative methods". Mar Freshw Behav Phy 42(5):363–372

May P (2006) The mammalian superior colliculus: laminar structure and connections. Prog Brain Res 151:321–378

Mayes A, Montaldi D, Migo E (2007) Associative memory and the medial temporal lobes. Trends Cogn Sci 11(3):126–135

Mazzatenta A, Caleo M, Baldaccini N, Maffei L (2001) A comparative morphometric analysis of the optic nerve in two cetacean species, the striped dolphin (*Stenella coeruleoalba*) and fin whale (*Balaenoptera physalus*). Vis Neurosci 18:319–325

McArdle B (1988) The structural relationship: regression in biology. Can J Zool 66(11):2329–2339

McFarland W, Morgane P, Jacobs M (1969) Ventricular system of the brain of the dolphin, *Tursiops truncatus*, with comparative anatomical observations and relations to brain specializations. J Comp Neurol 135(3):275–367

McHugh T, Saykin A, Wishart H, Flashman L, Cleavinger H, Rabin L, Mamourian A, Shen L (2007) Hippocampal volume and shape analysis in an older adult population. Clin Neuropsychol 21(1):130–145

Meredith M, Stein B (1986) Visual, auditory, and somatosensory convergence on cells in superior colliculus results in multisensory integration. J Neurophysiol 56(3):640–662

Meyer J (1981) A quantitative comparison of the parts of the brains of two Australian marsupials and some eutherian mammals. Brain Behav Evol 18(1–2):60–71

Møhl B, Wahlberg M, Madsen P, Heerfordt A, Lund A (2003) The monopulsed nature of sperm whale clicks. J Acoust Soc Am 114(2):1143–1154

Montie E, Schneider G, Ketten D, Marino L, Touhey K, Hahn M (2007) Neuroanatomy of the subadult and fetal brain of the Atlantic White-sided Dolphin (*Lagenorhynchus acutus*) from in situ magnetic resonance images. Anat Rec 290(12):1459–1479

Montie E, Schneider G, Ketten D, Marino L, Touhey K, Hahn M (2008) Volumetric neuroimaging of the Atlantic White-Sided Dolphin (*Lagenorhynchus acutus*) brain from in situ magnetic resonance images. Anat Rec 291(3):263–282

Montie E, Wheeler E, Pussini N, Battey T, Barakos J, Dennison S, Colegrove K, Gulland F (2010) Magnetic resonance imaging quality and volumes of brain structures from live and post-mortem imaging of California sea lions with clinical signs of domoic acid toxicosis. Dis Aquat Org 91(3):243–256

Moore P, Dankiewicz L, Houser D (2008) Beamwidth control and angular target detection in an echolocating bottlenose dolphin (*Tursiops truncatus*). J Acoust Soc Am 124(5):3324–3332

Morey R, Petty C, Xu Y, Hayes J, Wagner H II, Lewis D, LaBar K, Styner M, McCarthy G (2009) A comparison of automated segmentation and manual tracing for quantifying hippocampal and amygdala volumes. Neuroimage 45(3):855–866

Morgane P, McFarland W, Jacobs M (1982) The limbic lobe of the dolphin brain: a quantitative cytoarchitectonic study. J Hirnforsch 23(5):465–552

Mortensen H, Pakkenberg B, Dam M, Dietz R, Sonne C, Mikkelsen B, Eriksen N (2014) Quantitative relationships in delphinid neocortex. Front Neuroanat 8:1–10

Ness A (1967) A measure of asymmetry of the skulls of odontocete whales. J Zool 153(2):209–221
Nummela S, Wägar T, Hemilä S, Reuter T (1999) Scaling of the cetacean middle ear. Hear Res 133(1):71–81
Oelschläger H (2008) The dolphin brain—a challenge for synthetic neurobiology. Brain Res Bull 75(2):450–459
Oelschläger H, Oelschläger J (2009) Brain. In: Perrin WF, Wursig B, Thewissen J (eds) Encyclopedia of marine mammals. Elsevier, Oxford
Oelschläger H, Haas-Rioth M, Fung C, Ridgway S, Knauth M (2007) Morphology and evolutionary biology of the dolphin (*Delphinus* sp.) brain—MR imaging and conventional histology. Brain Behav Evol 71(1):68–86
Oelschläger H, Ridgway S, Knauth M (2010) Cetacean brain evolution: Dwarf sperm whale (*Kogia sima*) and common dolphin (*Delphinus delphis*)–an investigation with high-resolution 3D MRI. Brain Behav Evol 75:33–62
Pack A, Herman L (1995) Sensory integration in the bottle nosed dolphin: immediate recognition of complex shapes across the senses of echolocation and vision. J Acoust Soc Am 98(2): 722–733
Pakkenberg B, Gundersen H (1997) Neocortical neuron number in humans: effect of sex and age. J Comp Neurol 384:312–320
Panin M, Gabai G, Ballarin C, Peruffo A, Cozzi B (2012) Evidence of melatonin secretion in cetaceans: plasma concentration and extrapineal HIOMT-like presence in the bottlenose dolphin *Tursiops truncatus*. Gen Comp Endocr 177(2):238–245
Patzke N, Spocter M, Bertelsen M, Haagensen M, Chawana R, Streicher S, Kaswera C, Gilissen E, Alagaili A, Mohammed O (2013) In contrast to many other mammals, cetaceans have relatively small hippocampi that appear to lack adult neurogenesis. Brain Struct Funct 1–23. Accessed 7 Oct 2015
Payne R, Webb D (1971) Orientation by means of long range acoustic signaling in baleen whales. Ann NY Acad Sci 188(1):110–141
Pfrieger F, Barres B (1997) Synaptic efficacy enhanced by glial cells in vitro. Science 277(5332):1684–1687
Pierson R, Corson P, Sears L, Alicata D, Magnotta V, O'Leary D, Andreasen N (2002) Manual and semiautomated measurement of cerebellar subregions on MR images. Neuroimage 17(1):61–76
Pilleri G (1972) Cerebral anatomy of the Platanistidae (*Platanista gangetica, Platanista indi, Pontoporia blainvillei, Inia geoffrensis*). Investig Cetacea 4:44–70
Pilleri G, Gihr M (1969) On the anatomy and behaviour of Risso's dolphin (*Grampus griseus* G. Cuvier). Investig Cetacea 1:74-93. Accessed 26 Jan 2015
Pilleri G, Gihr M (1970) The central nervous system of the mysticete and odontocete whales. Investig Cetacea 2:87–135
Pilleri G, Gihr M (1972) Contribution to the knowledge of the cetaceans of Pakistan with particular reference to the genera *Neomeris, Sousa, Delphinus, and Tursiops* and description of a new Chinese porpoise (*Neomeris asiaeorientalis*). Investig Cetacea 4:107–162
Pirlot P, Kamiya T (1985) Qualitative and quantitative brain morphology in the Sirenian *Dugong dugong* Erxl. J Zool Syst Evol Res 23(2):147–155
Poole J, Payne K, Langbauer W, Moss C (1988) The social contexts of some very low frequency calls of African elephants. Behav Ecol Sociobiol 22(6):385–392
Poth C, Fung C, Güntürkün O, Ridgway S, Oelschläger H (2005) Neuron numbers in sensory cortices of five delphinids compared to a physeterid, the pygmy sperm whale. Brain Res Bull 66(4):357–360
Quester R, Schröder R (1997) The shrinkage of the human brain stem during formalin fixation and embedding in paraffin. J Neurosci Meth 75(1):81–89
Rattenborg N, Amlaner C, Lima S (2000) Behavioral, neurophysiological and evolutionary perspectives on unihemispheric sleep. Neurosci Biobehav Rev 24(8):817–842
Reader S, Laland K (2002) Social intelligence, innovation, and enhanced brain size in primates. Proc Nat Acad Sci 99(7): 4436–4441
Reep R, O'Shea T (1990) Regional brain morphometry and lissencephaly in the Sirenia. Brain Behav Evol 35(4):185–194
Reep R, Finlay B, Darlington R (2007) The limbic system in mammalian brain evolution. Brain Behav Evol 70:57–70
Renaud D, Popper A (1975) Sound localization by the bottlenose porpoise *Tursiops truncatus*. J Exp Biol 63(3):569–585
Ridgway S (1986) Physiological observations on dolphin brains. In: Schusterman R, Thomas J, Wood F (eds) Dolphin cognition and behavior: a comparative approach. pp 31–60. Accessed 26 Jan 2015
Ridgway S (1990) The central nervous system of the bottlenose dolphin. In: Leatherwood S, Reeves R (eds) The bottlenose dolphin. pp 69–97. Accessed 8 Nov 2013
Ridgway S (2000) The auditory central nervous system of dolphins. In: Au W, Popper A, Fay R (eds) Hearing by whales and dolphins. Springer, New York, pp 273–293
Ridgway S, Brownson R (1984) Relative brain sizes and cortical surface areas in odontocetes. Acta Zool Fenn 172:149–152
Ridgway S, Hanson A (2014) Sperm whales and killer whales with the largest brains of all toothed whales show extreme differences in cerebellum. Brain Behav Evol 83(4):1–9
Ridgway S, Tarpley R (1996) Brain mass comparisons in Cetacea. Proc Int Assoc Aquat Anim Med 27:55–57
Ridgway S, Bullock T, Carder D, Seeley R, Woods D, Galambos R (1981) Auditory brainstem response in dolphins. Proc Natl Acad Sci 78(3):1943–1947
Ridgway S, Marino L, Lipscomb T (2002) Description of a poorly differentiated carcinoma within the brainstem of a white whale (*Delphinapterus leucas*) from magnetic resonance images and histological analysis. Anat Rec 268(4):441–449
Ridgway S, Houser D, Finneran J, Carder D, Keogh M, Van Bonn W, Smith C, Scadeng M, Dubowitz D, Mattrey R (2006) Functional imaging of dolphin brain metabolism and blood flow. J Exp Biol 209(15):2902–2910
Rilling J, Insel T (1999a) Differential expansion of neural projection systems in primate brain evolution. Neuroreport 10(7): 1453–1459
Rilling J, Insel T (1999b) The primate neocortex in comparative perspective using magnetic resonance imaging. J Hum Evol 37(2):191–223
Ringo J (1991) Neuronal interconnection as a function of brain size. Brain Behav Evol 38(1):1–6
Roth G, Dicke U (2005) Evolution of the brain and intelligence. Trends Cogn Sci 9(5):250–257
Ruscher K, Freyer D, Karsch M, Isaev N, Megow D, Sawitzki B, Priller J, Dirnagl U, Meisel A (2002) Erythropoietin is a paracrine mediator of ischemic tolerance in the brain: evidence from an in vitro model. J Neurosci 22(23):10291–10301
Säljö A, Bao F, Jingshan S, Hamberger A, Hansson H, Haglid K (2002) Exposure to short-lasting impulse noise causes neuronal c-Jun expression and induction of apoptosis in the adult rat brain. J Neurotraum 19(8):985–991
Schlenska G (1974) Volumen und Oberflächenmessungen an Gehirnen verschiedener Säugetiere im Vergleich zu einem errechneten Modell. J Hirnforsch 15:401–408
Schulz G, Crooijmans H, Germann M, Scheffler K, Müller-Gerbl M, Müller B (2011) Three-dimensional strain fields in human brain resulting from formalin fixation. J Neurosci Methods 202(1): 17–27

Seiffert E (2007) A new estimate of afrotherian phylogeny based on simultaneous analysis of genomic, morphological, and fossil evidence. BMC Evol Biol 7(1):224

Shoshani J, Kupsky W, Marchant G (2006) Elephant brain: Part I: gross morphology, functions, comparative anatomy, and evolution. Brain Res Bull 70(2):124–157

Shultz S, Dunbar R (2006) Both social and ecological factors predict ungulate brain size. Proc R Soc B 273(1583):207–215

Sinha S, Moss C (2007) Vocal premotor activity in the superior colliculus. J Neurosci 27(1):98–110

Širović A, Hildebrand J, Wiggins S (2007) Blue and fin whale call source levels and propagation range in the Southern Ocean. J Acoust Soc Am 122(2):1208–1215

Smith R (2005) Relative size versus controlling for size. Curr Anthropol 46(2):249–273

Stein B, Meredith M, Huneycutt W, McDade L (1989) Behavioral indices of multisensory integration: orientation to visual cues is affected by auditory stimuli. J Cogn Neurosci 1(1):12–24

Stephan H (1960) Methodische studien über den quantitativen vergleich architektonischer struktureinheiten des gehirns. Z Wiss Zool 164:143–172

Stephan H, Frahm H, Baron G (1981) New and revised data on volumes of brain structures in insectivores and primates. Folia Primatol 35:1–29

Swanson R, Farrell K, Stein B (1997) Astrocyte energetics, function, and death under conditions of incomplete ischemia: a mechanism of glial death in the penumbra. Glia 21(1):142–153

Sweatt J (2003) The hippocampus serves a role in multimodal information processing, and memory consolidation. Mechanisms of memory. Elsevier Academic Press, Oxford

Tarpley R, Ridgway S (1994) Corpus callosum size in delphinid cetaceans. Brain Behav Evol 44(3):156–165

Tyack P (1999) Communication and cognition. In: Reynolds JE, Rommel SA (eds) Biology of marine mammals. Smithsonian Institution Press, Washington, pp 287–323

Tyack P (2000) Functional aspects of cetacean communication. In: Mann J, Connor R, Tyack P, Whitehead H (eds) Cetacean societies: field studies of dolphins and whales. University of Chicago Press, Chicago, pp 270–307

Tyack P, Clark C (2000) Communication and acoustic behavior of dolphins and whales. In: Au W, Popper A, Fay R (eds) Hearing by whales and dolphins. Springer, New York, pp 156–224

Ullian E, Sapperstein S, Christopherson K, Barres B (2001) Control of synapse number by glia. Science 291(5504):657–661

Valentine D, Moss C (1997) Spatially selective auditory responses in the superior colliculus of the echolocating bat. J Neurosci 17(5):1720–1733

Verkhratsky A, Butt A (2013) Neuroglia: definition, classification, evolution, numbers, development. Glial physiology and pathophysiology, 1st edn. Wiley, New York, pp 73–104

von Fersen L, Schall U, Güntürkün O (2000) Visual lateralization of pattern discrimination in the bottlenose dolphin (*Tursiops truncatus*). Behav Brain Res 107(1):177–181

Walhovd K, Westlye L, Amlien I, Espeseth T, Reinvang I, Raz N, Agartz I, Salat D, Greve D, Fischl B (2011) Consistent neuroanatomical age-related volume differences across multiple samples. Neurobiol Aging 32(5):916–932

Walløe S, Eriksen N, Dabelsteen T, Pakkenberg B (2010) A neurological comparative study of the harp seal (*Pagophilus groenlandicus*) and harbor porpoise (*Phocoena phocoena*) brain. Anat Rec 293(12):2129–2135

Wartzok D, Ketten D (1999) Marine mammal sensory systems. In: Reynolds J, Rommel S (eds) Biology of marine mammals. Smithsonian Institution Press, Washington, pp 117–174

Washington S, Kanwal J (2012) Sex-dependent hemispheric asymmetries for processing frequency-modulated sounds in the primary auditory cortex of the mustached bat. J Neurophysiol 108(6):1548–1566

Watts D, Strogatz S (1998) Collective dynamics of 'small-world' networks. Nature 393(6684):440–442

Waxman S (1980) Determinants of conduction velocity in myelinated nerve fibers. Muscle Nerve 3(2):141–150

Wen Q, Chklovskii D (2005) Segregation of the brain into gray and white matter: a design minimizing conduction delays. Plos Comput Biol 1(7):e78

Whitehead H, Mann J (2000) Female reproductive strategies of cetaceans. In: Mann J, Connor R, Tyack P, Whitehead H (eds) Cetacean societies: field studies of dolphins and whales. University of Chicago Press, Chicago, pp 219–246

Wislocki G (1929) The hypophysis of the porpoise (*Tursiops truncatus*). Arch Surg 18(4):1403–1412

Wirsig B (2009) Intelligence and cognition. In: Perrin W, Wirsig B, Thewissen J (eds) Encyclopedia of marine mammals, 2nd edn. Academic Press, Cambridge, pp 616–623

Yaman S, von Fersen L, Dehnhardt G, Güntürkün O (2003) Visual lateralization in the bottlenose dolphin (*Tursiops truncatus*): evidence for a population asymmetry? Behav Brain Res 142(1):109–114

Yamazaki Y, Hozumi Y, Kaneko K, Sugihara T, Fujii S, Goto K, Kato H (2007) Modulatory effects of oligodendrocytes on the conduction velocity of action potentials along axons in the alveus of the rat hippocampal CA1 region. Neuron Glia Biol 3(04):325–334

Zhang K, Sejnowski T (2000) A universal scaling law between gray matter and white matter of cerebral cortex. Proc Nat Acad Sci 97(10):5621–5626

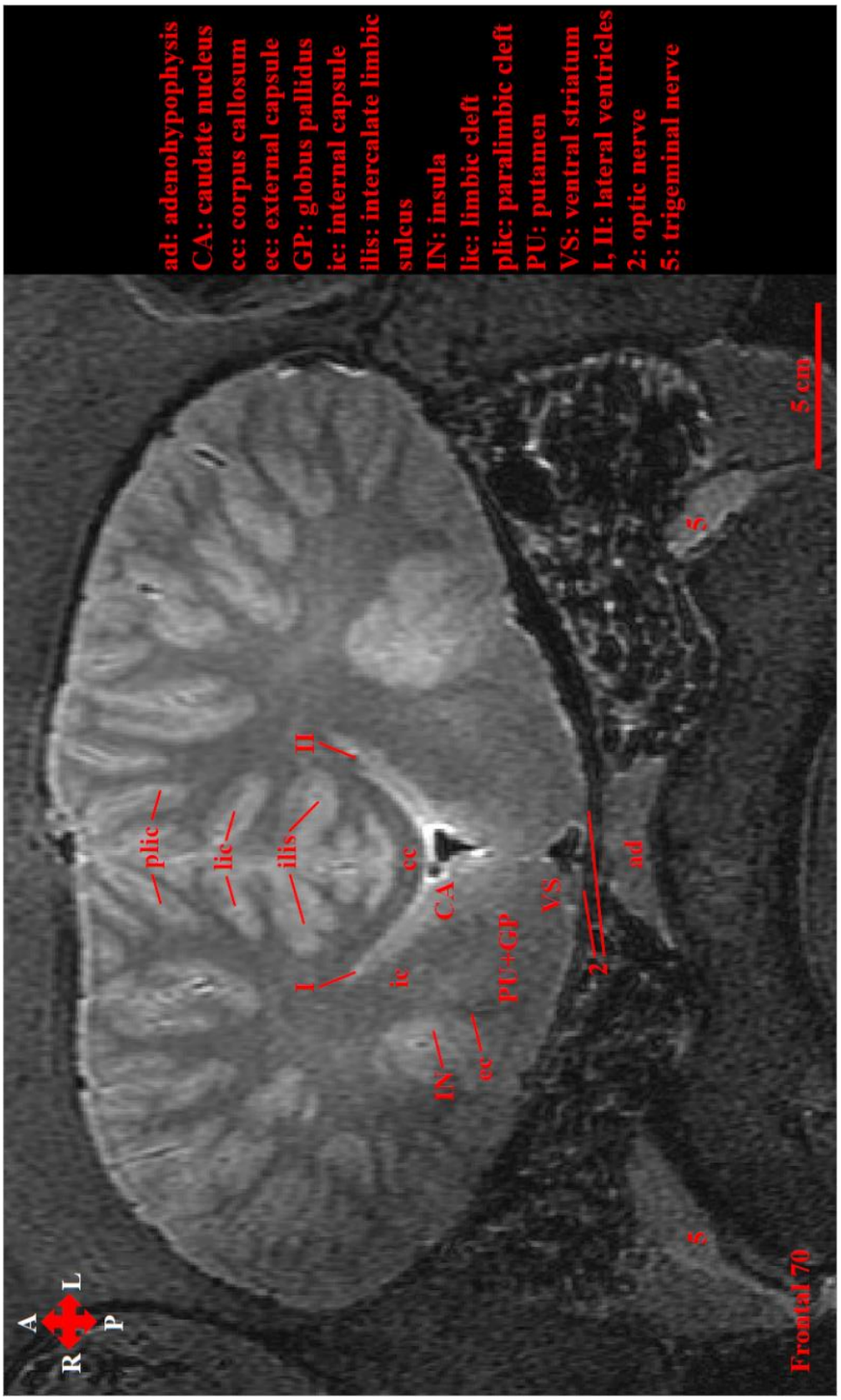

S. Figure 2.1: Annotated frontal, horizontal, and sagittal MR images of the *O. orca* brain. Anatomical directions: A (anterior), P (posterior), D (dorsal), V (ventral), R (right), and L (left).

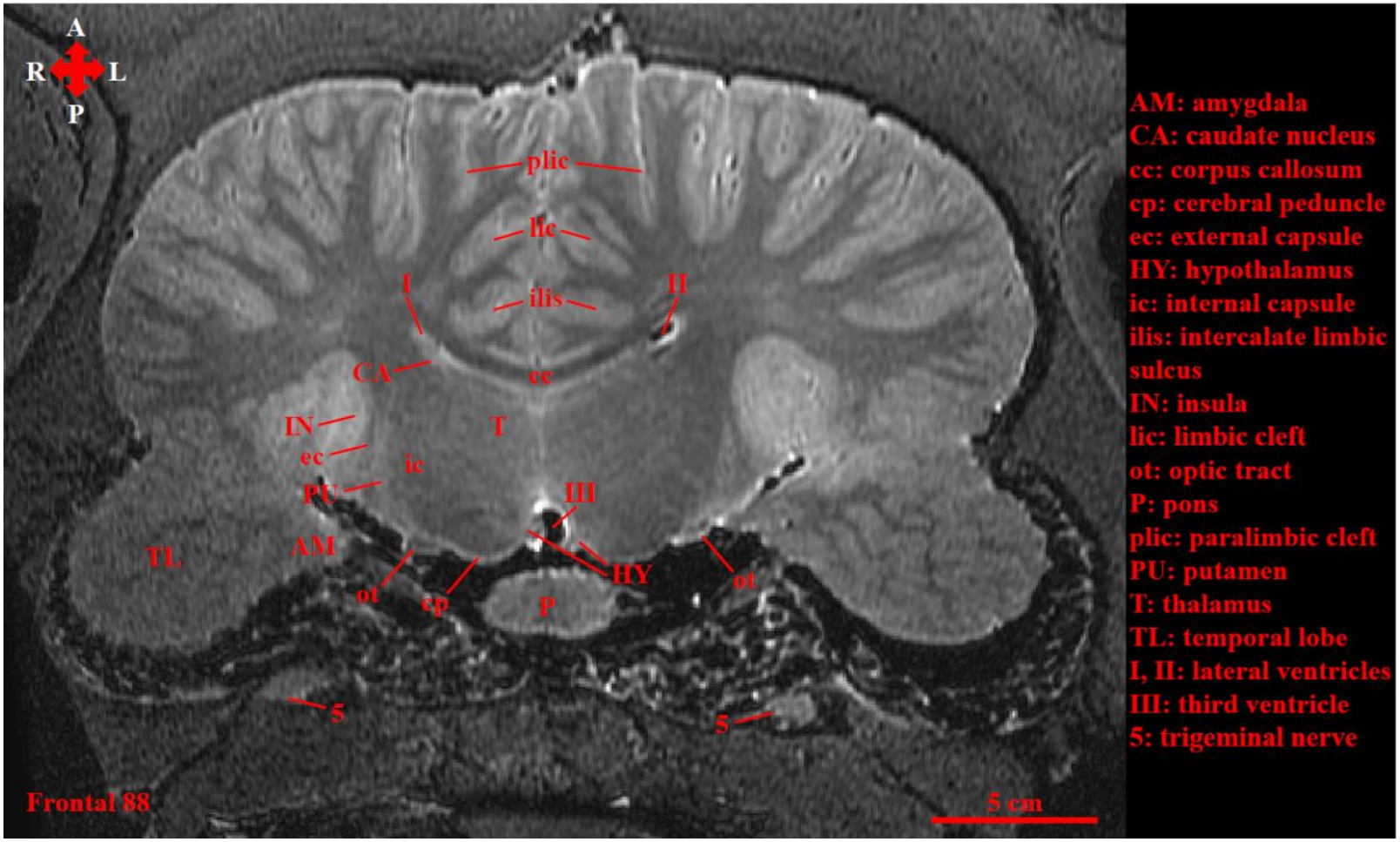

S. Figure 2.1: Annotated frontal, horizontal, and sagittal MR images of the *O. orca* brain. Anatomical directions: A (anterior), P (posterior), D (dorsal), V (ventral), R (right), and L (left).

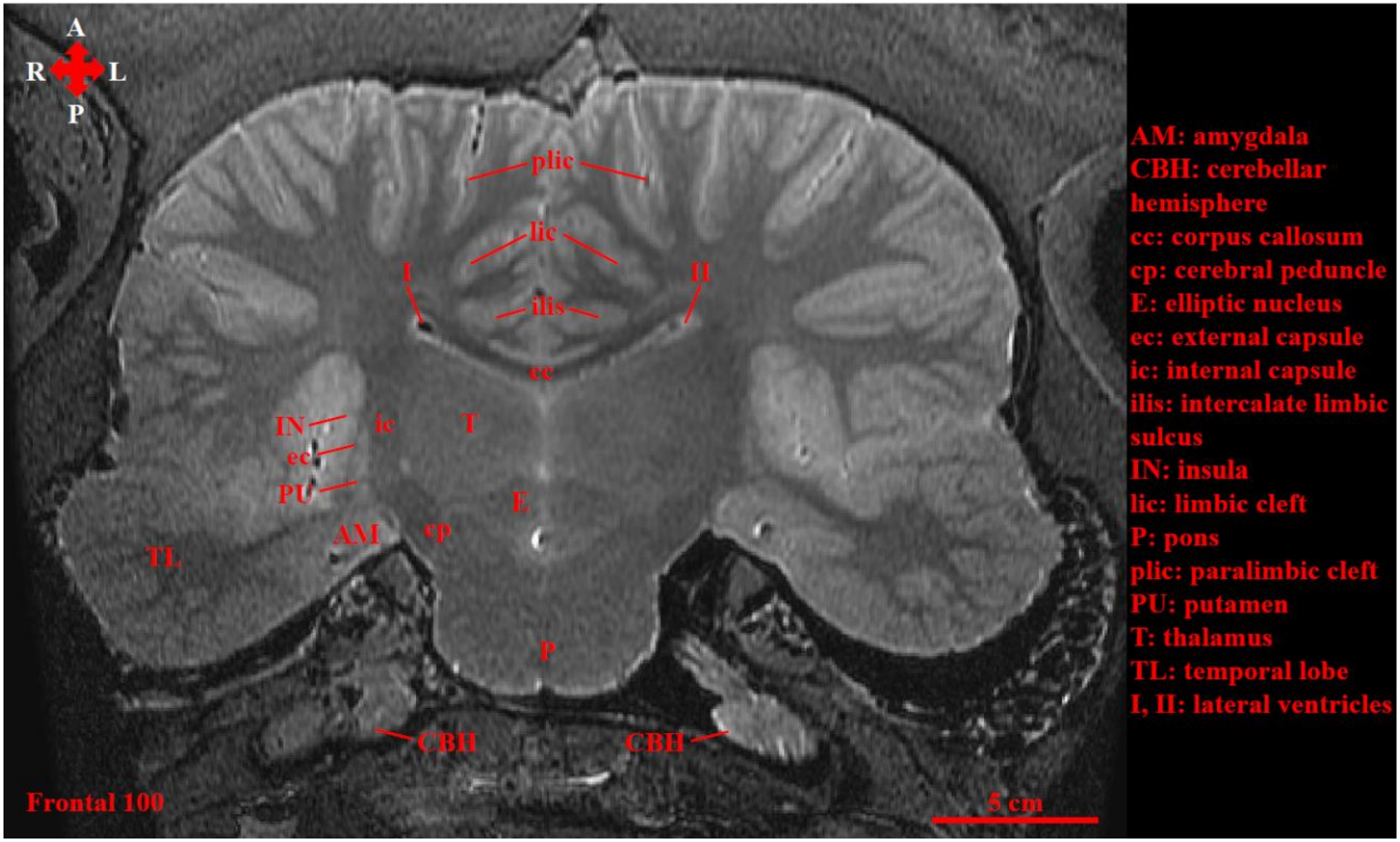

S. Figure 2.1: Annotated frontal, horizontal, and sagittal MR images of the *O. orca* brain. Anatomical directions: A (anterior), P (posterior), D (dorsal), V (ventral), R (right), and L (left).

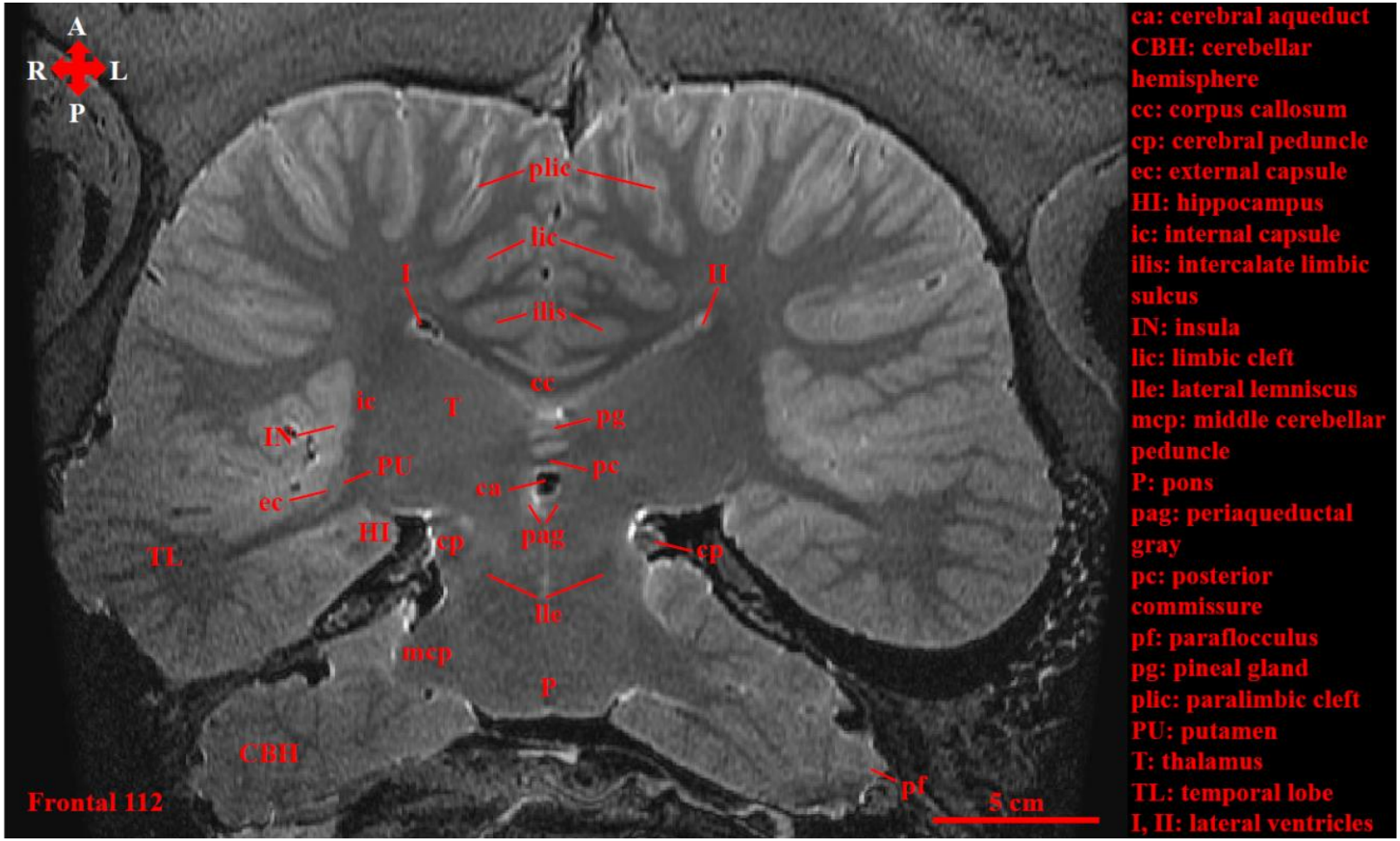

S. Figure 2.1: Annotated frontal, horizontal, and sagittal MR images of the *O. orca* brain. Anatomical directions: A (anterior), P (posterior), D (dorsal), V (ventral), R (right), and L (left).

S. Figure 2.1: Annotated frontal, horizontal, and sagittal MR images of the *O. orca* brain. Anatomical directions: A (anterior), P (posterior), D (dorsal), V (ventral), R (right), and L (left).

S. Figure 2.1: Annotated frontal, horizontal, and sagittal MR images of the *O. orca* brain. Anatomical directions: A (anterior), P (posterior), D (dorsal), V (ventral), R (right), and L (left).

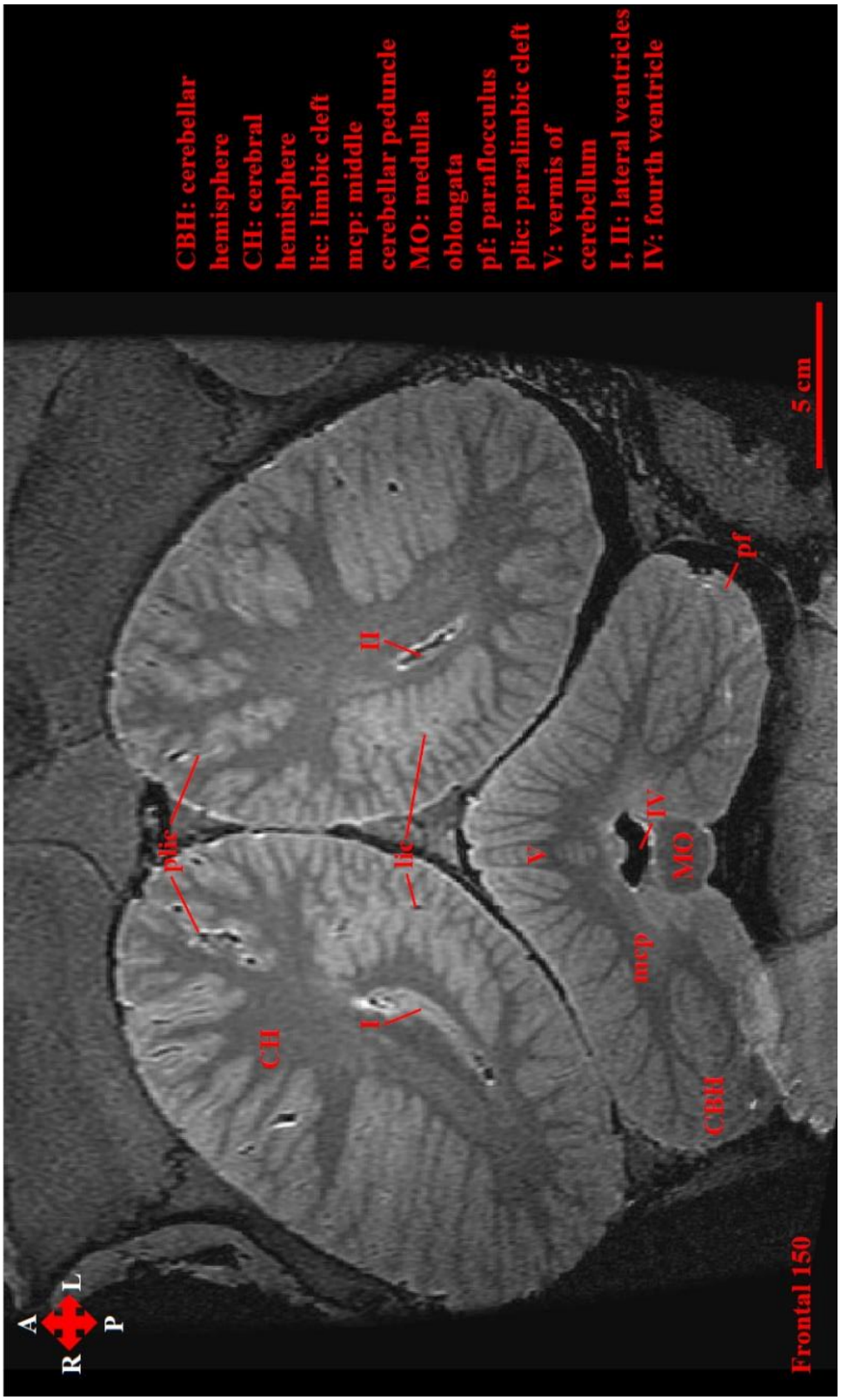

S. Figure 2.1: Annotated frontal, horizontal, and sagittal MR images of the *O. orca* brain. Anatomical directions: A (anterior), P (posterior), D (dorsal), V (ventral), R (right), and L (left).

S. Figure 2.1: Annotated frontal, horizontal, and sagittal MR images of the *O. orca* brain. Anatomical directions: A (anterior), P (posterior), D (dorsal), V (ventral), R (right), and L (left).

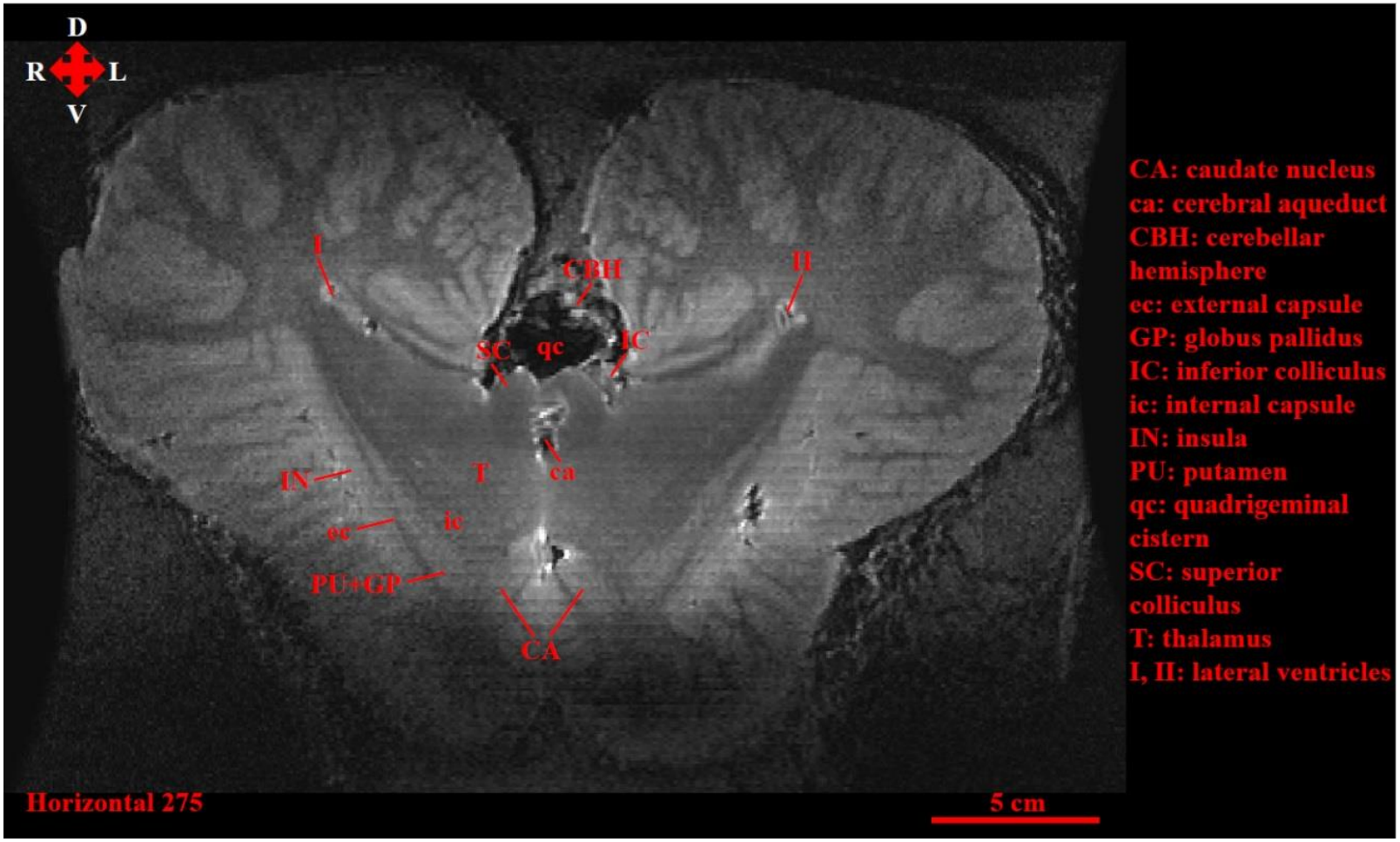

S. Figure 2.1: Annotated frontal, horizontal, and sagittal MR images of the *O. orca* brain. Anatomical directions: A (anterior), P (posterior), D (dorsal), V (ventral), R (right), and L (left).

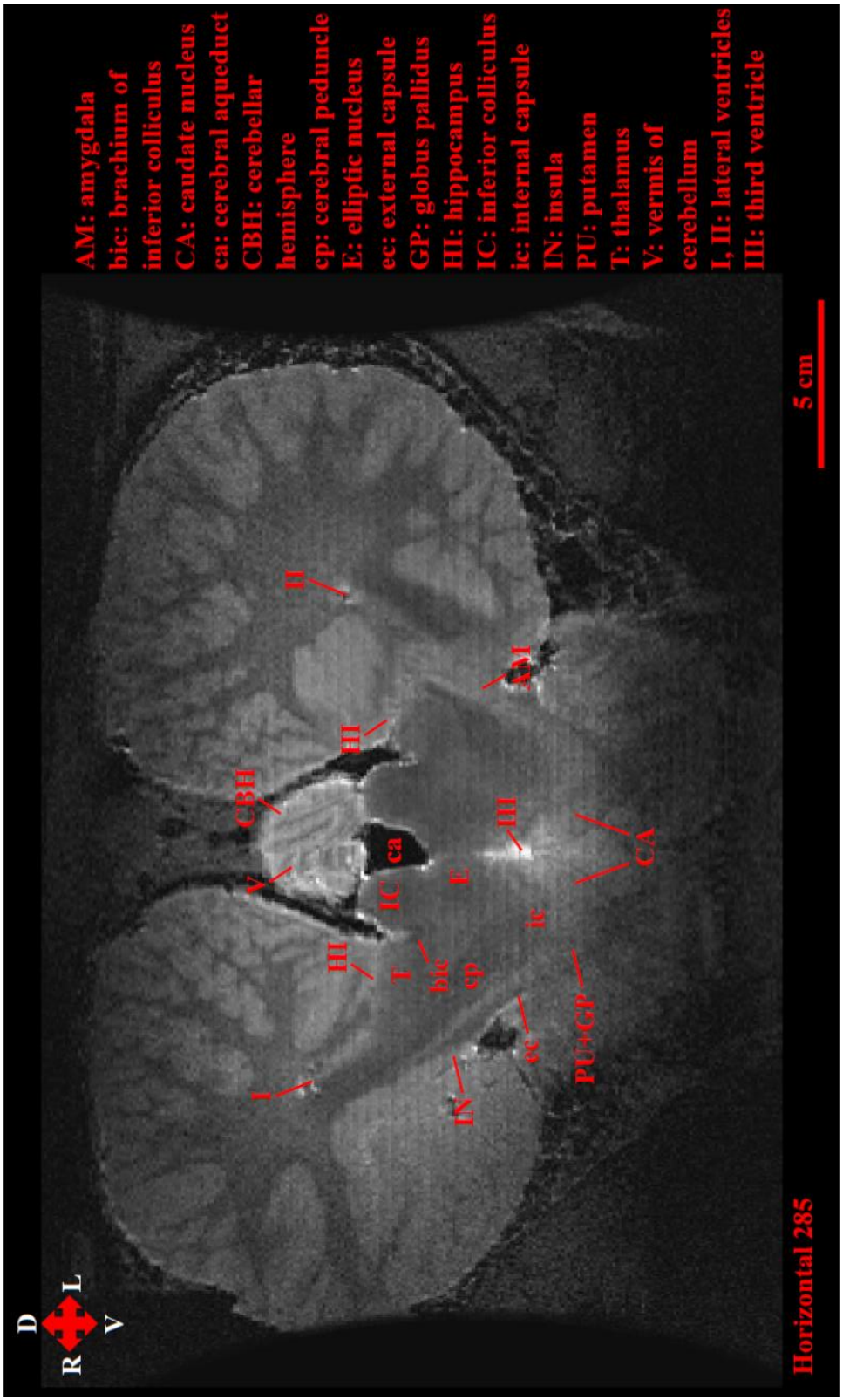

S. Figure 2.1: Annotated frontal, horizontal, and sagittal MR images of the *O. orca* brain. Anatomical directions: A (anterior), P (posterior), D (dorsal), V (ventral), R (right), and L (left).

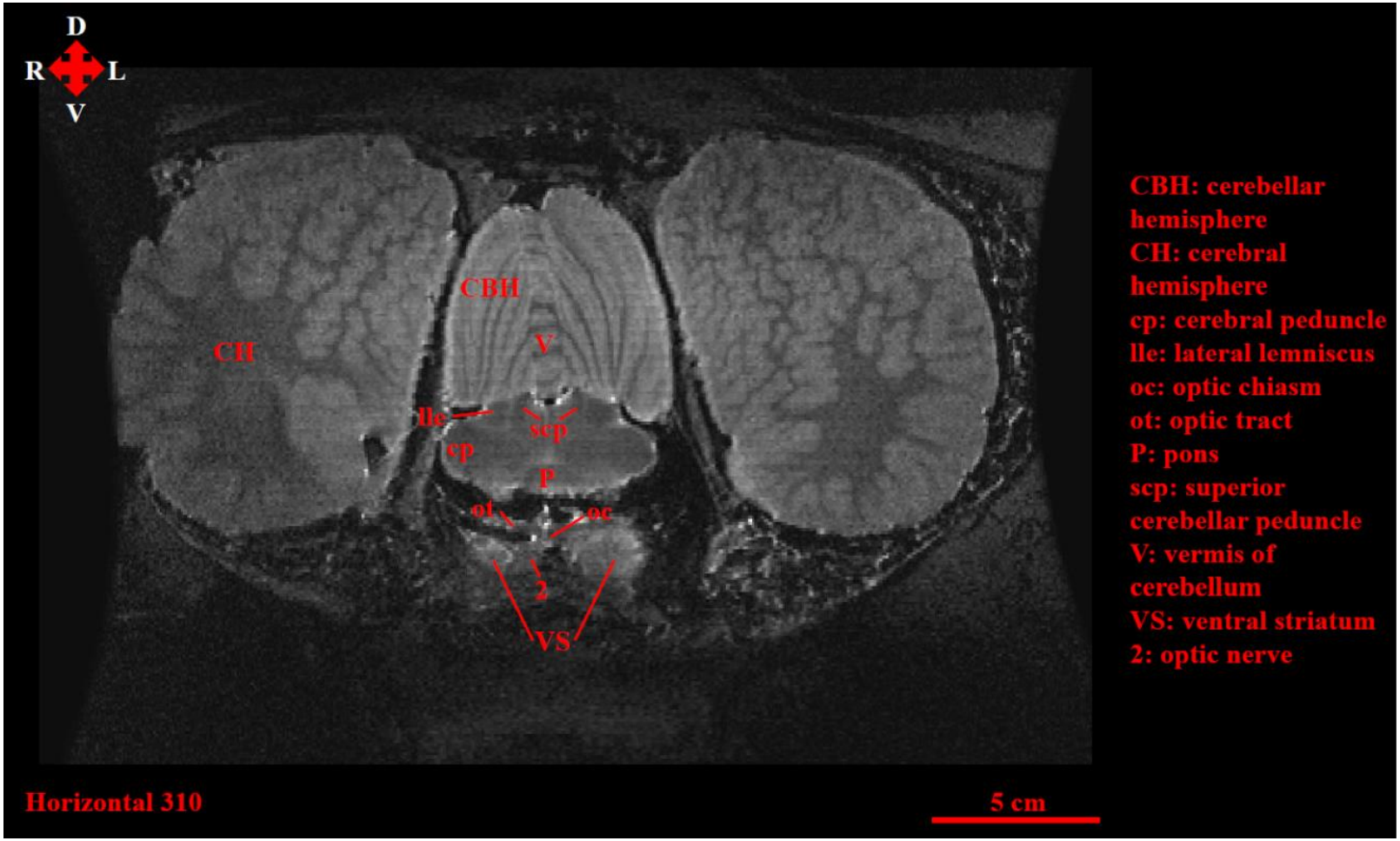

S. Figure 2.1: Annotated frontal, horizontal, and sagittal MR images of the *O. orca* brain. Anatomical directions: A (anterior), P (posterior), D (dorsal), V (ventral), R (right), and L (left).

S. Figure 2.1: Annotated frontal, horizontal, and sagittal MR images of the *O. orca* brain. Anatomical directions: A (anterior), P (posterior), D (dorsal), V (ventral), R (right), and L (left).

S. Figure 2.1: Annotated frontal, horizontal, and sagittal MR images of the *O. orca* brain. Anatomical directions: A (anterior), P (posterior), D (dorsal), V (ventral), R (right), and L (left).

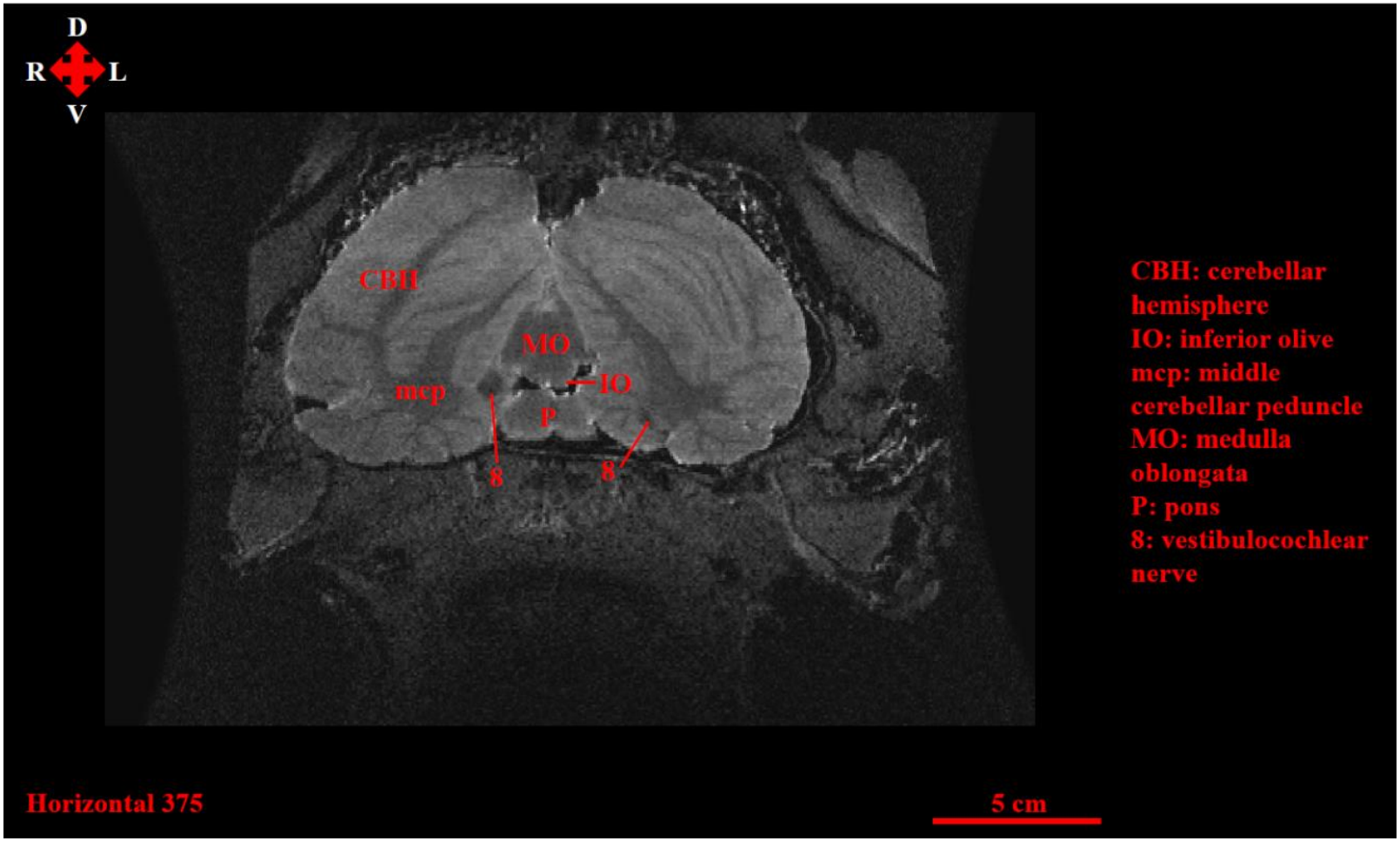

S. Figure 2.1: Annotated frontal, horizontal, and sagittal MR images of the *O. orca* brain. Anatomical directions: A (anterior), P (posterior), D (dorsal), V (ventral), R (right), and L (left).

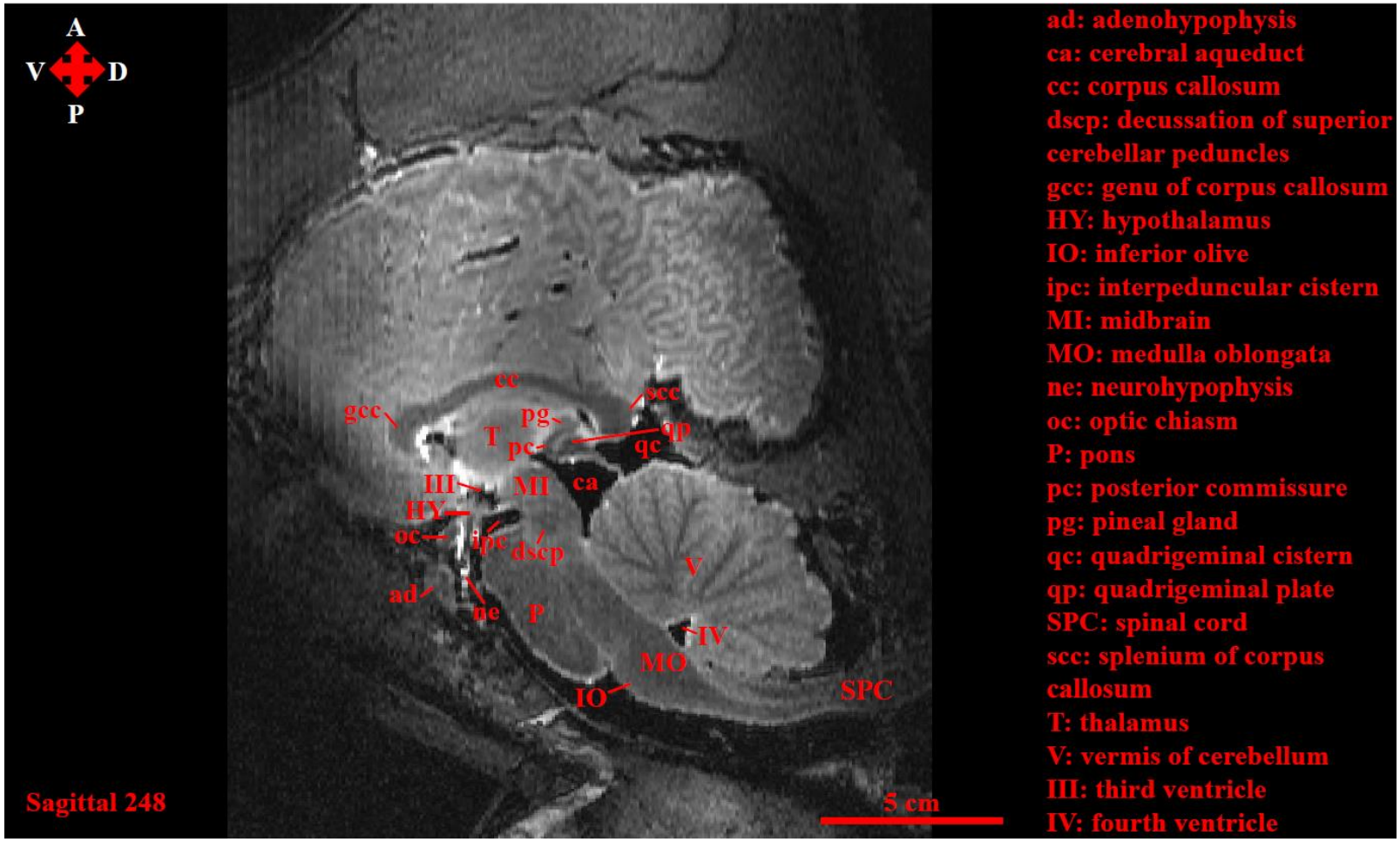

S. Figure 2.1: Annotated frontal, horizontal, and sagittal MR images of the *O. orca* brain. Anatomical directions: A (anterior), P (posterior), D (dorsal), V (ventral), R (right), and L (left).

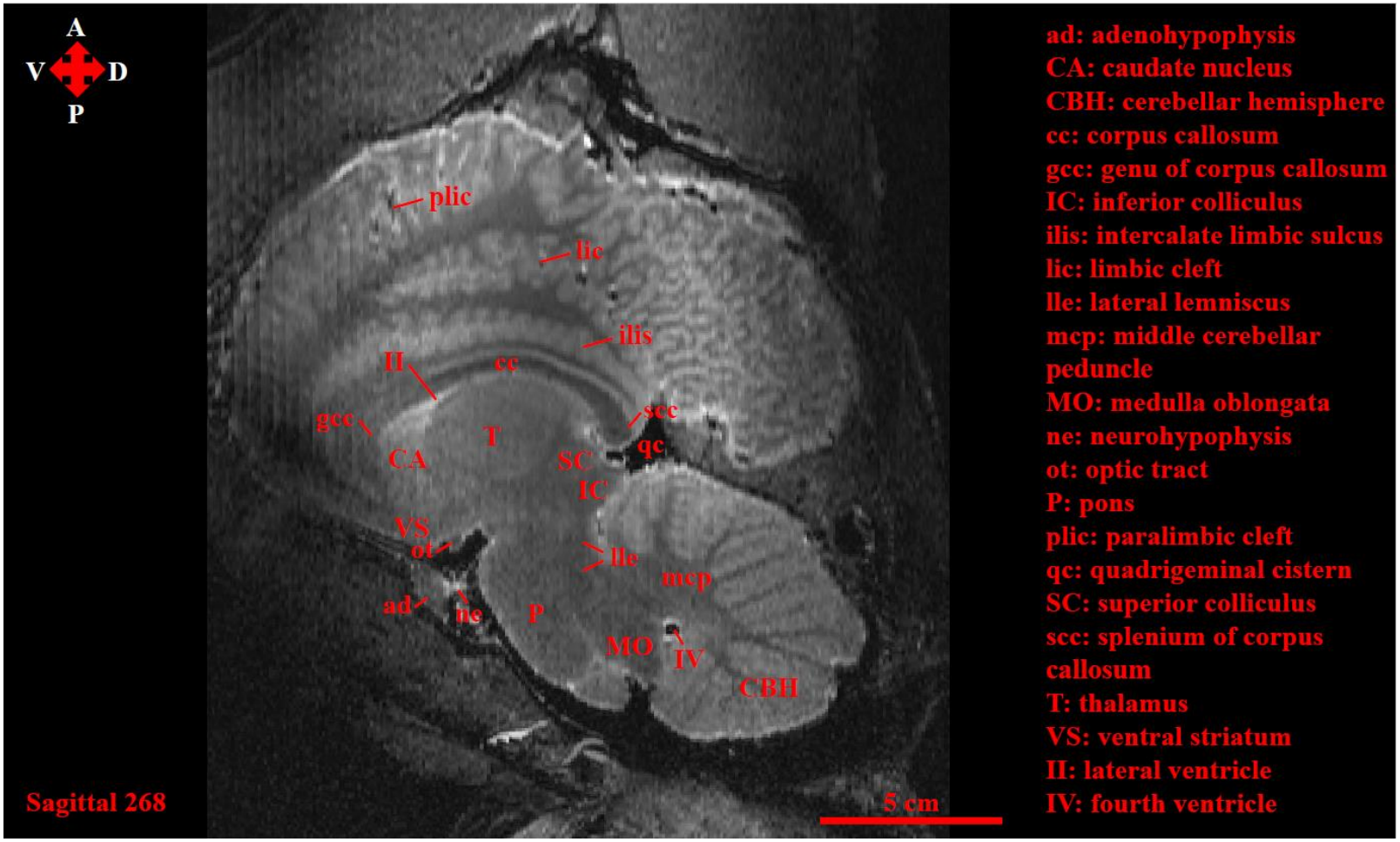

S. Figure 2.1: Annotated frontal, horizontal, and sagittal MR images of the *O. orca* brain. Anatomical directions: A (anterior), P (posterior), D (dorsal), V (ventral), R (right), and L (left).

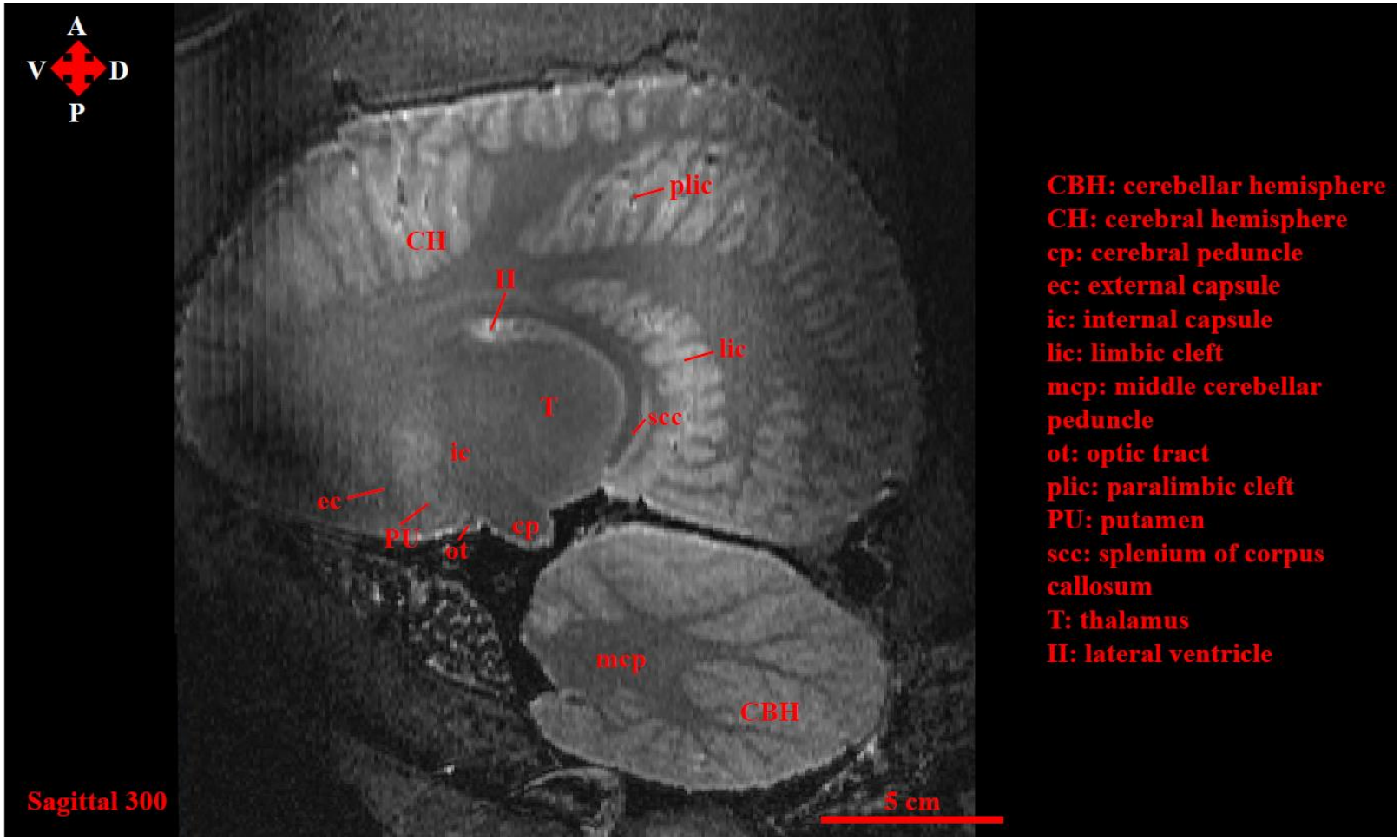

S. Figure 2.1: Annotated frontal, horizontal, and sagittal MR images of the *O. orca* brain. Anatomical directions: A (anterior), P (posterior), D (dorsal), V (ventral), R (right), and L (left).

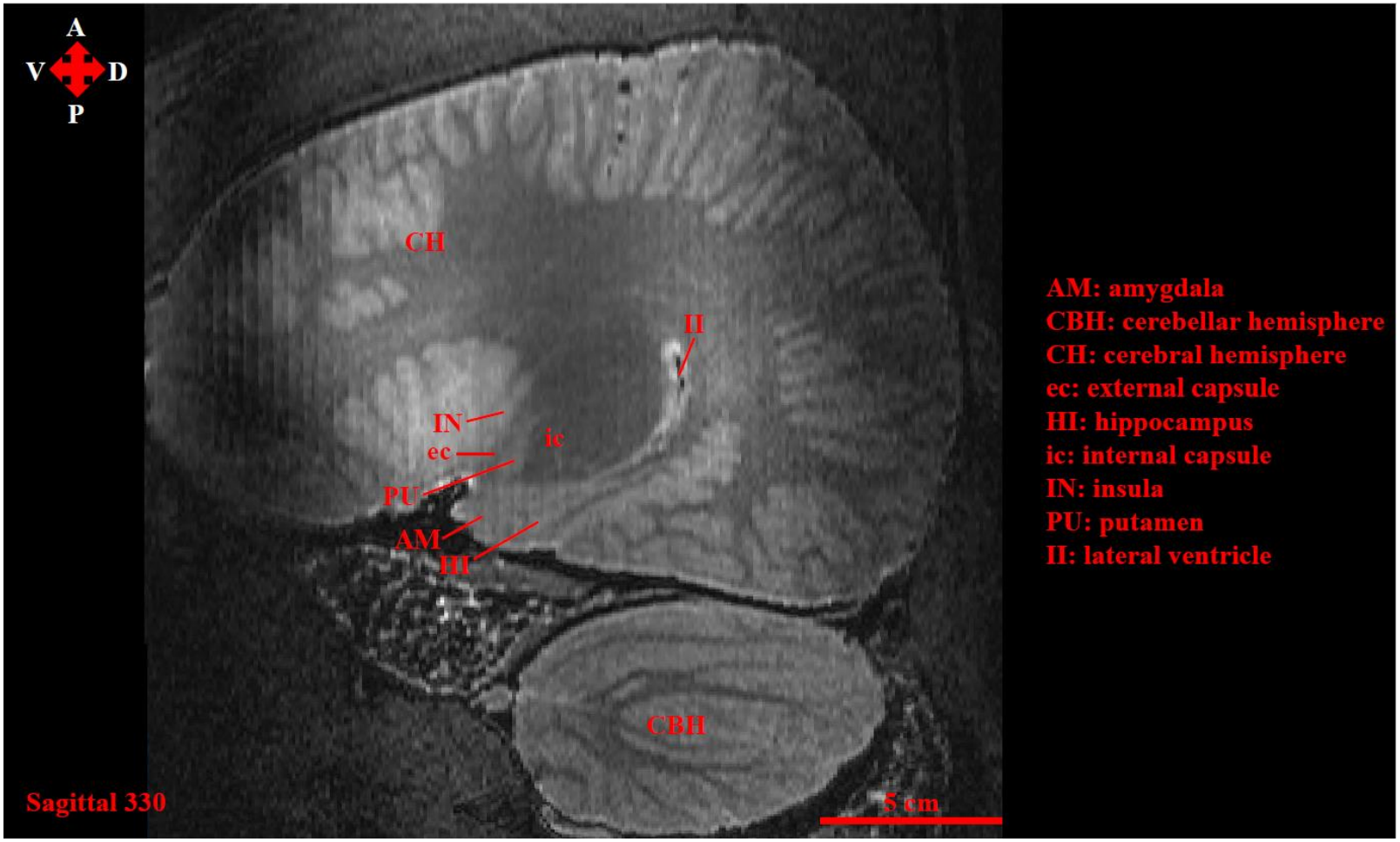

S. Figure 2.1: Annotated frontal, horizontal, and sagittal MR images of the *O. orca* brain. Anatomical directions: A (anterior), P (posterior), D (dorsal), V (ventral), R (right), and L (left).

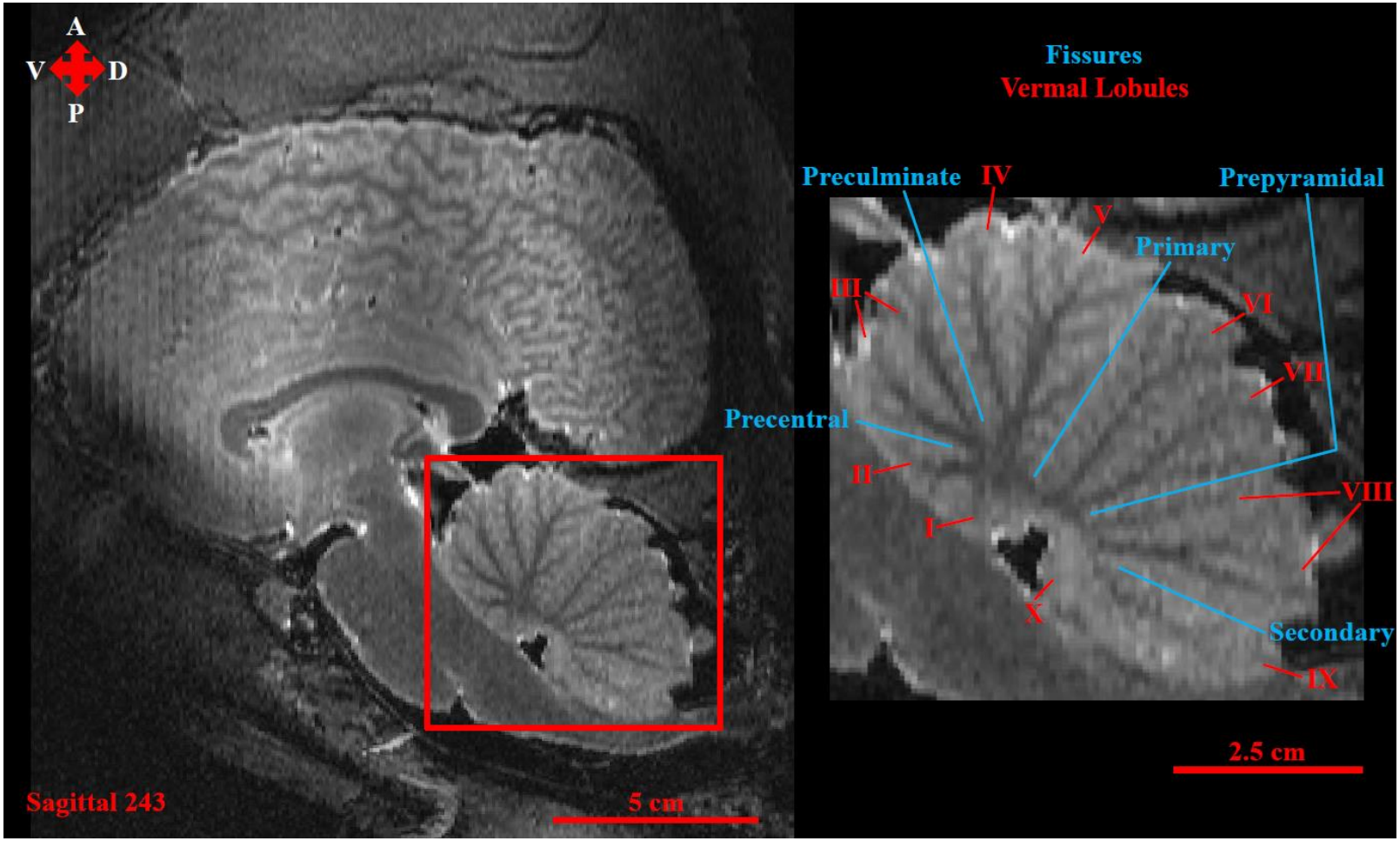

S. Figure 2.1: Annotated frontal, horizontal, and sagittal MR images of the *O. orca* brain. Anatomical directions: A (anterior), P (posterior), D (dorsal), V (ventral), R (right), and L (left).

Acknowledgements

Chapter 2, in its entirety, is a reprint of the peer-reviewed publication as it appears in Brain Structure and Function 2016. Citation: Wright, Alexandra; Scadeng, Miriam; Stec, Dominik; Dubowitz, Rebecca; Ridgway, Sam; St. Leger, Judy. 2016. Neuroanatomy of the killer whale (*Orcinus orca*): a magnetic resonance imaging investigation of structure with insights on function and evolution. *Brain Structure & Function*, 1–20. doi:10.1007/s00429-016-1225-x. The dissertation author was the primary investigator and author of this publication.

Chapter 3. Diffusion tractography reveals pervasive asymmetry of cerebral white matter tracts in the bottlenose dolphin (*Tursiops truncatus*)

Abstract

Brain enlargement is associated with concomitant growth of interneuronal distance, increased conduction time, and reduced neuronal interconnectivity. Recognition of these functional constraints led to the hypothesis that large-brained mammals should exhibit greater structural and functional brain lateralization. As a taxon with the largest brains in the animal kingdom, Cetacea provides a unique opportunity to examine asymmetries of brain structure and function. In the present study, diffusion tensor imaging and tractography were used to investigate cerebral white matter asymmetry in the bottlenose dolphin (*Tursiops truncatus*). Widespread white matter asymmetries were observed with the preponderance of tracts exhibiting leftward structural asymmetries. Leftward lateralization may reflect differential processing and execution of behaviorally variant sensory and motor functions by the cerebral hemispheres. The arcuate fasciculus, an association tract linked to human language evolution, was isolated and exhibited rightward asymmetry suggesting a right hemisphere bias for conspecific vocalizations unlike that of most mammals. This study represents the first examination of cetacean white matter asymmetry and constitutes an important step toward understanding potential drivers of structural asymmetry and its role in underpinning functional and behavioral lateralization in cetaceans.

Keywords

Arcuate fasciculus; Asymmetry; Bottlenose dolphin (*Tursiops truncatus*); Diffusion tensor imaging (DTI); Tractography; White matter

Introduction

Asymmetries of brain structure and function are found throughout the vertebrates (Rogers and Andrew 2002), varying in type and magnitude. An asymmetric or lateralized brain is characterized by anatomical or functional differences between its bilateral components, such as the cerebral hemispheres, cortical areas, or cerebral white matter tracts. It has been hypothesized that the extent of brain lateralization increases with increasing brain size (Ringo 1991; Ringo et al. 1994). This relationship is thought to arise through mechanisms to (1) avoid extreme and untenable brain enlargement consequent to the maintenance of complete neuronal interconnectivity (i.e., the number of neurons in which an individual neuron is directly connected) and (2) mitigate increased interhemispheric conduction delay in large brains resultant from longer transmission distances. The Ringo hypothesis contends that constraints on interconnectivity and conduction time inherent to the evolution of large brains may impose strict limits on global processing and favor local processing of related functions leading to the development of brain lateralization. Studies of cortical arealization (Northcutt and Kaas 1995; Kaas 2013) and hemispheric interconnectivity (Rilling and Insel 1999; Olivares, Michalland, and Aboitiz 2000; Olivares, Montiel, and Aboitiz 2001) provide evidence for enhanced local processing in large-brained mammals and suggest that greater structural

and functional lateralization may arise from increased intrahemispheric connections and hemispheric isolation via reduced commissural linkage.

Cetaceans (whales, dolphins, and porpoises) have the largest brains in the animal kingdom (Pilleri and Gihr 1970; Ridgway and Brownson 1984; Ridgway and Tarpley 1996; Ridgway and Hanson 2014). In accordance with the Ringo hypothesis (Ringo 1991; Ringo et al. 1994), a high degree of lateralization would be expected for large cetacean brains. Moreover, deviation from an otherwise evolutionarily conserved cerebral scaling law (Hofman 1989; Wright et al. 2016) in addition to selective pressures of the aquatic environment favoring continuous vigilance (Ridgway, Houser, et al. 2006; Ridgway, Carder, et al. 2006; Ridgway et al. 2009; Branstetter et al. 2012) would be predictive of increased hemispheric lateralization and functional independence of the cerebral hemispheres. Indeed, structural, functional, and behavioral lateralization has been observed throughout the Cetacea, including both the Odontoceti (echolocating toothed whales, dolphins, and porpoises) and Mysticeti (non-echolocating baleen whales). Asymmetry of cortical surface area (Ridgway and Brownson 1984) and subcortical and midbrain structure volumes (Montie et al. 2008; Wright et al. 2016) have been observed in a number of species of the cetacean family Delphinidae. Morphological asymmetry has also been reported for certain midbrain nuclei of balaenopterid mysticetes (Pilleri and Gihr 1970). Behavioral asymmetries indirectly linked to functional lateralization have been widely documented in odontocetes and mysticetes spanning various sensory, motor, cognitive, and social functions (MacNeilage 2013). Arguably the most striking form of functional lateralization observed in odontocetes is that of

unihemispheric slow wave sleep, a state of hemispheric incoherence (i.e., one cerebral hemisphere produces sleeping electroencephalograms (EEGs) while the contralateral hemisphere produces waking EEGs) thought to be important for the maintenance of locomotion, surface respiration, and vigilance toward conspecifics, predators, and prey by one cerebral hemisphere while simultaneously permitting sleep in the contralateral hemisphere (Supin et al. 1978; Goley 1999; Rattenborg, Amlaner, and Lima 2000; Ridgway 2002; Lyamin et al. 2008).

Though observations of anatomical, functional, and behavioral asymmetry have been reported in Cetacea, no previous studies have investigated white matter asymmetry in large cetacean brains and its potential functional implications. Therefore, the present study examined the extent of cerebral white matter asymmetry in *Tursiops truncatus*, a delphinid with an average absolute brain size larger than that of *Homo sapiens* and a relative brain size exceeding that of nonhuman anthropoid primates (Ridgway and Brownson 1984; Marino 1998). Diffusion tensor imaging (DTI) and tractography were used for the identification, measurement, and three-dimensional (3D) reconstruction of *T. truncatus* white matter tracts of the association, projection, and commissural fiber systems. The bilateral cerebral white matter tracts of this large *T. truncatus* brain exhibited pronounced lateralization associated with brain enlargement, unique cerebral scaling, and environmental selection pressures. The observation of pervasive asymmetry in cerebral white matter architecture of *T. truncatus* is proposed to reflect differential perception, processing, and production of social and nonsocial sensory signals and motor actions.

Materials and Methods

Specimen

The specimen examined was the formalin-fixed brain of a captive, 27-year-old, male *T. truncatus* (NAY, body length: 302 cm, body weight: 284 kg). The fresh mass of the specimen was 2093 g. Within 3 hours of death, the specimen was extracted, fixed whole in 10% phosphate-buffered formalin, and placed on a shaker to facilitate thorough penetration of the fixative. The specimen was kept for approximately 6 years in regularly changed buffered formalin. The cause of death was phytobezoar asphyxiation and non-neurological in nature.

Two additional specimens (i.e., one *T. truncatus* brain and one *Pseudorca crassidens* brain) were available for inclusion in this study but suboptimal data quality using the imaging protocol described below prohibited DTI analysis. This was potentially due to prolonged storage in fixative (i.e., approximately 20 years in buffered formalin).

Image acquisition and processing

Imaging was conducted at the University of California - San Diego Center for Functional Magnetic Resonance Imaging (fMRI) using a General Electric 3.0 T Signa 750 MRI system with an eight-channel head coil. T2-weighted [fast spin echo, repetition time (TR) = 5500 ms, echo time (TE) = 80 ms, matrix = 256 x 384 (re-gridded onto a 512 x 512 matrix), voxel size = 0.39 x 0.39 x 3 mm, field of view (FOV) = 200 mm, two-dimensional (2D) acquisition with 4 averages, 12 min collection] and T1-weighted [gradient echo, TR = 7.5 ms, TE = 3.2 ms, inversion time (TI) = 400 ms,

matrix = 256 x 256, flip angle = 11°, voxel size = 0.78 x 0.78 x 1.2 mm, FOV = 200 mm, 3D acquisition, 15 min collection] high-resolution anatomical images were acquired in the axial plane.

Diffusion tensor images were acquired in the axial plane using a single-shot echo planar imaging (EPI) sequence with diffusion-encoding along 60 directions, *b* value = 3000 s/mm^2, six non-diffusion weighted images (b_o), slice thickness = 3 mm, TR = 8 s, TE = 82 ms, 4 averages, matrix = 128 × 128 mm (automatically re-gridded onto a 128 × 128 matrix), FOV = 200 mm, 56 axial slices, and voxel size 0.78 × 0.78 × 3 mm. The DTI acquisition was repeated 3 times for a total scan time of 105 min.

Diffusion tensor imaging data were prepared using FMRIB Software Library (FSL), version 5.0.2.2 (http://www.fmrib.ox.ac.uk/fsl). Images from each DTI acquisition were concatenated (3 total) and corrected for eddy currents using the "eddy" tool provided by FSL. Eddy corrected DTI acquisitions were then fit to a diffusion model for each voxel using the FMRIB Diffusion Toolbox (FDT; (Behrens et al. 2003)). The diffusion tensor model was diagonalized to yield the three eigenvalues of the tensor in order to calculate fractional anisotropy (FA), mean diffusivity (M_D), axial diffusivity (A_D), and radial diffusivity (R_D) maps. R_D maps were calculated as the average of the second and third eigenvalue. The FA and the main eigenvector maps were converted and imported into DtiStudio for fiber tracking analysis.

Tractography and 3D reconstruction

Fiber tracking (i.e., streamline tracking) was performed in DtiStudio (Jiang et al. 2006) using the fiber assignment by continuous tracking (FACT) method (Mori et al. 1999). Tracking was terminated when the local fractional anisotropy (FA) fell below the FA threshold of 0.1, or when the tract-turning angle exceeded the angular threshold of 55^{o}. The selected FA threshold exceeded the cerebral gray matter FA of 0.04 ± 0.01 (mean ± standard deviation). The reduced diffusivity and anisotropy of this formalin-fixed specimen (Miller et al. 2011) necessitated a lower FA threshold compared to the default FA threshold (i.e., FA = 0.20) often used for *in vivo H. sapiens* studies.

A multiple region of interest (ROI) approach was used to reconstruct cerebral white matter tracts. ROIs were identified and manually delineated using FA maps, directionally encoded color maps (red: left-right, green: dorsal-ventral, blue: anterior-posterior), or HSV color images where appropriate. ROI placement was performed by one author (AKW) and replicated for each tract 3 times during different sessions on separate days. The ROI protocols implemented for each white matter tract are summarized in the Appendix. 3D volume rendering of the cerebrum and white matter tracts was performed using AMIRA software (FEI Visualization Sciences Group, Burlington, MA, USA).

Eight cerebral white matter tracts of the association, projection, and commissural fiber systems were reconstructed. The association tracts identified included the arcuate fasciculus, cingulum, external capsule and superior longitudinal fasciculus system. Moreover, the components of the superior longitudinal fasciculus system (SLF I, SLF II, and SLF III) were identified and isolated. The anterior thalamic radiation, corticocaudate

tract (i.e., the white matter of the caudate tail), and fornix comprised the projection tracts isolated. The forceps minor of the corpus callosum was the only commissural tract that could be reliably reconstructed.

Quantitative Analysis

Measurements of the volume [number of voxels containing at least one fiber (i.e., streamline) * voxel size; (Hagmann et al. 2006)], fiber number [number of reconstructed streamlines penetrating the ROI(s); (Jiang et al. 2006)], mean fiber length (mean length of reconstructed streamlines; (Jiang et al. 2006)), FA (degree of anisotropic diffusion; (Beaulieu 2014)), mean diffusivity (M_D; magnitude of diffusivity; (Beaulieu 2014)), axial diffusivity (A_D; parallel diffusivity; (Beaulieu 2014)), and radial diffusivity (R_D; perpendicular diffusivity; (Beaulieu 2014)) were acquired for each tract. Asymmetries of each tract-specific measurement were assessed by calculating the lateralization index (LI; (Vernooij et al. 2007)) according to the following equation:

$$LI\ (X) = (X_{Left} - X_{Right}) / (X_{Left} + X_{Right})$$

where X is the tract measurement (e.g., volume or FA). Lateralization index values ranged between -1 and 1. Positive values indicate that tract measurement X_{Left} is greater than tract measurement X_{Right}, whereas negative values indicate that tract measurement X_{Right} is greater than tract measurement X_{Left}. Index values approaching 0 ($-0.1 \leq LI\ (X) \leq 0.1$; (Vernooij et al. 2007; Seghier 2008)) indicate a comparable tract measurement X between the right and left cerebral hemispheres and thus, the absence of asymmetry. Calculations of the relative volume and relative fiber number were performed for each

tract to determine the percentage of the total volume or total fiber number occupied by the left and right tracts. The assessment of asymmetry was not performed for the forceps minor of the corpus callosum or fornix.

Results

3D reconstructions of the anterior thalamic radiation, arcuate fasciculus, cingulum, corticocaudate tract, external capsule, forceps minor of the corpus callosum, fornix, and superior longitudinal fasciculus system are shown in Figs. 1 and 2. Reconstructions of the sub-tracts of the superior longitudinal fasciculus system (SLF I, SLF II, and SLF III) are displayed in Fig. 2. Tract-specific measurements (repeated measures mean ± standard deviation) of volume, fiber number, mean fiber length, FA, M_D, A_D, and R_D are provided in Online Resources 1 and 2.

Asymmetries were found for the relative volumes of all of the tracts examined, with the exception of the anterior thalamic radiation, superior longitudinal fasciculus system, and sub-tract SLF II (Fig 3a). Rightward asymmetry was observed for the relative volumes of the arcuate fasciculus and SLF I, whereas the corticocaudate tract, cingulum, external capsule, and SLF III were leftwardly asymmetric. Asymmetries in relative fiber number were observed for nearly all tracts and were generally greater in magnitude than the volumetric asymmetries (Fig 3b). All of the asymmetric tracts examined exhibited a leftward bias in relative fiber number, except for the arcuate fasciculus and sub-tract SLF I which were right lateralized. Pronounced lateralization of relative fiber number was observed for the right arcuate fascicle and left SLF III, with each representing 79% and 94% of the total fiber number, respectively. Of all of the

tracts examined, the superior longitudinal fasciculus system and sub-tract SLF II were the only tracts to exhibit symmetry of relative fiber number.

Lateralization indices for tract volume, fiber number, and mean fiber length are shown in Fig. 4. Volumetric LI values indicated leftward asymmetries for all of the white matter tracts, except for the arcuate fasciculus and sub-tract SLF I, which were right lateralized, and the anterior thalamic radiation, superior longitudinal fasciculus system, and sub-tract SLF II, which exhibited no asymmetry ($-0.1 \leq$ LI (Volume) ≤ 0.1). Fiber number LI values indicated asymmetry for all of the tracts examined, except for the superior longitudinal fasciculus system and sub-tract SLF II. Positive LI values for fiber number were observed for the anterior thalamic radiation, corticocaudate tract, cingulum, external capsule, and SLF III, whereas the rightwardly asymmetric arcuate fasciculus and SLF I exhibited negative LI values. LI values corresponding to fiber number were greater than LI values for tract volume for all of the asymmetrical tracts excluding sub-tract SLF I. Asymmetry of mean fiber length was less widespread than that of volume and fiber number, with only a third of the tracts demonstrating lateralization. Of the six bilateral tracts examined, only the superior longitudinal fasciculus system exhibited consistent symmetry of LI values across tract-specific measurements of volume, fiber number, and mean fiber length. However, parcellation of the superior longitudinal fasciculus system into its subcomponents revealed pronounced lateralization of SLF I and SLF III. The preponderance of asymmetrical tracts and sub-tracts were left lateralized (Fig. 4).

There was an absence of lateralization ($-0.1 \leq$ LI (X) ≤ 0.1) for the measurements of FA, M_D, A_D, and R_D in all of the tracts examined (Online Resource 3), which suggests

that the tract-specific measurements of volume, fiber number, and mean fiber length were not confounded by these parameters and were indeed asymmetric. Moreover, symmetry of microstructural diffusion parameters and uniformity of the structural T1 dataset indicate that macrostructural asymmetries were not due to tissue damage or incomplete fixation of the specimen.

Discussion

The present study represents the first investigation of cerebral white matter asymmetry in a cetacean. Given the difficulty of obtaining cetacean specimens, particularly those of suitable quality for DTI analysis (*see Materials and Methods*), only one *T. truncatus* specimen was included in this investigation. Based on its species-appropriate brain mass (Pilleri and Gihr 1970; Tarpley and Ridgway 1994; Marino 1998) and comparatively normal appearance on structural MR images (Marino et al. 2001; Ridgway, Houser, et al. 2006; Hanson et al. 2013), it is not suspected that the macrostructural white matter asymmetry observed in this *T. truncatus* specimen was anomalous. Moreover, the demonstration of stability of macro- and microstructural white matter asymmetry in *H. sapiens* with aging (Takao et al. 2010; Stamatakis et al. 2011; Takao, Hayashi, and Ohtomo 2013; but cf. Ardekani et al. 2007; Bennett et al. 2010) suggests that the structural asymmetries, or lack thereof, observed in this 27-year-old *T. truncatus* were not associated with senescence. However, future DTI studies are required to examine *T. truncatus* specimens of varying age, sex, ecotype, and wild/captive status to increase confidence in the seminal results of this study and their interpretation.

The findings of this investigation suggest widespread structural asymmetries of cerebral white matter in this *T. truncatus* and provide support for the hypothesis that large brains should exhibit pronounced lateralization (Ringo 1991; Ringo et al. 1994). Moreover, the sparse reconstruction of the corpus callosum in this *T. truncatus* (Figs. 1 & 2) in parallel with various reports on the diminutive size of the cetacean corpus callosum relative to the volume of the cerebral hemispheres (Tarpley and Ridgway 1994; Keogh and Ridgway 2008; Montie et al. 2008; Manger et al. 2010; Berns et al. 2015; Wright et al. 2016) correspond to observations and predictions of reduced interhemispheric connectivity with brain enlargement (Ringo 1991; Ringo et al. 1994; Rilling and Insel 1999; Olivares, Michalland, and Aboitiz 2000; Olivares, Montiel, and Aboitiz 2001). In addition, it is quite plausible that distinctive structural scaling and selective pressures of the aquatic environment have also contributed to white matter asymmetry in *T. truncatus* and potentially other members of the order Cetacea. To address constraints on neuronal interconnectivity and transmission times associated with increased brain size, *T. truncatus* and other members of the cetacean superfamily Delphinoidea may have been selected for a unique cerebral scaling strategy that could further maximize brain lateralization. Whereas all other mammals exhibit allometric scaling of cerebral white matter (i.e., a disproportionate expansion of white matter compared to gray matter) (Barton and Harvey 2000; Zhang and Sejnowski 2000), the cerebral white matter of delphinoids scales isometrically with increasing brain size (Hofman 1989; Wright et al. 2016). Mammalian white matter hyperscaling is thought to arise from the need for thicker axons to increase conduction velocity in large brains that have greater interneuronal distances and consequently, require longer axonal connections (Chklovskii and Stevens

2000; Zhang and Sejnowski 2000; Changizi 2001); however, disproportionate expansion of white matter is insufficient to maintain complete neuronal interconnectivity and overcome significant transmission delays potentially promoting the clustering of related functions and ultimately, brain lateralization (Ringo 1991; Ringo et al. 1994; Changizi 2001). Without the compensatory mechanism of white matter hyperscaling, it may be suggested that the brains of delphinoids, and potentially other cetaceans, would be characterized by fewer connections and greater asymmetry than expected for a brain of the same size subject to typical mammalian allometric scaling. Moreover, the demands of an aquatic existence may necessitate continuous vigilance resulting in an extreme form of functional lateralization, unihemispheric slow wave sleep (Lyamin et al. 2008; Branstetter et al. 2012), feasibly supported by reduced interhemispheric connectivity (Figs. 1 & 2; Tarpley and Ridgway 1994) and the prevalent intrahemispheric white matter asymmetries revealed in this study (Figs. 2, 3, & 4).

The cerebral white matter asymmetry reported for *T. truncatus* complements previous evidence for structural, functional, and behavioral lateralization in Cetacea. Furthermore, examination of prior investigations in light of the findings of this study may provide insights into the functional significance of the structural lateralization observed. Along with neuroanatomical asymmetries of cortical surface area (Ridgway and Brownson 1984), gray matter volume (Montie et al. 2008; Wright et al. 2016), and intrahemispheric white matter volume and fiber number, delphinids and the wider Odontoceti exhibit varying degrees of asymmetry of the surrounding cranium and epicranial complex (i.e., an assemblage of nasal structures responsible for acoustic signal

generation; (Ness 1967; Cranford, Amundin, and Norris 1996)). Odontocete cranial and epicranial asymmetry may be related to the evolution of echolocation; however, it may alternatively be associated with laryngeal asymmetry facilitating prey capture (MacLeod et al. 2007) or directional hearing in water (Renaud and Popper 1975; Branstetter and Mercado 2006; Fahlke et al. 2011). Moreover, it has been proposed that epicranial asymmetry may facilitate the production of complex and diverse acoustic signals and cause marked lateralization of emitted sounds, resulting in the generation of a wide leftward beam and narrow rightward beam (Cranford, Amundin, and Norris 1996; Huggenberger, Vogl, and Oelschläger 2010; Frainer, Huggenberger, and Moreno 2015). Relevant to this interpretation is the demonstration of directional bias for the production of functionally distinct acoustic signals by delphinoids, including the *T. truncatus* of the present study (NAY; (Ridgway et al. 2009)), with their independently and simultaneously operable phonic lips (i.e., sound generators; (Cranford et al. 2011; Ridgway et al. 2015)). The delphinoids *T. truncatus*, *P. crassidens*, and *Phocoena phocoena* demonstrate a preference for emitting echolocation signals (i.e., predominantly nonsocial high-frequency, broad-band clicks) from the right pair of phonic lips (Ridgway et al. 2009; Madsen, Wisniewska, and Beedholm 2010; Madsen et al. 2013) and communication signals (i.e., social lower frequency whistles) from the left pair of phonic lips (Ridgway et al. 2009; Madsen et al. 2013). Since the presentation of auditory as well as visual and somatosensory stimuli evokes larger responses in the contralateral cerebral hemisphere in delphinoids (Bullock et al. 1968; Bullock and Ridgway 1972; Supin et al. 1978; Ridgway and Carder 1990; Ridgway et al. 2015), the directional emittance of behaviorally distinct sounds could promote differential processing by the right hemisphere for social

communicative information and the left hemisphere for nonsocial echolocative information. Specifically, the returning echoes of high frequency clicks generated by the right pair of phonic lips should reach the ipsilateral jaw first leading to earlier processing of echolocation information by the contralateral left hemisphere; whereas, perception of lower frequency whistles produced by the left pair of phonic lips should occur more rapidly with the ipsilateral jaw leading to earlier processing of communication signals in the contralateral right hemisphere. The aforesaid auditory schema for the asymmetric production, perception, and processing of acoustic signals of differing frequencies by delphinoids finds support in the Double Filtering by Frequency (DFF) theory proposed by Ivry and Roberston (1998). DFF theory is largely based on pitch perception experiments which indicate a left hemisphere bias for processing relatively high-frequency sounds and a right hemisphere bias for processing relatively low-frequency sounds (Ivry and Lebby 1993; Ivry and Robertson 1998). The pervasive white matter asymmetry of this *T. truncatus* (Figs. 2, 3, & 4) may underpin this proposed functional lateralization of frequency processing and the lateralized production of high-frequency echolocation clicks and lower frequency communication whistles observed *in vita* (NAY; (Ridgway et al. 2009)).

Of relevance to the lateralized processing of lower frequency communication signals in *T. truncatus* is the arcuate fasciculus (Figs. 1 & 2). In anthropoid primates, the arcuate fasciculus connects the frontal, parietal, and temporal lobes (Rilling et al. 2008; Rilling et al. 2012; Thiebaut de Schotten et al. 2012). Arcuate terminations in *H. sapiens* include Broca's territory (i.e., speech production), Wernicke's area (i.e., speech

comprehension), and proximal areas (Catani, Jones, and Ffytche 2005; Rilling et al. 2008). Moreover, the arcuate fasciculus of the primates *Pan troglodytes* and *Macaca mulatta* connects homologs of Broca's and Wernicke's areas (Catani, Jones, and Ffytche 2005; Rilling et al. 2012) associated with the production of orofacial expressions (Petrides, Cadoret, and Mackey 2005) and communicative signals (i.e., gestural and vocal signaling; (Taglialatela et al. 2008)) as well as the perception of conspecific vocalizations (Gil-da-Costa et al. 2006). Compared to nonhuman primates, the arcuate fasciculus of *H. sapiens* is considerably different exhibiting unique structural elaboration and cortical terminations thought to be associated with the evolution of language (Rilling et al. 2008). In *H. sapiens* and *P. troglodytes*, the arcuate fasciculus is predominantly left lateralized (Catani et al. 2007; Glasser and Rilling 2008; Thiebaut de Schotten et al. 2011; Rilling et al. 2012; Fernández-Miranda et al. 2014) indicating a left hemisphere specialization for species-specific communication. In contrast, the arcuate fasciculus of *T. truncatus* exhibited pronounced rightward asymmetry (Figs. 2, 3, & 4). If the arcuate terminations of *T. truncatus* are functionally homologous to that of primates, then this finding may suggest a right hemisphere bias for conspecific vocalization in agreement with behavioral observations demonstrating directional bias for the production of social communication signals (i.e., lower frequency whistles; (Ridgway et al. 2009; Madsen et al. 2013)). Interestingly, the right hemisphere bias for conspecific vocalizations proposed for *T. truncatus* contrasts with substantial evidence for left lateralization of communicative functions in nearly all other mammals studied to date (Ocklenburg, Ströckens, and Güntürkün 2013). A recent DTI study identified a direct auditory pathway from the inferior colliculus to the ipsilateral temporal lobe in the delphinids, *Delphinus delphis* and

Stenella attenuata (Berns et al. 2015); however, structural asymmetry of this pathway was not assessed in that study nor could it be evaluated in the present study due to susceptibility artifacts in the data localized in the brainstem. It would be of interest in future DTI investigations of *T. truncatus* and other cetaceans to compare the lateralization of this direct auditory pathway to that of the arcuate fasciculus. In addition to the proposed functional lateralization of conspecific acoustic signals, arcuate asymmetry may also be relevant to accumulating reports of behavioral lateralization in delphinoids regarding visual (Karenina et al. 2010; Thieltges et al. 2011; Karenina, Giljov, Glazov, et al. 2013; Karenina, Giljov, Ivkovich, et al. 2013; Yeater et al. 2014) and somatosensory (Johnson and Moewe 1999; Sakai et al. 2006; Hill et al. 2015) social signaling.

Regarding the proposed left hemisphere bias for the perception, processing, and production of nonsocial echolocation signals (i.e., high frequency clicks), it is interesting to note that in *T. truncatus* the majority of bilateral tracts were left lateralized. Increased tract size could reflect greater axonal diameter, axon abundance, or degree of myelination, all of which are factors associated with increased conduction velocity (Hursh 1939; Waxman 1980). The symmetries of microstructural diffusion parameters (i.e., FA, M_D, A_D, and R_D) found for all tracts and sub-tracts suggest that increased white matter volume and potentially higher conduction velocity is correlated with greater axon abundance in this *T. truncatus*; however, future histological studies are needed to determine the extent to which asymmetrical tract volumes reflect differences in axonal diameter, abundance, or myelination in cetaceans. Ultimately, the preponderance of

enlarged tracts in the left cerebral hemisphere of *T. truncatus* (Figs. 2, 3, & 4) could reflect a requirement for rapid analysis of high frequency echolocation signals transmitted within an aquatic medium that quadruples sound velocity. Widespread leftward structural asymmetries along with lateralized production of echolocation clicks by the right pair of phonic lips (Ridgway et al. 2009; Madsen, Wisniewska, and Beedholm 2010; Madsen et al. 2013; Ridgway et al. 2015) suggest a left hemisphere bias for nonsocial echolocative vocalization. Moreover, the cetacean left hemisphere has previously been implicated in predatory locomotor activity. Odontocetes and mysticetes both exhibit rightward biases during foraging behaviors including strand, mud plume, and lunge feeding, fish chasing and herding, and rolling during feeding dives (MacNeilage 2013; Karenina et al. 2016). The observation of largely left lateralized bilateral tracts in *T. truncatus* may be correlated with both echolocative function and the strong rightward action asymmetries observed in Cetacea allowing for rapid and responsive perception and pursuit of prey.

Brain enlargement, isometric cerebral white matter scaling, and the unique demands of the aquatic environment may each potentially contribute to the widespread intrahemispheric white matter asymmetries observed in the present study of the *T. truncatus* brain. As the first investigation of cetacean white matter asymmetry, this study provides a heretofore undescribed neuroanatomical basis for functional and behavioral lateralization in delphinids and potentially other cetaceans. Reviewing the available literature, pervasive asymmetry of white matter architecture is tentatively proposed to reflect lateralization of social and nonsocial sensory and motor functions. Moreover, the

detection of a right lateralized arcuate fasciculus raises interesting and important questions about the nature of cetacean communication and the plasticity of hemispheric specialization. Future DTI or fMRI studies of *T. truncatus* and other cetaceans are needed to characterize cerebral white matter asymmetry across a wide range of individuals and species, and more specifically, to establish the predominant directionality of arcuate lateralization and elucidate the function of arcuate cortical terminations. The growing availability of wide-bore MRI systems capable of accommodating larger animals may facilitate future fMRI studies of delphinids. With proper preparation, delphinids can be trained to slide out of the water and sit in a scanner (Ridgway, Houser, et al. 2006). Moreover, delphinids can echolocate while out of water (Finneran et al. 2010). With such animals and imaging equipment, great progress can be made in understanding the organization and function of the cetacean brain.

Appendix: ROI protocols

The reconstruction protocols for each tract of interest involved different permutations of three DtiStudio operations, OR, AND, or NOT (Jiang et al. 2006). The OR operation permitted the initial selection of fibers with the placement of the first ROI on an anatomical landmark. Placement of a second ROI with the AND operation restricted the selected fibers to those that penetrated both the first and second ROIs. ROIs applied with the NOT operation removed the circumscribed subset of fibers from the previously selected tract.

Arcuate fasciculus

In mid-sagittal view, select the coronal slice 18 mm anterior to the splenium of the corpus callosum. In this coronal slice, draw the first ROI (OR operation) around the superior longitudinal fasciculus core and branches of the suprasylvian, ectosylvian, and perisylvian gyri, located dorsolateral to the internal capsule. Place a second ROI (AND operation) around the temporally-projecting fibers of the arcuate fasciculus on the axial slice 21 mm dorsal to the genu of the corpus callosum when viewed mid-sagittally.

Anterior thalamic radiation

In mid-sagittal view, select the coronal slice 12 mm anterior to the splenium of the corpus callosum. In this coronal slice, draw the first ROI (OR operation) around the entire thalamus. Draw a second ROI (AND operation) around the anterior limb of the internal capsule in the coronal slice at the level of the anteriormost portion of the genu of the corpus callosum when viewed mid-sagittally. Place subsequent ROIs (NOT operation) to remove: (a) fibers extending to the contralateral hemisphere; (b) fibers extending ventrally and posteriorly from the thalamus; (c) callosal fibers; (d) corticocaudate fibers; and (e) stray fibers.

Cingulum

In mid-sagittal view, select the coronal slice at the level of the anteriormost portion of the genu of the corpus callosum. In this coronal slice, draw the first ROI (OR operation) around the cingulum, located dorsal to the corpus callosum. Place a second ROI (AND operation) around the cingulum on the coronal slice 15 mm posterior to the genu of the corpus callosum (near the callosal midpoint) when viewed mid-sagittally.

Draw subsequent ROIs (NOT operation) to remove: (a) callosal fibers; and (b) stray fibers.

Corticocaudate tract

In mid-sagittal view, select the axial slice at the level of the dorsalmost portion of the body of the corpus callosum. In this axial slice, draw the first ROI (OR operation) around the caudate nucleus. Place a second ROI (AND operation) around the caudate nucleus in the coronal slice at the level of the mid-splenium of the corpus callosum when viewed mid-sagittally. Place subsequent ROIs (NOT operation) to remove: (a) anterior fibers extending ventrally; (b) callosal fibers; (c) corona radiata fibers; (d) internal capsule fibers; (e) thalamic fibers; and (f) stray fibers.

External capsule

In mid-sagittal view, select the coronal slice at the level of the anteriormost portion of the fornix. In this coronal slice, draw the first ROI (OR operation) around the external capsule, located lateral to the internal capsule. Place subsequent ROIs (NOT operation) to remove: (a) fibers extending to the contralateral hemisphere; (b) internal capsule fibers; and (c) stray fibers.

Forceps minor of the corpus callosum

In mid-sagittal view, select the coronal slice at the level of the anteriormost portion of the genu of the corpus callosum. In this coronal slice, draw the first ROI (OR operation) around the genu of the corpus callosum. The callosal genu and first ROI exhibit a distinct butterfly shape. Place subsequent ROIs (NOT operation) to remove: (a)

fibers extending posteriorly from the genu; (b) cingulum fibers; (c) internal capsule fibers; (d) obvious non-bilaterally projecting fibers apparent in the anterior and ventral portions of the forceps minor; and (e) stray fibers. In order to isolate the bilaterally projecting fibers of the forceps minor, place a final ROI (AND operation) around the genu of the corpus callosum when viewed mid-sagittally.

Fornix

In mid-sagittal view, select the coronal slice 3 mm posterior to the anteriormost portion of the fornix. In this coronal slice, draw the first ROI (OR operation) around the fornix, located ventral to the corpus callosum and septum pellucidum tract. Place subsequent ROIs (NOT operation) to remove: (a) fibers medial to the anterior columns of the fornix; (b) callosal fibers; and (c) septum pellucidum tract fibers.

Superior longitudinal fasciculus

In mid-sagittal view, select the coronal slice 18 mm anterior to the splenium of the corpus callosum. In this coronal slice, draw the first ROI (OR operation) around the superior longitudinal fasciculus core and branches of the suprasylvian, ectosylvian, and perisylvian gyri, located dorsolateral to the internal capsule. Place a second ROI (AND operation) around the superior longitudinal fasciculus core and branches in the coronal slice at the level of the anteriormost portion of the genu of the corpus callosum when viewed mid-sagittally. Place subsequent ROIs (NOT operation) to remove: (a) arcuate fasciculus fibers; (b) external capsule fibers; (c) internal capsule fibers; (d) lateral gyrus fibers; and (e) stray fibers.

In order to isolate the subcomponents of the superior longitudinal fasciculus system (SLF I, SLF II, SLF III), placement of additional ROIs on the coronal slice 18 mm anterior to the splenium of the corpus callosum is required. For SLF I, a ROI (AND operation) was drawn around the white matter of the suprasylvian gyrus. For SLF II, a ROI (AND operation) was drawn around the white matter of the ectosylvian gyrus. Due to the lack of an apparent demarcation between the SLF I and SLF II within the superior longitudinal fasciculus core, an arbitrary line was drawn from the lateralmost base of the SLF I branch to the dorsalmost portion of the lateral ventricle to separate SLF I and SLF II core fibers. A ROI (AND operation) was drawn around the white matter of the perisylvian gyrus to isolate SLF III.

Funding

AKW was supported by the National Science Foundation Graduate Research Fellowship Program, Scripps Institution of Oceanography Graduate Department, and University of California, San Diego Graduate Division. The funders had no role in the study design, data collection, analysis, or interpretation, preparation of the manuscript, or decision to publish.

Acknowledgements

Chapter 3, in its entirety, has been submitted for publication as it may appear in Brain Structure and Function 2016. Wright, Alexandra K.; Theilmann, Rebecca J.; Ridgway, Sam H., Scadeng, Miriam. (*in review*). Diffusion tractography reveals pervasive asymmetry of cerebral white matter tracts in the bottlenose dolphin (*Tursiops*

truncatus). The dissertation author was the primary investigator and author of this publication.

References

Ardekani, S, A Kumar, G Bartzokis, and U Sinha. 2007. "Exploratory Voxel-Based Analysis of Diffusion Indices and Hemispheric Asymmetry in Normal Aging." *Magn Reson Imaging* 25: 154–67. doi:10.1016/j.mri.2006.09.045.

Barton, R A, and P H Harvey. 2000. "Mosaic Evolution of Brain Structure in Mammals." *Nature* 405 (6790): 1055–58. doi:10.1038/35016580.

Beaulieu, C. 2014. "The Biological Basis of Diffusion Anisotropy." In *Diffusion MRI: From Quantitative Measurement to in-Vivo Neuroanatomy*, edited by H Johansen-Berg and T E J Behrens, 2nd ed., 155–83. Elsevier Academic Press. doi:10.1016/B978-0-12-374709-9.00006-7.

Behrens, T E J, M W Woolrich, M Jenkinson, H Johansen-Berg, R G Nunes, S Clare, P M Matthews, J M Brady, and S M Smith. 2003. "Characterization and Propagation of Uncertainty in Diffusion-Weighted MR Imaging." *Magn Reson Med* 50: 1077–88. doi:10.1002/mrm.10609.

Bennett, Ilana J., David J. Madden, Chandan J. Vaidya, Darlene V. Howard, and James H. Howard. 2010. "Age-Related Differences in Multiple Measures of White Matter Integrity: A Diffusion Tensor Imaging Study of Healthy Aging." *Hum Brain Mapp* 31: 378–90. doi:10.1002/hbm.20872.

Berns, G S, P F Cook, S Foxley, S Jbabdi, K L Miller, and L Marino. 2015. "Diffusion Tensor Imaging of Dolphin Brains Reveals Direct Auditory Pathway to Temporal Lobe." *P Roy Soc B* 282: 20151203. doi:http://dx.doi.org/10.1098/rspb.2015.1203.

Branstetter, B K, J J Finneran, E A Fletcher, B C Weisman, and S H Ridgway. 2012. "Dolphins Can Maintain Vigilant Behavior through Echolocation for 15 Days without Interruption or Cognitive Impairment." *Plos One* 7 (10): e47478. doi:http://dx.doi.org/10.1371/journal.pone.0047478.

Branstetter, B K, and E Mercado. 2006. "Sound Localization by Cetaceans." *Int J Comp Psychol* 19: 26–61. doi:http://escholarship.org/uc/item/28c0q755.

Bullock, T H, and S H Ridgway. 1972. "Evoked Potentials in the Central Auditory System of Alert Porpoises to Their Own and Artifical Sounds." *J Neurobiol* 3 (1): 79–99. doi:10.1007/978-1-4684-9427-3_35.

Bullock, T. H., A. D. Grinnell, E. Ikezono, K. Kameda, Y. Katsuki, M. Nomoto, O. Sato, N. Suga, and K. Yanagisawa. 1968. "Electrophysiological Studies of Central

Auditory Mechanisms in Cetaceans." *Z Vergl Physiol* 59 (2): 117–56. doi:10.1007/BF00339347.

Catani, M, M P G Allin, M Husain, L Pugliese, M M Mesulam, R M Murray, and D K Jones. 2007. "Symmetries in Human Brain Language Pathways Correlate with Verbal Recall." *P Nat Acad Sci* 104 (43): 17163–68. doi:10.1073/pnas.0702116104.

Catani, M, D K Jones, and D H Ffytche. 2005. "Perisylvian Language Networks of the Human Brain." *Ann Neurol* 57 (1): 8–16. doi:10.1002/ana.20319.

Changizi, M A. 2001. "Principles Underlying Mammalian Neocortical Scaling." *Bio Cybern* 84 (3): 207–15. doi:10.1007/s004220000205.

Chklovskii, D B, and C F Stevens. 2000. "Wiring Optimization in the Brain." In *Advances in Neural Information Processing Systems 12*, 12:103–7. MIT Press.

Cranford, T W, M Amundin, and K S Norris. 1996. "Functional Morphology and Homology in the Odontocete Nasal Complex: Implications for Sound Generation." *J Morphol* 228 (3): 223–85. doi:10.1002/(SICI)1097-4687(199606)228:3<223::AID-JMOR1>3.0.CO;2-3.

Cranford, T W, W R Elsberry, W G Van Bonn, J A Jeffress, M S Chaplin, D J Blackwood, D A Carder, T Kamolnick, M A Todd, and S H Ridgway. 2011. "Observation and Analysis of Sonar Signal Generation in the Bottlenose Dolphin (Tursiops Truncatus): Evidence for Two Sonar Sources." *J Exp Mar Biol Ecol* 407 (1). Elsevier B.V.: 81–96. doi:10.1016/j.jembe.2011.07.010.

Fahlke, J M, P D Gingerich, R C Welsh, and A R Wood. 2011. "Cranial Asymmetry in Eocene Archaeocete Whales and the Evolution of Directional Hearing in Water." *P Natl Acad Sci* 108 (35): 14545–48. doi:10.1073/pnas.1108927108.

Fernández-Miranda, J C, Y Wang, S Pathak, L Stefaneau, T Verstynen, and Fang C Yeh. 2014. "Asymmetry, Connectivity, and Segmentation of the Arcuate Fascicle in the Human Brain." *Brain Struct Funct* 220: 1665–80. doi:10.1007/s00429-014-0751-7.

Finneran, J J, D S Houser, P W Moore, B K Branstetter, J S Trickey, and S H Ridgway. 2010. "A Method to Enable a Bottlenose Dolphin (Tursiops Truncatus) to Echolocate While out of Water." *J Acoust Soc Am* 128 (3): 1483–89. doi:10.1121/1.3471915.

Frainer, G, S Huggenberger, and I B Moreno. 2015. "Postnatal Development of Franciscana's (Pontoporia Blainvillei) Biosonar Relevant Structures with Potential Implications for Function, Life History, and Bycatch." *Mar Mamm Sci*, 1–20. doi:10.1111/mms.12211.

Gil-da-Costa, R, A Martin, M A Lopes, M Muñoz, J B Fritz, and A R Braun. 2006. "Species-Specific Calls Activate Homologs of Broca's and Wernicke's Areas in the Macaque." *Nature Neurosci* 9 (8): 1064–70. doi:10.1038/nn1741.

Glasser, M. F., and J. K. Rilling. 2008. “DTI Tractography of the Human Brain’s Language Pathways.” *Cereb Cortex* 18 (11): 2471–82. doi:10.1093/cercor/bhn011.

Goley, P D. 1999. “Behavioral Aspects of Sleep in Pacific White-Sided Dolphins (Lagenorhynchus Obliquidens, Gill 1865).” *Mar Mamm Sci* 15 (4): 1054–64. doi:10.1111/j.1748-7692.1999.tb00877.x.

Hagmann, P, L Cammoun, R Martuzzi, P Maeder, S Clarke, J P Thiran, and R Meuli. 2006. “Hand Preference and Sex Shape the Architecture of Language Networks.” *Human Brain Mapping* 27 (10): 828–35. doi:10.1002/hbm.20224.

Hanson, A, W Grisham, C Sheh, J Annese, and S H Ridgway. 2013. “Quantitative Examination of the Bottlenose Dolphin Cerebellum.” *Anat Rec* 296: 1215–28. doi:10.1002/ar.22726.

Hill, H M, S Dietrich, D Yeater, M McKinnon, M Miller, S Aibel, and A Dove. 2015. “Developing a Catalog of Socio-Sexual Behaviors of Beluga Whales (Delphinapterus Leucas).” *Anim Behav Cogn* 2 (2): 105–23. doi:10.12966/abc.05.01.2015.

Hofman, M A. 1989. “On the Evolution and Geometry of the Brain in Mammals.” *Prog Neurobiol* 32 (2): 137–58. doi:10.1016/0301-0082(89)90013-0.

Huggenberger, S, T J Vogl, and H H A Oelschläger. 2010. “Epicranial Complex of the La Plata Dolphin (Pontoporia Blainvillei): Topographical and Functional Implications.” *Mar Mamm Sci* 26 (2): 471–81. doi:10.1111/j.1748-7692.2009.00349.x.

Hursh, J B. 1939. “Conduction Velocity and Diameter of Nerve Fibers.” *Am J Physiol* 127: 131–39.

Ivry, R B, and P C Lebby. 1993. “Hemispheric Differences in Auditory Perception Are Similar to Those Found in Visual Perception.” *Psychol Sci* 4 (1): 41–45. http://www.jstor.org/stable/40062501.

Ivry, R B, and L C Robertson. 1998. *The Two Sides of Perception*. MIT Press.

Jiang, H, P C M van Zijl, J Kim, G D Pearlson, and S Mori. 2006. “DtiStudio: Resource Program for Diffusion Tensor Computation and Fiber Bundle Tracking.” *Comput Meth Prog Bio* 81 (2): 106–16. doi:http://dx.doi.org/10.1016/j.cmpb.2005.08.004.

Johnson, C M, and K Moewe. 1999. “Pectoral Fin Preference during Contact in Commerson’s Dolphins (Cephalorynchus Commersoni).” *Aquat Mamm* 25: 73–78.

Kaas, J H. 2013. “The Evolution of Brains from Early Mammals to Humans.” *WIREs Cogn Sci* 4 (1): 33–45. doi:10.1002/wcs.1206.

Karenina, K, A Giljov, V Baranov, L Osipova, V Krasnova, and Y Malashichev. 2010. “Visual Laterality of Calf–mother Interactions in Wild Whales.” *Plos One* 5 (11): e13787. doi:http://dx.doi.org/10.1371/journal.pone.0013787.

Karenina, K, A Giljov, D Glazov, and Y Malashichev. 2013. “Social Laterality in Wild Beluga Whale Infants: Comparisons between Locations, Escort Conditions, and Ages.” *Behav Ecol Sociobiol* 67 (7): 1195–1204. doi:10.1007/s00265-013-1545-2.

Karenina, K, A Giljov, T Ivkovich, A Burdin, and Y Malashichev. 2013. “Lateralization of Spatial Relationships between Wild Mother and Infant Orcas, Orcinus Orca.” *Anim Behav* 86 (6): 1225–31. doi:doi:10.1016/j.anbehav.2013.09.025.

Karenina, K, A Giljov, T Ivkovich, and Y Malashichev. 2016. “Evidence for the Perceptual Origin of Right-Sided Feeding Biases in Cetaceans.” *Anim Cogn* 19 (1). Springer Berlin Heidelberg: 239–43. doi:10.1007/s10071-015-0899-4.

Keogh, M J, and S H Ridgway. 2008. “Neuronal Fiber Composition of the Corpus Callosum within Some Odontocetes.” *Anat Rec* 291 (7): 781–89. doi:10.1002/ar.20701.

Lyamin, O I, P R Manger, S H Ridgway, L M Mukhametov, and J M Siegel. 2008. “Cetacean Sleep: An Unusual Form of Mammalian Sleep.” *Neurosci Biobehav R* 32 (8): 1451–84. doi:doi:10.1016/j.neubiorev.2008.05.023.

MacLeod, C D, J S Reidenberg, M Weller, M B Santos, J Herman, J Goold, and G J Pierce. 2007. “Breaking Symmetry: The Marine Environment, Prey Size, and the Evolution of Asymmetry in Cetacean Skulls.” *Anat Rec* 290 (6): 539–45. doi:10.1002/ar.20539.

MacNeilage, P F. 2013. “Vertebrate Whole-Body-Action Asymmetries and the Evolution of Right Handedness: A Comparison between Humans and Marine Mammals.” *Dev Psychobiol* 55 (6): 577–87. doi:10.1002/dev.21114.

Madsen, P T, M Lammers, D Wisniewska, and K Beedholm. 2013. “Nasal Sound Production in Echolocating Delphinids (Tursiops Truncatus and Pseudorca Crassidens) Is Dynamic, but Unilateral: Clicking on the Right Side and Whistling on the Left Side.” *J Exp Biol* 216 (21): 4091–4102. doi:10.1242/jeb.091306.

Madsen, P T, D Wisniewska, and K Beedholm. 2010. “Single Source Sound Production and Dynamic Beam Formation in Echolocating Harbour Porpoises (Phocoena Phocoena).” *J Exp Biol* 213 (18): 3105–10. doi:10.1242/jeb.044420.

Manger, P R, J Hemingway, M Haagensen, and E Gilissen. 2010. “Cross-Sectional Area of the Elephant Corpus Callosum: Comparison to Other Eutherian Mammals.” *Neurosci* 167 (3): 815–24. doi:10.1016/j.neuroscience.2010.02.066.

Marino, L. 1998. “A Comparison of Encephalization between Odontocete Cetaceans and Anthropoid Primates.” *Brain Behav Evol* 51 (4): 230–38. doi:10.1159/000006540.

Marino, L, K D Sudheimer, T L Murphy, K K Davis, D Pabst, W A McLellan, J K Rilling, and J I Johnson. 2001. “Anatomy and Three-Dimensional Reconstructions of the Brain of a Bottlenose Dolphin (Tursiops Truncatus) from Magnetic

Resonance Images." *Anat Rec* 264 (4): 397–414. doi:10.1002/ar.10018.

Miller, K L, C J Stagg, G Douaud, S Jbabdi, S M. Smith, T E J Behrens, M Jenkinson, et al. 2011. "Diffusion Imaging of Whole, Post-Mortem Human Brains on a Clinical MRI Scanner." *NeuroImage* 57 (1): 167–81. doi:10.1016/j.neuroimage.2011.03.070.

Montie, E W, G Schneider, D R Ketten, L Marino, K E Touhey, and M E Hahn. 2008. "Volumetric Neuroimaging of the Atlantic White-Sided Dolphin (Lagenorhynchus Acutus) Brain from in Situ Magnetic Resonance Images." *Anat Rec* 291 (3): 263–82. doi:10.1002/ar.20654.

Mori, S, B J Crain, V P Chacko, and P C M van Zijl. 1999. "Three-Dimensional Tracking of Axonal Projections in the Brain by Magnetic Resonance Imaging." *Ann Neurol* 45 (2): 265–69. doi:10.1002/1531-8249(199902)45:2<265::AID-ANA21>3.0.CO;2-3.

Ness, A R. 1967. "A Measure of Asymmetry of the Skulls of Odontocete Whales." *J Zool* 153 (2): 209–21. doi:10.1111/j.1469-7998.1967.tb04060.x.

Northcutt, R G, and J H Kaas. 1995. "The Emergence and Evolution of Mammalian Neocortex." *Trends Neurosci* 18 (9): 373–79. doi:10.1016/0166-2236(95)93932-N.

Ocklenburg, S, F Ströckens, and O Güntürkün. 2013. "Lateralisation of Conspecific Vocalisation in Non-Human Vertebrates." *Laterality* 18 (1): 1–31. doi:10.1080/1357650X.2011.626561.

Olivares, R, S Michalland, and F Aboitiz. 2000. "Cross-Species and Intraspecies Morphometric Analysis of the Corpus Callosum." *Brain Behav Evol* 55 (1): 37–43. doi:10.1159/000006640.

Olivares, R, J Montiel, and F Aboitiz. 2001. "Species Differences and Similarities in the Fine Structure of the Mammalian Corpus Callosum." *Brain Behav Evol* 57 (0006-8977 (Print)): 98–105. doi:10.1159/000047229.

Petrides, M, G Cadoret, and S Mackey. 2005. "Orofacial Somatomotor Responses in the Macaque Monkey Homologue of Broca's Area." *Nature* 435: 1235–38. doi:10.1038/nature03628.

Pilleri, G, and M Gihr. 1970. "The Central Nervous System of the Mysticete and Odontocete Whales." In *Investigations on Cetacea*, 2:87–135.

Rattenborg, N C, C J Amlaner, and S L Lima. 2000. "Behavioral, Neurophysiological and Evolutionary Perspectives on Unihemispheric Sleep." *Neurosci Biobehav Rev* 24 (8): 817–42. doi:10.1016/S0149-7634(00)00039-7.

Renaud, D L, and A N Popper. 1975. "Sound Localization by the Bottlenose Porpoise Tursiops Truncatus." *J Exp Biol* 63 (3): 569–85.

Ridgway, S H. 2002. "Asymmetry and Symmetry in Brain Waves from Dolphin Left and

Right Hemispheres: Some Observations after Anesthesia, during Quiescent Hanging Behavior, and during Visual Obstruction." *Brain Behav Evol* 60 (5): 265–74. doi:10.1159/000067192.

Ridgway, S H, and R H Brownson. 1984. "Relative Brain Sizes and Cortical Surface Areas in Odontocetes." *Acta Zool Fenn* 172: 149–52.

Ridgway, S H, and D A Carder. 1990. "Tactile Sensitivity, Somatosensory Responses, Skin Vibrations, and the Skin Surface Ridges of the Bottle-Nose Dolphin, Tursiops Truncatus." In *Sensory Abilities of Cetaceans*, 163–79. Springer. doi:10.1007/978-1-4899-0858-2_9.

Ridgway, S H, D Carder, J Finneran, M Keogh, T Kamolnick, M Todd, and A Goldblatt. 2006. "Dolphin Continuous Auditory Vigilance for Five Days." *J Exp Biol* 209 (18): 3621–28. doi:10.1242/jeb.02405.

Ridgway, S H, and A C Hanson. 2014. "Sperm Whales and Killer Whales with the Largest Brains of All Toothed Whales Show Extreme Differences in Cerebellum." *Brain Behav Evol* 83 (4): 1–9. doi:10.1159/000360519.

Ridgway, S H, D Houser, J Finneran, D Carder, M Keogh, W Van Bonn, C Smith, M Scadeng, D Dubowitz, and R Mattrey. 2006. "Functional Imaging of Dolphin Brain Metabolism and Blood Flow." *J Exp Biol* 209 (15): 2902–10. doi:10.1242/jeb.02348.

Ridgway, S H, M Keogh, D Carder, J Finneran, T Kamolnick, M Todd, and A Goldblatt. 2009. "Dolphins Maintain Cognitive Performance during 72 to 120 Hours of Continuous Auditory Vigilance." *J Exp Biol* 212 (10): 1519–27. doi:10.1242/jeb.027896.

Ridgway, S H, D Samuelson Dibble, K Van Alstyne, and D Price. 2015. "On Doing Two Things at Once: Dolphin Brain and Nose Coordinate Sonar Clicks, Buzzes and Emotional Squeals with Social Sounds during Fish Capture." *J Exp Biol* 218: 3987–95. doi:10.1242/jeb.130559.

Ridgway, S H, and R J Tarpley. 1996. "Brain Mass Comparisons in Cetacea." *P Int Assoc Aquat Anim Med* 27: 55–57.

Rilling, J K, M F Glasser, S Jbabdi, J Andersson, and T M Preuss. 2012. "Continuity, Divergence, and the Evolution of Brain Language Pathways." *Front Evol Neurosci* 3 (11): 1–6. doi:10.3389/fnevo.2011.00011.

Rilling, J K, M F Glasser, T M Preuss, Xi Ma, T Zhao, X Hu, and T E J Behrens. 2008. "The Evolution of the Arcuate Fasciculus Revealed with Comparative DTI." *Nature Neuroscience* 11 (4): 426–28. doi:10.1038/nn2072.

Rilling, J K, and T R Insel. 1999. "Differential Expansion of Neural Projection Systems in Primate Brain Evolution." *Neuroreport* 10 (7): 1453–59.

Ringo, J L. 1991. “Neuronal Interconnection as a Function of Brain Size.” *Brain Behav Evol* 38 (1): 1–6. doi:10.1159/000114375.

Ringo, J L, R W Doty, S Demeter, and P Y Simard. 1994. “Time Is of the Essence: A Conjecture That Hemispheric Specialization Arises from Interhemispheric Conduction Delay.” *Cereb Cortex* 4: 331–43. doi:10.1093/cercor/4.4.331.

Rogers, L J, and R Andrew. 2002. *Comparative Vertebrate Lateralization*. Edited by L J Rogers and R Andrew. Cambridge University Press.

Sakai, M, T Hishii, S Takeda, and S Kohshima. 2006. “Laterality of Flipper Rubbing Behaviour in Wild Bottlenose Dolphins (Tursiops Aduncus): Caused by Asymmetry of Eye Use?” *Behav Brain Res* 170 (2): 204–10. doi:10.1016/j.bbr.2006.02.018.

Seghier, ML. 2008. “Laterality Index in Functional MRI: Methodological Issues.” *Magn Reson Imaging* 26. Elsevier Inc.: 594–601. doi:10.1016/j.mri.2007.10.010.

Stamatakis, EA, MA Shafto, G Williams, P Tam, and LK Tyler. 2011. “White Matter Changes and Word Finding Failures with Increasing Age.” *Plos One* 6 (1): e14496. doi:10.1371/journal.pone.0014496.

Supin, A Y, L M Mukhametov, T F Ladygina, V V Popov, A M Mass, and I G Polyakova. 1978. “Electrophysiological Studies of the Dolphin’s Brain.” *Izd Nauka*.

Taglialatela, J P, J L Russell, J A Schaeffer, and W D Hopkins. 2008. “Communicative Signaling Activates ‘Broca’s’ Homolog in Chimpanzees.” *Curr Biol* 18 (5): 343–48. doi:10.1016/j.cub.2008.01.049.

Takao, H, O Abe, H Yamasue, S Aoki, K Kasai, H Sasaki, and K Ohtomo. 2010. “Aging Effects on Cerebral Asymmetry: A Voxel-Based Morphometry and Diffusion Tensor Imaging Study.” *Magn Reson Imaging* 28. Elsevier Inc.: 65–69. doi:10.1016/j.mri.2009.05.020.

Takao, H, N Hayashi, and K Ohtomo. 2013. “White Matter Microstructure Asymmetry: Effects of Volume Asymmetry on Fractional Anisotropy Asymmetry.” *Neurosci* 231. IBRO: 1–12. doi:10.1016/j.neuroscience.2012.11.038.

Tarpley, R J, and S H Ridgway. 1994. “Corpus Callosum Size in Delphinid Cetaceans.” *Brain Behav Evol* 44 (3): 156–65. doi:10.1159/000113587.

Thiebaut de Schotten, M, F Dell’Acqua, R Valabregue, and M Catani. 2012. “Monkey to Human Comparative Anatomy of the Frontal Lobe Association Tracts.” *Cortex* 48. Elsevier Srl: 82–96. doi:10.1016/j.cortex.2011.10.001.

Thiebaut de Schotten, M, D H Ffytche, A Bizzi, F Dell’Acqua, M Allin, Muriel Walshe, R Murray, S C Williams, D G M Murphy, and M Catani. 2011. “Atlasing Location, Asymmetry and Inter-Subject Variability of White Matter Tracts in the Human Brain with MR Diffusion Tractography.” *NeuroImage* 54 (1). Elsevier Inc.: 49–59.

doi:10.1016/j.neuroimage.2010.07.055.

Thieltges, H, A Lemasson, S Kuczaj, M Böye, and C Blois-Heulin. 2011. "Visual Laterality in Dolphins When Looking at (Un)familiar Humans." *Anim Cogn* 14 (2): 303–8. doi:10.1007/s10071-010-0354-5.

Vernooij, MW, M Smits, PA Wielopolski, GC Houston, GP Krestin, and A van der Lugt. 2007. "Fiber Density Asymmetry of the Arcuate Fasciculus in Relation to Functional Hemispheric Language Lateralization in Both Right- and Left-Handed Healthy Subjects: A Combined fMRI and DTI Study." *NeuroImage* 35. Elsevier Inc.: 1064–76. doi:10.1016/j.neuroimage.2006.12.041.

Waxman, S G. 1980. "Determinants of Conduction Velocity in Myelinated Nerve Fibers." *Muscle Nerve* 3 (2): 141–50. doi:10.1002/mus.880030207.

Wright, Alexandra, Miriam Scadeng, Dominik Stec, Rebecca Dubowitz, S H Ridgway, and Judy St. Leger. 2016. "Neuroanatomy of the Killer Whale (Orcinus Orca): A Magnetic Resonance Imaging Investigation of Structure with Insights on Function and Evolution." *Brain Struct Funct*, 1–20. doi:10.1007/s00429-016-1225-x.

Yeater, D B, H M Hill, N Baus, H Farnell, and S A Kuczaj II. 2014. "Visual Laterality in Belugas (Delphinapterus Leucas) and Pacific White-Sided Dolphins (Lagenorhynchus Obliquidens) When Viewing Familiar and Unfamiliar Humans." *Anim Cogn* 17 (6): 1245–59. doi:10.1007/s10071-014-0756-x.

Zhang, K, and T J Sejnowski. 2000. "A Universal Scaling Law between Gray Matter and White Matter of Cerebral Cortex." *P Nat Acad Sci* 97 (10): 5621–26. doi:10.1073/pnas.090504197.

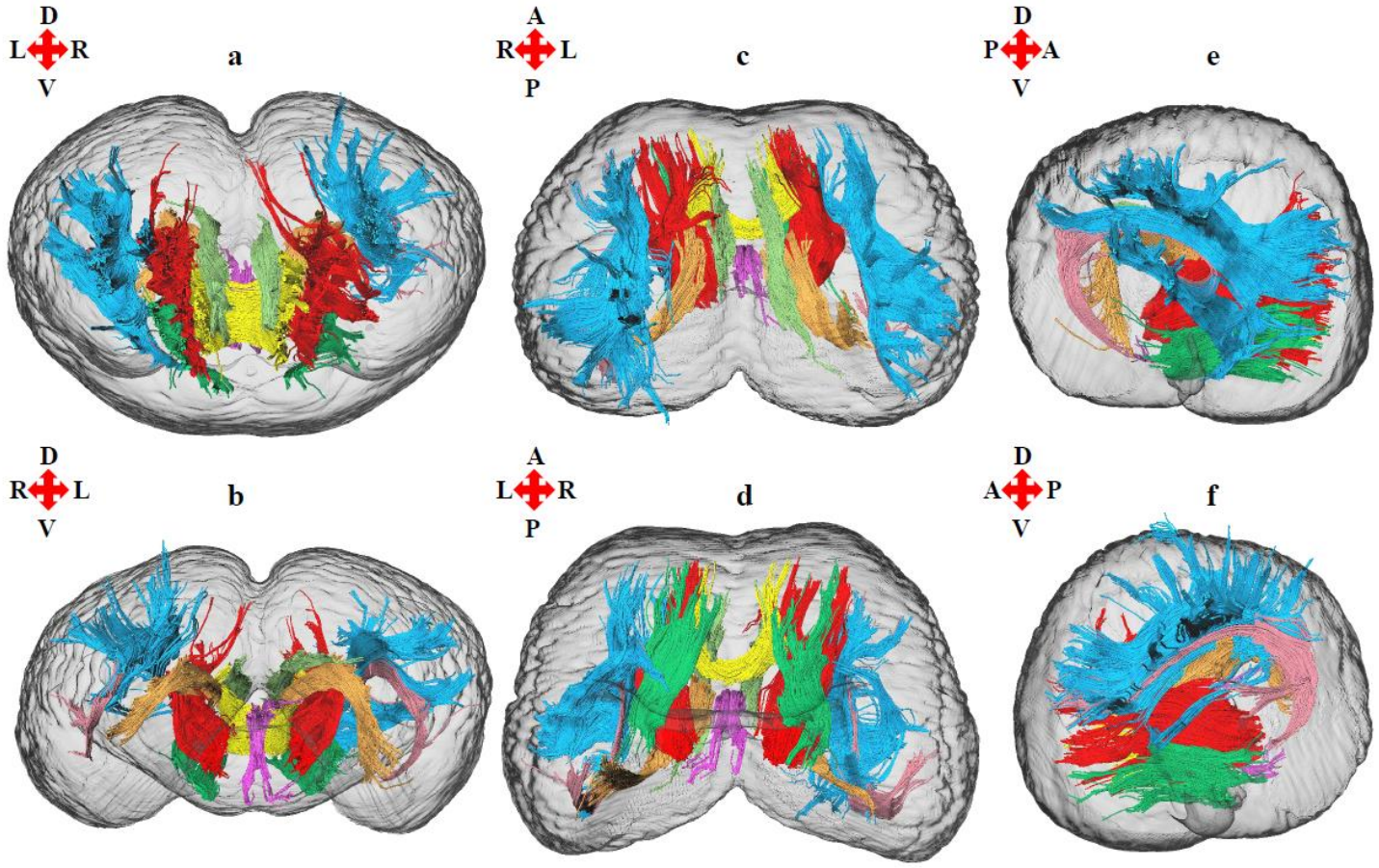

Figure 3.1: (a) Anterior, (b) posterior, (c) dorsal, (d) ventral, (e) left parasagittal, and (f) right parasagittal views of the *T. truncatus* cerebral surface (*translucent dark gray*) and underlying white matter tracts of the anterior thalamic radiation (*red*), arcuate fasciculus (rose), cingulum (*light green*), corticocaudate tract (*orange*), external capsule (*dark green*), forceps minor of the corpus callosum (*yellow*), fornix (*fuchsia*), and superior longitudinal fasciculus system (*light blue*). Color designations are consistent across figures; however, the superior longitudinal fasciculus system in Fig. 2 reflects parcellation of the sub-tracts, SLF I, SLF II, and SLF III).

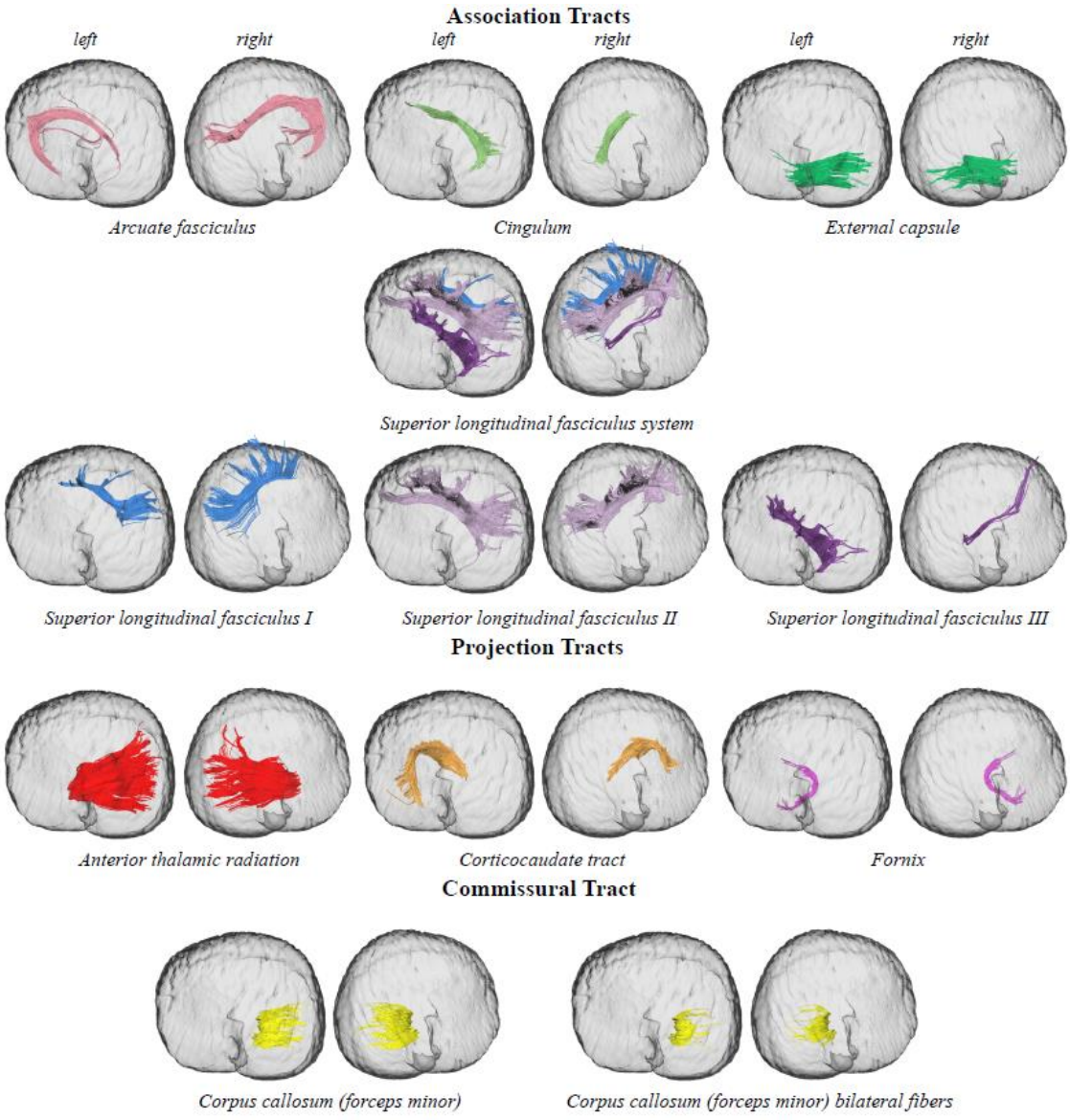

Figure 3.2: Left and right parasagittal views of the *T. truncatus* cerebral surface (*translucent dark gray*) and underlying white matter tracts of the association, projection, and commissural fiber systems. Color designations are consistent across figures; however, the superior longitudinal fasciculus system in this figure reflects parcellation of the sub-tracts, SLF I, SLF II, and SLF III.

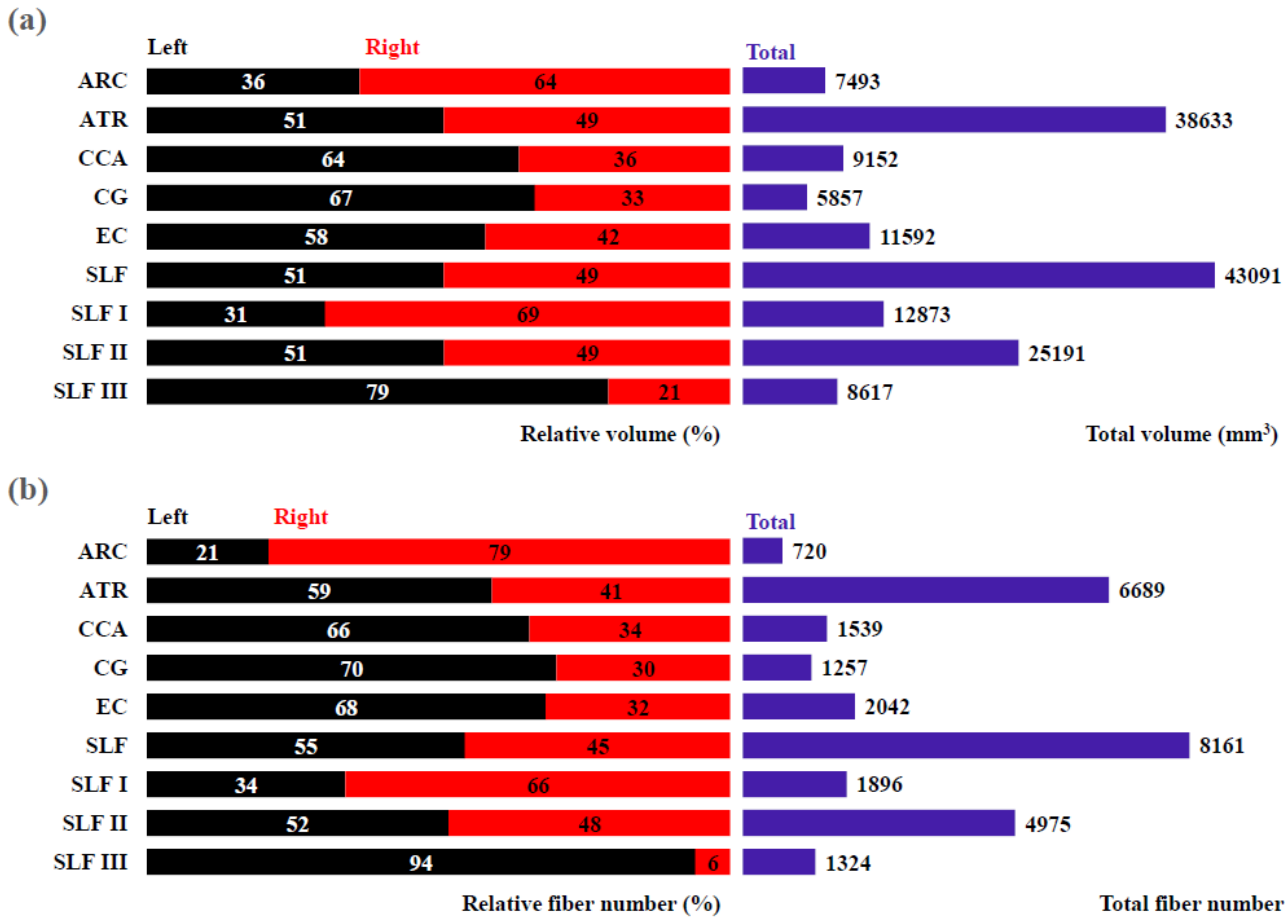

Figure 3.3: (a) Total volume (mm^3, *purple*) and relative volume (%) for each tract (left, *black*; right, *red*) and (b) total fiber number (*purple*) and relative fiber number (%) for each tract (left, *black*; right, *red*). Left and right tracts combined represent 100% of the total volume or total fiber number. *ARC (arcuate fasciculus), ATR (anterior thalamic radiation), CCA (corticocaudate tract), CG (cingulum), EC (external capsule), SLF (superior longitudinal fasciculus system), SLF I (superior longitudinal fasciculus I), SLF II (superior longitudinal fasciculus II), SLF III (superior longitudinal fasciculus III).*

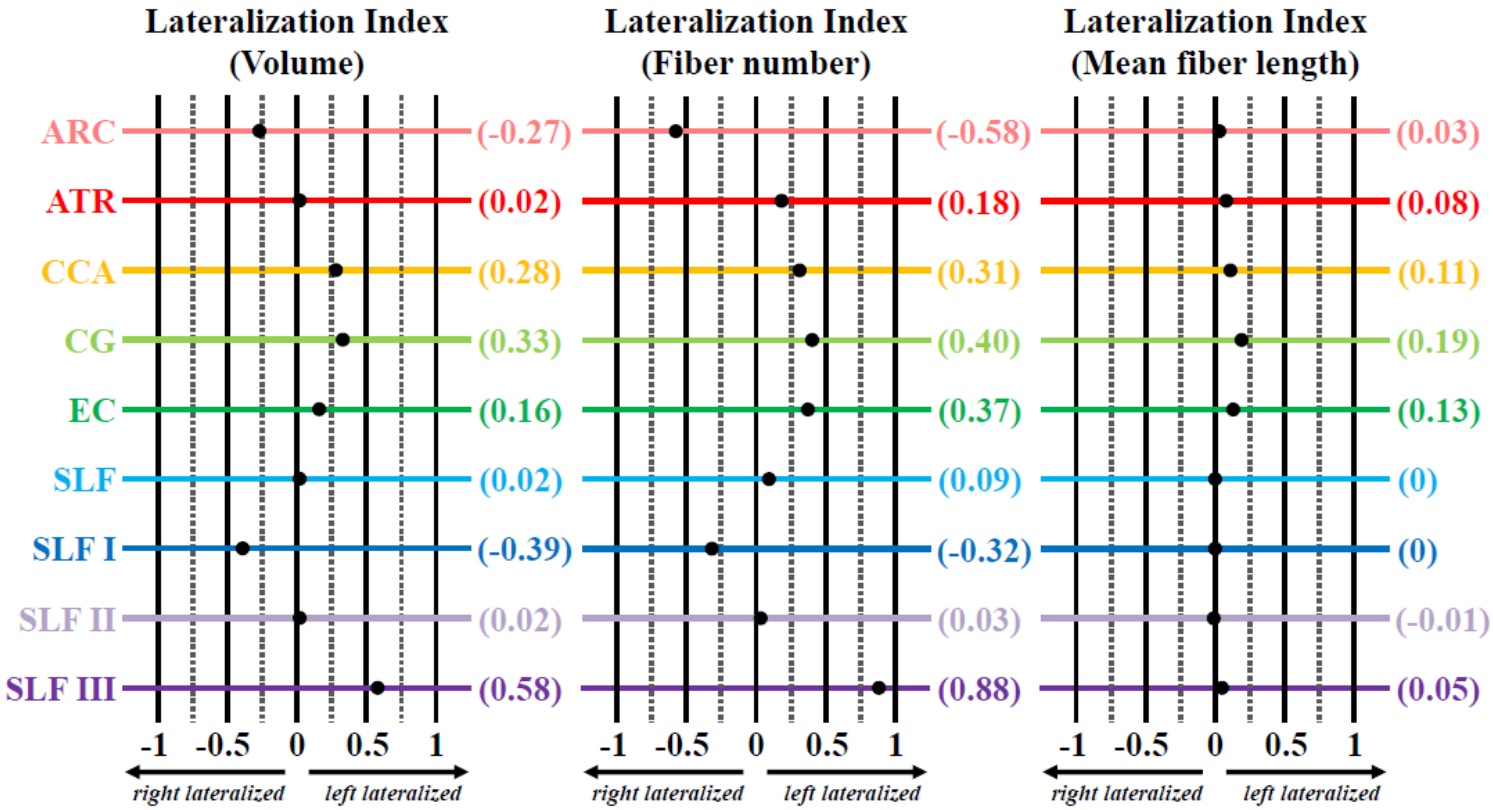

Figure 3.4: Lateralization index (LI) for the volume, fiber number, and mean fiber length of the arcuate fasciculus (ARC, *rose*) anterior thalamic radiation (ATR, *red*), corticocaudate tract (CCA, *orange*), cingulum (CG, *light green*), external capsule (EC, *dark green*), superior longitudinal fasciculus system (SLF, *light blue*), superior longitudinal fasciculus I (SLF I, *dark blue*), superior longitudinal fasciculus II (SLF II, *light purple*), and superior longitudinal fasciculus III (SLF III, *dark purple*). Tract-specific LI values for each measurement are shown in parentheses on the right. Color designations are consistent across figures; however, the superior longitudinal fasciculus system in Fig. 2 reflects parcellation of the sub-tracts, SLF I, SLF II, and SLF III.

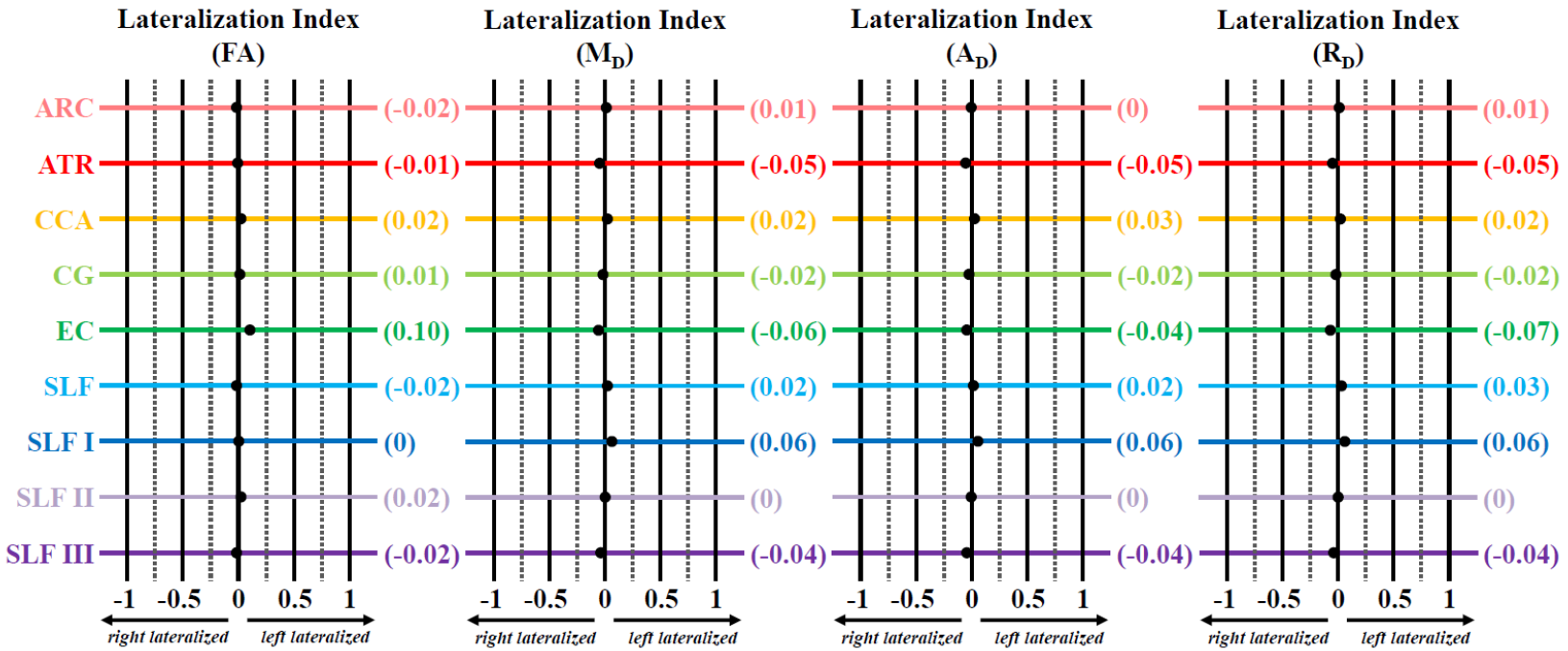

S. Figure 3.1: Lateralization index (LI) for the FA, M_D, A_D, and R_D of the arcuate fasciculus (ARC, *rose*) anterior thalamic radiation (ATR, *red*), corticocaudate tract (CCA, *orange*), cingulum (CG, *light green*), external capsule (EC, *dark green*), superior longitudinal fasciculus system (SLF, *light blue*), superior longitudinal fasciculus I (SLF I, *dark blue*), superior longitudinal fasciculus II (SLF II, *light purple*), and superior longitudinal fasciculus III (SLF III, *dark purple*). Tract-specific LI values for each measurement are shown in parentheses on the right. Color designations are consistent across figures; however, the superior longitudinal fasciculus system in Fig. 2 reflects parcellation of the sub-tracts, SLF I, SLF II, and SLF III.

S. Table 3.1 Repeated measures mean and standard deviation (± SD) for macrostructural tract-specific parameters of volume, fiber number, and mean fiber length in *T. truncatus* (N=1)

Tracts		Volume (mm^3) *Mean ± SD*	Fiber number *Mean ± SD*	Mean fiber length (mm) *Mean ± SD*
ARC				
	Left	2734 ± 0	150 ± 0	110 ± 0
	Right	4760 ± 0	570 ± 0	105 ± 0
ATR				
	Left	19653 ± 1298	3955 ± 355	60.0 ± 0.5
	Right	18980 ± 278	2734 ± 75	50.9 ± 0.1
CCA				
	Left	5839 ± 149	1009 ± 68	45.3 ± 1.4
	Right	3313 ± 241	530 ± 70	36.5 ± 1.7
CCFM				
	CCFM	10894 ± 168	2321 ± 56	25.1 ± 0.3
	CCFMBi	4775 ± 93	807 ± 56	31.0 ± 0.6
CG				
	Left	3895 ± 5	882 ± 1	57.7 ± 0
	Right	1962 ± 31	374 ± 6	39.1 ± 0.1
EC				
	Left	6727 ± 305	1396 ± 71	40.9 ± 0.9
	Right	4866 ± 248	646 ± 52	31.5 ± 0.5
FX				
		2355 ± 96	386 ± 27	38.2 ± 1.4
SLF				
	Left	21924 ± 0	4450 ± 0	65.2 ± 0
	Right	21167 ± 124	3711 ± 36	65.0 ± 0.2
	SLF I			
	Left	3938 ± 330	645 ± 73	56.4 ± 1.2
	Right	8935 ± 556	1251 ± 68	56.2 ± 0.1
	SLF II			
	Left	12838 ± 168	2573 ± 63	68.6 ± 0
	Right	12353 ± 434	2402 ± 67	69.7 ± 0.3
	SLF III			
	Left	6818 ± 0	1245 ± 0	62.6 ± 0
	Right	1799 ± 0	79.0 ± 0	56.8 ± 0

ARC (arcuate fasciculus), ATR (anterior thalamic radiation), CCA (corticocaudate tract), CCFM (corpus callosum - forceps minor), CCFMBi (corpus callosum - forceps minor, bilateral fibers), CG (cingulum), EC (external capsule), FX (fornix), SLF (superior longitudinal fasciculus system), SLF I (superior longitudinal fasciculus I), SLF II (superior longitudinal fasciculus II), SLF III (superior longitudinal fasciculus III)

S. Table 3.2 Repeated measures mean and standard deviation (± SD) for microstructural tract-specific parameters of fractional anisotropy (FA), mean diffusivity (M_D), axial diffusivity (A_D), and radial diffusivity (R_D) in *T. truncatus* (N=1)

Tracts		FA *Mean ± SD*	M_D (mm^2/s) *Mean ± SD*	A_D (mm^2/s) *Mean ± SD*	R_D (mm^2/s) *Mean ± SD*
ARC					
	Left	0.20 ± 0	1.91E-04 ± 0	2.31E-04 ± 0	1.70E-04 ± 0
	Right	0.21 ± 0	1.87E-04 ± 0	2.29E-04 ± 0	1.67E-04 ± 0
ATR					
	Left	0.28 ± 0	2.04E-04 ± 0	2.63E-04 ± 0	1.74E-04 ± 1.04E-06
	Right	0.28 ± 0	2.25E-04 ± 0	2.92E-04 ± 0	1.91E-04 ± 0
CCA					
	Left	0.24 ± 0	2.74E-04 ± 2.52E-06	3.43E-04 ± 2.32E-06	2.40E-04 ± 2.62E-06
	Right	0.23 ± 0	2.62E-04 ± 2.54E-06	3.25E-04 ± 3.23E-06	2.30E-04 ± 2.14E-06
CCFM					
	CCFM	0.32 ± 0	2.12E-04 ± 0	2.85E-04 ± 0	1.76E-04 ± 0
	CCFMBi	0.32 ± 0	2.08E-04 ± 0	2.81E-04 ± 0	1.72E-04 ± 0
CG					
	Left	0.23 ± 0	2.16E-04 ± 0	2.71E-04 ± 0	1.89E-04 ± 0
	Right	0.23 ± 0	2.26E-04 ± 0	2.83E-04 ± 0	1.97E-04 ± 0
EC					
	Left	0.28 ± 0	2.51E-04 ± 1.80E-06	3.26E-04 ± 2.50E-06	2.14E-04 ± 1.50E-06
	Right	0.23 ± 0	2.83E-04 ± 1.70E-06	3.53E-04 ± 2.23E-06	2.48E-04 ± 1.50E-06
FX					
		0.18 ± 0	3.35E-04 ± 0	3.99E-04 ± 0	3.03E-04 ± 0

S. Table 3.2 continued Repeated measures mean and standard deviation (± SD) for microstructural tract-specific parameters of fractional anisotropy (FA), mean diffusivity (M_D), axial diffusivity (A_D), and radial diffusivity (R_D) in *T. truncatus* (N=1)

Tracts	FA *Mean ± SD*	M_D (mm^2/s) *Mean ± SD*	A_D (mm^2/s) *Mean ± SD*	R_D (mm^2/s) *Mean ± SD*
SLF				
Left	0.22 ± 0	1.80E-04 ± 0	2.21E-04 ± 0	1.60E-04 ± 0
Right	0.22 ± 0	1.72E-04 ± 0	2.14E-04 ± 0	1.51E-04 ± 0
SLF I				
Left	0.22 ± 0	1.84E-04 ± 0	2.29E-04 ± 1.15E-06	1.62E-04 ± 0
Right	0.23 ± 0	1.65E-04 ± 0	2.05E-04 ± 0	1.45E-04 ± 0
SLF II				
Left	0.23 ± 0	1.75E-04 ± 0	2.18E-04 ± 0	1.54E-04 ± 0
Right	0.23 ± 0	1.74E-04 ± 0	2.17E-04 ± 0	1.53E-04 ± 0
SLF III				
Left	0.18 ± 0	1.88E-04 ± 0	2.23E-04 ± 0	1.70E-04 ± 0
Right	0.18 ± 0	2.03E-04 ± 0	2.42E-04 ± 0	1.84E-04 ± 0

ARC (arcuate fasiculus), ATR (anterior thalamic radiation), CCA (corticocaudate tract), CCFM (corpus callosum - forceps minor), CCFMBi (corpus callosum - forceps minor, bilateral fibers), CG (cingulum), EC (external capsule), FX (fornix), SLF (superior longitudinal fasciculus system), SLF I (superior longitudinal fasciculus I), SLF II (superior longitudinal fasciculus II), SLF III (superior longitudinal fasciculus III)